

**Charles University**

**Faculty of Science**

Study program: Developmental and Cell Biology



**Mgr. Aneta Škarková**

The analysis of cancer invasion plasticity in a 3D environment  
Analýza plasticity invazivity nádorových buněk ve 3D prostředí

Doctoral thesis

Supervisor: Assoc. Prof. RNDr. Jan Brábek, PhD.

Prague, 2021

I hereby declare that I have carried out this work and have written the thesis independently based on my best knowledge and under the guidance of my supervisor. All sources and literature used have been cited properly and this work has not been used to obtain any other academic degree.

Prague, 3.6.2021

.....

Mgr. Aneta Škarková

I further declare that I have truthfully stated my contribution to the works published with collective authorship in the chapter “List of publications and author contribution “.

Prague, 3.6.2021

.....

Mgr. Aneta Škarková

.....

Supervisor: Assoc. Prof. RNDr. Jan Brábek, PhD.

## Acknowledgements

This thesis represents many months of my PhD work and brings my studies closer to a hopefully successful end. The years of my PhD were enriching, entertaining, but at times demanding and stressful, and I wish to thank those that helped me and supported me throughout.

I thank my supervisor, doc. RNDr. Jan Brábek, PhD, for all his valuable support and guidance, and doc. RNDr. Daniel Rösel, PhD for consultations and further help. I am grateful to Jan and Daniel for giving me the opportunity to become a part of the team of the Laboratory of Cancer Cell Invasion, which has provided me with a great, stimulatory scientific environment with a balance of collaborations and individual work, but also with friendships and encouragement in tough times. In this regard, I am especially thankful to Marie Charvátová for taking such good care of us.

I thank my closest family and friends for all their love and support - you know what you mean to me. Finally, I want to thank my husband Kryštof Škarka, for his endless love, patience, and encouragement.

## Table of contents

Acknowledgements .....	i
Table of contents .....	ii
Abstract .....	iii
Abstrakt .....	iv
List of abbreviations .....	v
Introduction .....	1
Cell migration: the good and the bad .....	1
The metastatic cascade .....	2
Cytoskeleton in cell migration .....	3
Cell migration modes: .....	5
Epithelial-mesenchymal transition and collective invasion .....	6
Mesenchymal invasion .....	8
Amoeboid invasion.....	9
Plasticity of cancer cell invasion.....	11
Plasticity governed by the cytoskeleton .....	13
Plasticity governed by mechanical cues .....	14
Plasticity governed by signalling within the tumour stroma .....	15
Inflammation in cancer invasion plasticity.....	16
Migrastatic therapy.....	17
Search for invasion plasticity mechanisms- aims of this thesis.....	18
List of publications and author contribution .....	18
Publication #1: Quantitative phase imaging unravels new insight into dynamics of mesenchymal and amoeboid cancer cell invasion.....	21
Publication #2: High throughput Transcriptomic and Proteomic Profiling of Mesenchymal-Amoeboid Transition in 3D Collagen .....	41
Publication #3: Sustained inflammatory signalling through Stat1/Stat2/IRF9 is associated with the amoeboid phenotype of melanoma cells .....	55
Discussion of results.....	78
Future challenges and perspectives .....	88
Concluding remarks .....	89
References .....	90

## Abstract

Cells have evolved multiple mechanisms of cellular motility ranging from the migration of large cell cohorts to specialized migration of individual cells. The wide range of invasion modes has been exploited by cancer cells to their advantage, which has rendered the metastatic process so difficult to defeat. To allow for a better understanding of cancer invasion plasticity, we have employed studies on cancer cells that adopt the proteolytically active, adhesion-dependent, elongated mesenchymal invasion mode, the protease-independent, low adhesion, rounded amoeboid invasion mode, or combination of both. To study invasion plasticity directly, we have established two model systems of the mesenchymal-amoeboid transition (MAT) that allow for regulated induction of MAT in 3D *in vitro* environments. Using these systems, MAT was induced in HT1080 fibrosarcoma cells and the acquisition of a motile, invasive amoeboid phenotype was confirmed. We then observed the mesenchymal and amoeboid invasion strategies within 3D collagen in more detail using a digital holographic microscope. Further, HT1080 cells before and after MAT were subject to high throughput proteomic and transcriptomic studies. Comparison of gene expression and protein levels of mesenchymal and amoeboid cells disclosed an inflammatory-like signature of amoeboid cells. To validate this finding, we tested the effect of activation and inhibition of Jak/Stat signalling on melanoma cell invasion phenotypes by various approaches and confirmed a pro-amoeboid role of inflammation-associated signalling. Altogether, we present novel findings on the regulation of cancer invasion plasticity.

Key words: metastasis, invasion plasticity, amoeboid, mesenchymal, MAT, 3D

## Abstrakt

Buňky si vyvinuly řadu mechanismů buněčného pohybu, od přesunu velkých buněčných kohort po specializovanou migraci jednotlivých buněk. Tuto širokou škálu invazivních fenotypů využily nádorové buňky ve svůj prospěch, čímž učinily metastatický proces těžko porazitelným. Pro lepší porozumění plasticitě invazivity nádorových buněk jsme studovali buňky využívající protáhlý, mesenchymální způsob migrace, který je závislý na proteolýze a adhezi, a buňky využívající kulatý, na proteázách a adhezivitě nezávislý améboidní pohyb i buňky využívající kombinaci obou. Pro přímé studium plasticity invazivity jsme zavedli dva modelové systémy mezenchymálně-améboidního přechodu (MAT), které umožňují regulovanou indukci MAT v 3D prostředí *in vitro*. S využitím těchto systémů jsme indukovali MAT v buňkách fibrosarkomové linie HT1080 a zároveň potvrdili přechod na funkční, invazivní améboidní fenotyp. Pomocí digitálního holografického mikroskopu jsme detailněji popsali mesenchymální i améboidní pohyb v 3D kolagenu. Dále jsme provedli proteomickou a transkriptomickou srovnávací analýzu HT1080 před a po MAT. Porovnání genové exprese a hladin proteinů v mezenchymálních a améboidních buňkách odhalilo aktivaci signalizace spojené se zánětem u améboidních buněk. Abychom toto zjištění potvrdili, testovali jsme účinek aktivace a inhibice Jak/Stat signalizace na invazivní fenotypy buněk melanomu různými přístupy a potvrdili jsme její pro-améboidní roli. V této disertační práci představuji námi získané nové poznatky o regulaci plasticity invazivity nádorových buněk.

Klíčová slova: metastáze, plasticita invazivity, améboidní, mesenchymální, MAT, 3D

## List of abbreviations

AMT	amoeboid to mesenchymal transition
Arp2/3	Actin-related proteins 2/3 complex
CAFs	cancer associated fibroblasts
CEBPB	CCAAT/enhancer-binding protein beta
CCHM	coherence-controlled holographic microscopy
DOCK3	dedicator of cytokinesis 3
ECM	extracellular matrix
EMT	epithelial-mesenchymal transition
GAP	GTPase activating protein
GDF15	growth differentiation factor 15
GDP	guanosine diphosphate
GEF	guanine nucleotide exchange factor
GTP	guanosine triphosphate
HIF1	hypoxia-inducible factor 1
icaRhoA	doxycycline-inducible constitutively active RhoA
IF	intermediate filament
IFIT1	interferon induced protein with tetratricopeptide repeats 1
IFITM3	interferon induced transmembrane protein 3
IFN	interferon
IL	interleukin
IRF9	interferon regulatory factor 9
ISGF3	interferon stimulated gene factor 3
Jak	Janus kinases
MAPK	mitogen-activated protein kinase
MAT	mesenchymal to amoeboid transition
mDia	mammalian Diaphanous-related
MLC	myosin light chain
MLCP	myosin light chain phosphatase
MMP	matrix metalloproteinase
MT	microtubule
MX1	MX dynamin like GTPase 1
NEDD9	neural precursor cell expressed, developmentally down-regulated 9
NFκB	nuclear factor kappa-light-chain-enhancer of activated B cells
NG2	neuron-glia antigen 2
NNMT	nicotinamide N-methyltransferase
PD-L1	programmed death-ligand 1
PEDF	pigment epithelium-derived factor
PI3K	phosphoinositide 3-kinases
ROCK	Rho associated protein kinase
RT-qPCR	reverse transcription - quantitative polymerase chain reaction
SERPINB2	serpin family B member 2
SOCS	suppressor of cytokine signaling
Stat	signal transducers and activators of transcription
STAT1	signal transducer and activator of transcription 1
TGFβ	transforming growth factor β
TNF	tumor necrosis factor
VASN	vasorin
WASP	Wiskott-Aldrich syndrome protein
WAVE	WASP family Verprolin-homologous protein

## Introduction

### Cell migration: the good and the bad

All forms of life are associated with movement, be it at organismal, multicellular, cellular level, or subcellular level. In higher, multicellular organisms, the migration of cells is a highly controlled mechanism underlying development and homeostatic processes, mainly exemplified as tissue renewal, repair after injury, and immune surveillance. On the contrary, when deregulated, it is the cause of multiple non-physiological events such as abrogated embryonic development, impaired wound healing and tissue repair, malfunctional immune response, and unfortunately also metastatic cancer.

To understand pathological states of cell migratory behaviour, it is important to perceive it also in its physiological state. Embryonic development represents the largest migratory event of cells, and as such, it is highly orchestrated and involves various migration strategies. Based on signalling cues, cells rearrange their mutual positions to establish novel structures, beginning with the formation of the three embryonic layers ectoderm, mesoderm and endoderm, and leading to the definite formation of tissues and organs. With respect to the diversity of these processes requiring cell motility, it should come as no surprise that multiple modes of cell migration have evolved, ranging from collective movement of cell cohorts and sheets to migration of individual, detached cells. This diversity in invasion modes applies to tumour invasion as well, and metastasis can be therefore thought of as physiological migratory processes gone awry and misused by invasive cancer cells.

In general, cell migration encompasses a series of steps that result in asymmetrical distribution of signalling molecules and cellular architecture in the direction of movement. This front-rear polarity, unlike apolar or apicobasal polarization of epithelial cells, leads to a distinct leading edge with the formation of cellular protrusions and a retracting cell rear. Spatial segregation of the front and rear enable cell body displacement along one axis, underlying directional persistence (Ridley et al., 2003). The repeating cycle of cell protrusion, adhesion, and rear contraction and retraction underlies the basic principle of cellular motility and is common to all invasion modes, albeit with modifications specific to particular invasion modes (Friedl and Wolf, 2003; Lauffenburger and Horwitz, 1996; Sheetz et al., 1999).



## The metastatic cascade

In the context of cancer, cell migration is often referred to as cell invasion and is an intrinsic feature of metastasis, a series of events resulting in cancer dissemination and formation of secondary tumours – metastases (**Fig. 1**)<sup>1</sup>. The cascade begins with cancer cells detaching from a primary tumour and is followed by their invasion through the tumour stroma and adjacent extracellular matrix, entering the bloodstream, extravasation, and final settlement at a secondary site. During this process, disseminated cancer cells must tackle the heterogeneous extracellular matrix (ECM), combat shear stress and anoikis, evade the immune system response and colonize the secondary site (Fares et al., 2020). The complexity of the individual steps renders this process largely ineffective, with only a tiny fraction, estimated to be less than 0,1% of all disseminated cells, completing the process (Chambers et al., 2002; Luzzi et al., 1998). The metastatic process thus selects for cancer cells with acquired resilience to multiple stress factors, which may underlie increased resistance of metastasis to therapy (Lambert et al., 2017). Moreover, the necessity to adapt to various environments, ranging from stiff tumour stroma to non-adhesive conditions within the bloodstream, may confer cells with invasion plasticity that would predispose them for successful invasion at secondary sites.

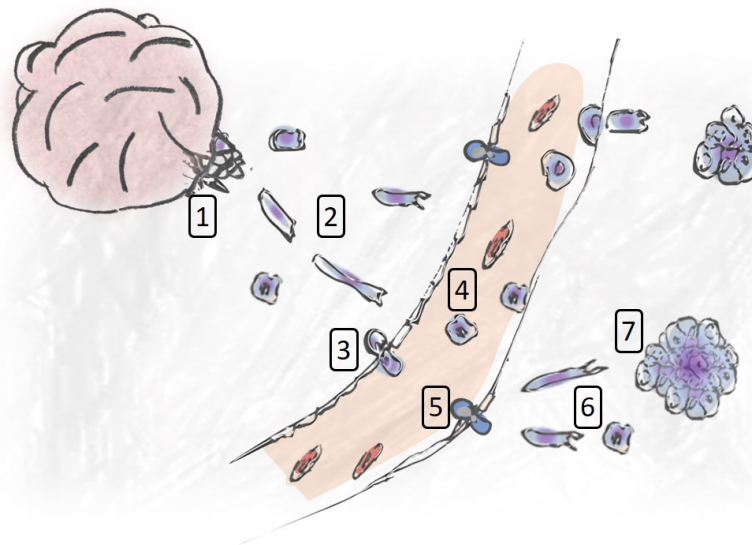


**Figure 1: Scheme of the metastatic cascade.** The process of metastasis encompasses a series of steps (1-7) that lead to the establishment of secondary tumours. 1) Detachment from the primary tumour. 2) Invasion through the adjacent extracellular matrix. 3) Intravasation into blood or lymphatic vessels. 4) Circulation in the vessel. 5) Extravasation through the basement membrane of vessels. 6) Invasion at the secondary site. 7) Proliferation and establishment of secondary tumours.

---

<sup>1</sup> All drawings in this thesis were created using Inkscape or were hand-drawn and further processed using basic image tools.

## Cytoskeleton in cell migration

Cell motility is necessarily accompanied by changes in the cell shape, which are driven by reorganization of the cytoskeleton. The most dynamic and rapid changes are dependent on actin polymerization, which drives propagation of protrusions, and actomyosin contractility, which enables retraction of the cell rear and builds up the cell cortex. Master regulators of actin dynamics are small GTPases of the Rho (*Ras homolog*) family - the most profound examples are Rac1/2/3, Cdc42 and RhoA/B/C, which represent the main signalling hubs regulating actin nucleation, polarity and cell contractility, respectively. Their activity is dependent on the binding of GTP (*guanosine triphosphate*), and its hydrolysis to GDP (*guanosine diphosphate*) leads to their inactivation. Rho GTPases thus exist in both active and inactive forms, and their cycling among these states is balanced out by numerous regulatory proteins. Guanine nucleotide exchange factors (GEFs) promote the exchange of GDP for GTP activating downstream signalling (Schmidt and Hall, 2002). On the other hand, GTPase activating proteins (GAPs) catalyse GTP hydrolysis promoting transition to the inactive state (Diekmann et al., 1995). RhoGTPases may be further regulated spatiotemporally by sequestration by guanine nucleotide dissociation factors (Dovas and Couchman, 2005). Given the fact that more than eighty GEFs and over seventy GAPs have been described, it clear that the activation of RhoGTPase signalling is largely tuneable and adaptable (Boureaux et al., 2007).

Both Rac1 and Cdc42 are key regulators of actin polymerization at the leading edge and drive the formation of actin-based protrusions, such as broad lamellipodia or thin, finger-like filopodia, (Ridley, 2006). Cdc42 and Rac1 signal via the WASP (*Wiskott-Aldrich syndrome protein*) and WAVE (*WASP family Verprolin-homologous protein*) protein complexes, respectively, leading to activation of Arp2/3 (*Actin-related proteins 2/3 complex*), which is a key actin nucleator (Eden et al., 2002; Rohatgi et al., 1999).

On the other hand, RhoA signalling is tightly coupled to the formation of stress fibres and actomyosin contractility (Amano et al., 2010; Ridley and Hall, 1992). The main effector of RhoA is ROCK (*Rho-associated protein kinase*), which promotes actomyosin contractility directly by phosphorylation of MLC (*myosin light chain*) (Amano et al., 1996) and indirectly by phosphorylation of MLCP (*myosin light chain phosphatase*), leading to its inactivation (Kimura et al., 1996). Another effector protein of RhoA is the formin mDia (*mammalian Diaphanous-related*), which is implicated in actin nucleation and polymerization (Watanabe et al., 1999). During cell migration, RhoA signalling is pre-dominantly activated at the cell rear, where contractile forces induce the retraction of the lagging end, although its activity is also detected at the leading edge preceding Rac1 and Cdc42 activation during membrane protrusion (Pertz et al., 2006).

Interestingly, RhoA and Rac1 signalling form an interconnected network with negative feedback loops (Byrne et al., 2016; Nguyen et al., 2018). For example, Rac1-GTP blocks activation of RhoA

via p190RhoGAP (Arthur and Burridge, 2001), and reciprocally, RhoA-GTP prevents Rac1 activation through FilGAP and ARHGAP22 (Sanz-Moreno et al., 2008).



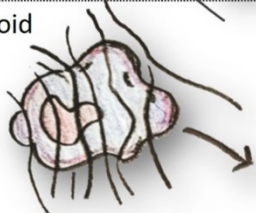
Altogether, Rho GTPase signalling governs actin dynamics, and modifying the balance between RhoA and Rac modulates cell contractile and protrusive forces, which is a key mechanism in invasion plasticity (Huang et al., 2014).

Apart from actin filaments, also microtubules (MTs) aid cell motility, and both actin and MTs signalling converge on RhoGTPases (Bouchet and Akhmanova, 2017). For example, TRIO, a GEF protein for Rac1, binds the growing tips of MTs, and Tiam1, another Rac1-GEF interacts with MT-associated proteins. Microtubules can regulate RhoA signalling through GEFH1, which is inactive when bound to MTs but becomes activated upon MT depolymerization leading to RhoA activation (Krendel et al., 2002). Reciprocally, RhoA can affect MT stabilization through mDia1 (Bartolini et al., 2008). Microtubules largely contribute to cell polarization, extending preferentially toward the leading edge, where they contribute to vesicular trafficking and localized delivery of cell migration-associated cargo proteins, including Rho GTPases (Osmani et al., 2010). Moreover, MTs have been implicated in regulating cellular adhesions, mainly through the transport of adhesion receptors and recycling of their components, and the targeting of stable adhesions by microtubules enhances their turnover rate (Seetharaman and Etienne-Manneville, 2019). Thus, apart from their fundamental role in cell division, MTs are key for multiple aspects of cell migration, including cell polarity, vesicle trafficking, stabilization of protrusions and turnover of adhesions at the leading edge.

While once considered largely static structural elements, it has recently become indisputable that also intermediate filaments (IFs) contribute to cell migration (Strouhalova et al., 2020). Vimentin, the most abundant IF, provides migrating cells with mechanical integrity necessary against compressive stress (Mendez et al., 2014) and protects the integrity of the nucleus by forming a cage-like structure around it (Patteson et al., 2019). Vimentin was shown to provide cells with stiffness, necessary for migration in dense environments (Messica et al., 2017) whereas its loss of promoted invasion through small pores (Patteson et al., 2019), pointing to a context-dependent role in migration. The exact mechanism remains to be elucidated, but it may involve GEFH1, as depletion of vimentin was shown to promote phosphorylation of GEFH1, resulting in the activation of RhoA (Jiu et al., 2017), a mechanism formerly described for MT depolymerization (Krendel et al., 2002).

### Cell migration modes:

Migrating cells can move collectively if they maintain cell-cell junctions (Haeger et al., 2015), or individually if cell-cell contacts are absent (**Fig. 2**). Although many intermediate migratory phenotypes exist, the prevailing classification distinguishes two individual invasion modes – amoeboid and mesenchymal. Amoeboid cells are often called “path-finding”, as these cells are not dependent on proteolytic degradation of the ECM, instead they actively deform their body and by enhancing contractility push through pores within the ECM, a process often accompanied by membrane blebbing. Conversely, mesenchymal invasion can be referred to as “path-generating”, because these cells require proteolytical degradation and adhesion to the ECM, resulting in more directional and persistent motility. The invasion modes, including underlying signalling, are described in more detail in the following chapters.

Invasion mode	Cell-cell contact	Cell-ECM contact	Proteolysis
Collective 	+	+	+
Mesenchymal 	-	+	+
Amoeboid 	-	-	-

**Figure 2: Basic classification of cancer invasion modes.** Collective invasion relies on cell-cell contact and cell-ECM contact, and requires proteolytical degradation of the extracellular matrix. Individually invading cells are generally classified as either mesenchymal, with profound cell-ECM contacts and ECM degradation, or amoeboid that do not require any stable contacts or proteolytical activity.

## Epithelial-mesenchymal transition and collective invasion

The translocation of cells during development often requires whole sheets or clusters of cells to move. This is enabled by maintaining cell-cell junctions within certain cells and disrupting them in others, whilst continuously preserving intercellular coordination (Haeger et al., 2015). To enable such reorganization, a specific programmatic switch, during which certain cells suppress epithelial features and gain mesenchymal characteristics, is activated. This process, tightly coupled to collective cell invasion, is termed the epithelial-mesenchymal transition (EMT) and is a crucial process during development, wound healing, and cancer (Baum et al., 2008; Kim et al., 2018).

EMT is a result of reciprocal reprogramming of intracellular signalling of cells and biochemical and structural composition of the ECM. A common trigger of the EMT is transforming growth factor  $\beta$  (TGF $\beta$ ) signalling, along with Wnt, Hedgehog, or Notch signalling pathways and activation of receptor tyrosine kinases, e.g. Ras, PI3K (*phosphoinositide 3-kinase*), and Src. These pro-invasive signalling pathways synergize with alterations of the microenvironment, such as stiffening or change in ECM components (D'Angelo et al., 2020). The process of EMT is orchestrated by transcriptional activity of pro-mesenchymal transcription factors, such as Snail or Twist, resulting in the expression of pro-migratory, mesenchymal genes (Lamouille et al., 2013). For example, the exchange of E-cadherin for N-cadherin and keratins for vimentin are common hallmarks of EMT.

During collective migration, only a subset of cells at the front undergoes the process of EMT, referred to as leader cells, while the remaining cell cohort is composed of so-called follower cells (**Fig. 3**). Leader cells lose apicobasal polarity typical of epithelial cells and transit to a front-rear organization. Furthermore, these cells typically display weakened cell-cell contacts, dynamic actin protrusions and secrete higher levels of membrane proteases capable of degrading the ECM (Nabeshima et al., 2000), creating space required for the forward movement of the cell cluster (**Fig. 3A**). Strikingly, recent findings show that specifically leading cells accumulate mRNA of pro-invasive molecules in the outmost region of their protrusions (Chrisafis et al., 2020). On the other hand, follower cells are tightly grouped due to intercellular contacts mediated by cadherins (Nabeshima et al., 1999) and these contacts are strong enough to keep the cell mass together when migrating through heterogeneous ECM (Vedula et al., 2014). The orchestration of leader cell invasive behaviour and compactness of following cells is common to all forms of collective invasion, although it is now evident that multiple hybrid phenotypes exist, where epithelial and mesenchymal markers are combined. This gives rise to the large variety of collectively migrating structures including sheets, strands and spherical clusters, which can greatly differ in cell numbers, ranging from a few cells to whole masses of cells (**Fig. 3B-C**). Recently, a hybrid collective amoeboid migration of cell clusters was described. It was shown that cells within the cluster may cooperate to form a supracellular actomyosin cortex around the cell cluster, which undergoes synchronized contraction at the rear that propels the cluster forward (Pagès et al., 2020).

Interestingly, during collective cancer cell migration, the leader cells are often replaced by cancer-associated fibroblasts (CAFs) that ensure matrix degradation and remodelling (Gaggioli et al., 2007). A different study showed that senescent cells can serve as leader cells and that their secretome enhances invasion (Kim et al., 2017). Overall, EMT leading to collective invasion is typical in carcinomas and histopathological analysis of patient samples suggests that collective migration is the prevalent mechanism for detachment of cancer cells from the tumour mass in solid tumours (Wang et al., 2016).

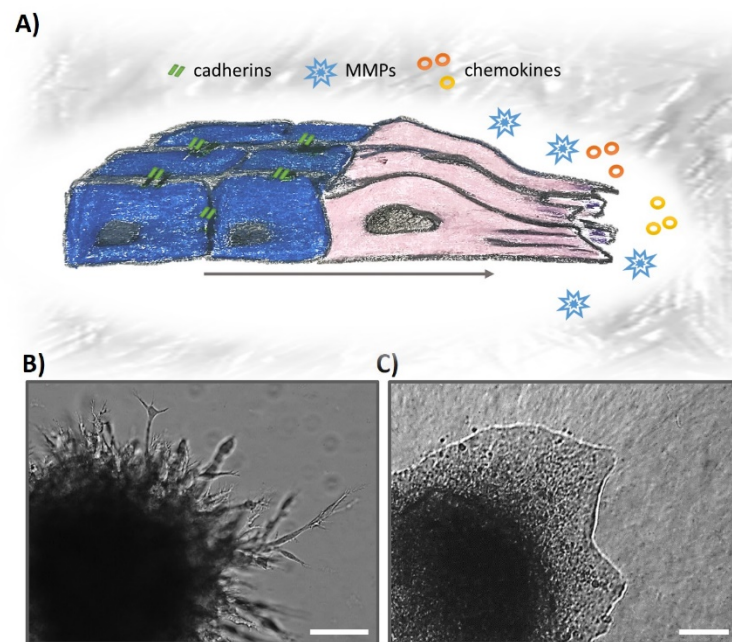


**Figure 3: Overview of collective invasion.** A) Leader cells (pink) secrete numerous pro-invasive molecules and secrete proteolytical enzymes, leading the way for follower cells (blue) that maintain cell-cell contacts and may contribute to the expansion of the cell sheet by proliferation. B-C) Wide-field image of strand-like (B) and sheet-like (C) collective invasion from cancer cell spheroids embedded in 3D collagen. Scale bars 100  $\mu\text{m}$ .

### Mesenchymal invasion

Mesenchymal invasion typically occurs in the presence of prominent cell-ECM adhesions but in the absence of intercellular adhesions. The cells' elongated shape, similar to that of fibroblasts, is enabled by protrusive activity at the leading edge and proteolytic degradation of the ECM forming tunnel-like paths that allow passage of the whole cell body (Friedl and Wolf, 2008) (**Fig. 4**).

Mesenchymally invading cells actively probe the ECM for adhesion sites by forming thin actin protrusions called filopodia, or actin bundles referred to as spikes (Jacquemet et al., 2015). Upon contact with the ECM, mesenchymal cells form adhesion structures, which serve to generate traction forces, anchor the cells and transmit signals from the ECM (Schwartz, 2010). The adhesions are mainly composed of integrins, which are coupled to the actin network, providing a structural link between the cell cytoskeleton and the ECM. Moreover, mesenchymal cells establish specialized adhesion structures that have ECM degrading ability, referred to as invadosomes. This term includes both podosomes formed by endothelial cells or monocytic cells and invadopodia, typical of cancer cells, which exhibit increased ECM degrading capacity (Linder et al., 2011). The degradation of the surrounding ECM is mediated by enzymes, both secreted and/or membrane-bound, with proteolytic activity such as MMPs (*matrix metalloproteinases*), ADAMs (*a disintegrin and metalloproteinase*), cathepsin proteinases, and serine proteinases, such as urokinase-type plasminogen activator (Basbaum and Werb, 1996).

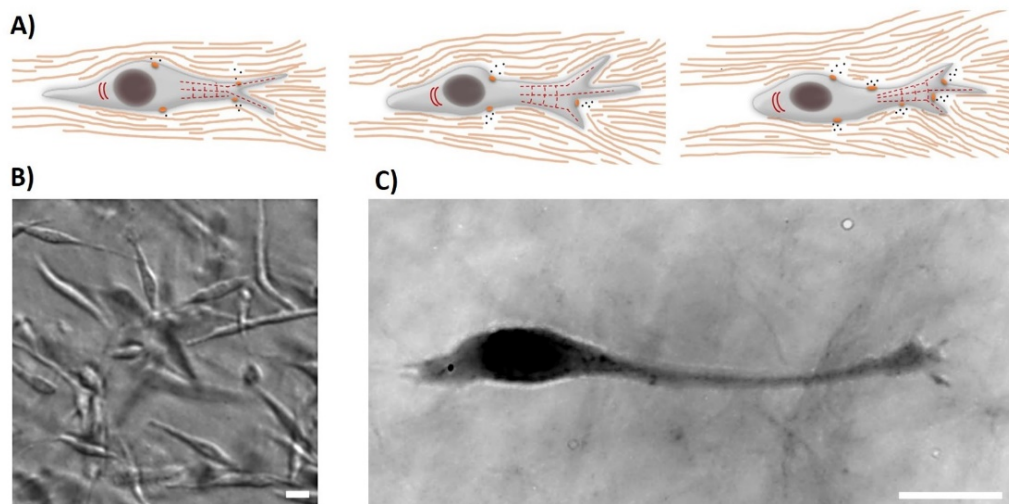


**Figure 4: Overview of mesenchymal invasion.** A) A scheme depicting mesenchymal invasion through a fibrillar environment. B) A representative image of mesenchymal cells embedded in 3D collagen. C) A mesenchymal cell within collagen imaged by digital holography microscopy. Scale bars 10  $\mu$ m.

Adhesion and ECM proteolysis are defining characteristics of mesenchymal invasion and both represent rate-limiting steps, restraining the speed of invasion (Friedl and Alexander, 2011). An invasive advantage of mesenchymal cells is their directional persistence, which is higher compared to amoeboid cells (Bouchet et al., 2016; Čermák et al., 2020). The invasive persistence is promoted by a clear front-rear polarity and the ability to degrade tunnels in the ECM by proteolysis, favouring unidirectional movement.

### Amoeboid invasion

Cells that do not degrade the ECM must navigate through the ECM to find pores large enough for the passage of the cell body, which requires dynamic cell shape plasticity (**Fig. 5**). The cell is propelled forward by contractile forces generated by the cortical actomyosin network, which builds up pressure leading to the formation of membrane blebs (Salbreux et al., 2012). The membrane blebs arise as a result of membrane detachment from the cell cortex, i.e., the cortical actomyosin network and associated proteins, and undergo expansion and retraction cycles. Importantly, the spatial distribution of membrane blebs dictates the directionality of invasion, which is regulated by the spatial distribution of the uropod proteins - ezrin, radixin and moesin (Lorentzen et al., 2011). Recently, a mechanism of membrane recycling by endocytosis at the cell rear and its trafficking to the leading front was described to drive adhesion-independent amoeboid migration (O'Neill et al., 2018).

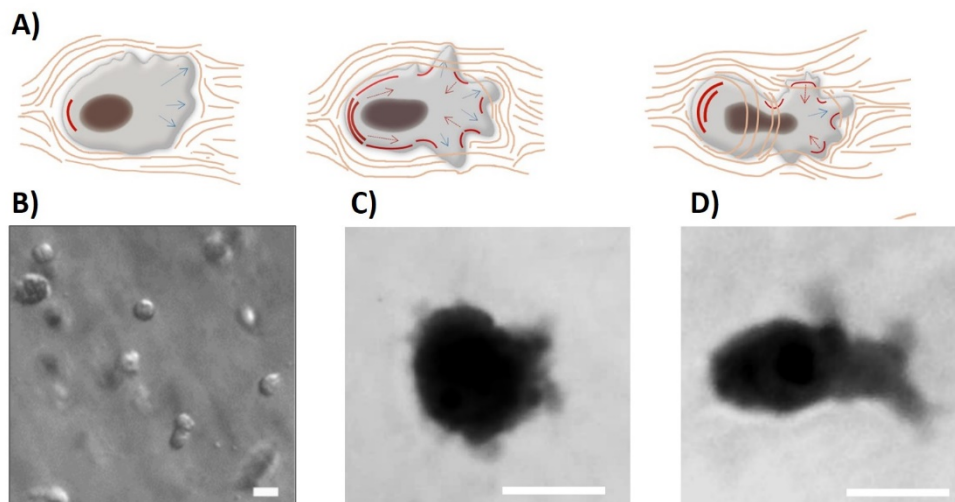


**Figure 5: Overview of amoeboid invasion.** A) A scheme depicting amoeboid invasion through a fibrillar environment. B) A representative image of amoeboid cells embedded in 3D collagen. C-D) A blebby amoeboid C) and pseudopodal amoeboid D) cell within collagen imaged by digital holography microscopy. Scale bars 10  $\mu\text{m}$ .



Unlike mesenchymal cells, amoeboid cells do not form stable ECM contacts. Accordingly, they have low expression of  $\beta$ 1-integrins. Instead, amoeboid cells can upregulate certain glycosaminoglycans that mediate low affinity, integrin independent ECM contacts (Schmidt and Friedl, 2010; Schmidt et al., 2020). As such, the formation of adhesions is not the rate-limiting step for amoeboid cells and they can migrate at the speed of 20  $\mu$ m/min, which superior to mesenchymal invasion (Krakhmal et al., 2015). However, due to the downregulated or missing proteolytical activity, the ECM pore size can restrict the translocation of the cell nucleus and halt the invasion of amoeboid cells (Wolf et al., 2013), and thus, the efficiency of amoeboid invasion is largely context-dependent.

Various amoeboid phenotypes have been observed in cancer cells, depending on the level of adhesion and contractility (Petrie and Yamada, 2016). These include blebby amoeboid cells, typically less motile with a round morphology with multiple blebs, and pseudopodal amoeboid cells, with a more polarized phenotype and larger, directional blebs (Liu et al., 2015; Tolde et al., 2018) (**Fig. 5C-D**). Further, in confining conditions and lack of adhesion, cells can transition to a fast migrating, stable bleb-based amoeboid mode. This type of amoeboid invasion is characterized by the formation of a single, large bleb, which is not rapidly retracted and instead persists as a result of a continuous flow of cortical actomyosin (Liu et al., 2015; Ruprecht et al., 2015).

## Plasticity of cancer cell invasion

The diversity of cancer invasion modes is further amplified by the fact that the cell invasion phenotypes are interconvertible, allowing cells to switch among them in order to adopt the most convenient mode in each situation. In addition to EMT, which drives the acquisition of a motile phenotype in originally epithelial cells, individually invading cells can promote their phenotype plasticity by switching between mesenchymal and amoeboid modes in transitions referred to as mesenchymal to amoeboid transition (MAT) and amoeboid to mesenchymal transition (AMT) (Friedl and Alexander, 2011; Gandalovičová et al., 2016; Panková et al., 2010). Cells can also regain epithelial traits in the so-called mesenchymal to epithelial transition, and there is ongoing debate as to whether this process is necessary for the establishment of secondary tumours (Jolly et al., 2017). Nevertheless, certain secondary metastases display increased epithelial markers compared to their paired primary tumours, suggesting that the process of re-differentiation may occur during secondary site colonization (Williams et al., 2019).

Especially cancer cells have become masters of invasion plasticity enabling them to metastasize through mechanically heterogeneous environments, ranging from very stiff tissue of the bone to very soft tissues, such as those of the brain. Moreover, invasion plasticity allows them to tackle therapeutical intervention and is often the cause of drug escape mechanisms (Gandalovičová et al., 2017). In cancer cell lines, there is a spontaneously large heterogeneity of cell invasion phenotypes, observed as varying cell morphologies within 3D environments, much larger than what is observed in 2D cultures. For example, melanoma cells can spontaneously acquire multiple phenotypes (Cooper et al., 2015). Importantly, the invasion modes are dynamically interconvertible, and phenotypic traits typical for either invasion mode may coexist within one cell. This was described in the case of rapid transitions between blebs, which are typical of amoeboid cells, and lamellipodia, which are associated with mesenchymal motility (Bergert et al., 2012). This rapid switching of membrane protrusions was later shown to be dependent on the degree of myosin II activity (Ghosh et al., 2021). Recently, a migration mode of breast cancer cells implementing both membrane blebs and integrin clustering was described (Guzman et al., 2017). Lobopodial migration is yet another example of a hybrid mode, characterized by blunt, cylindrical protrusions displaying both high actomyosin and high adhesion (Petrie et al., 2012). It is thus evident that cancer cells evolved various hybrid and transitional invasive phenotypes to their advantage (**Fig. 6**).

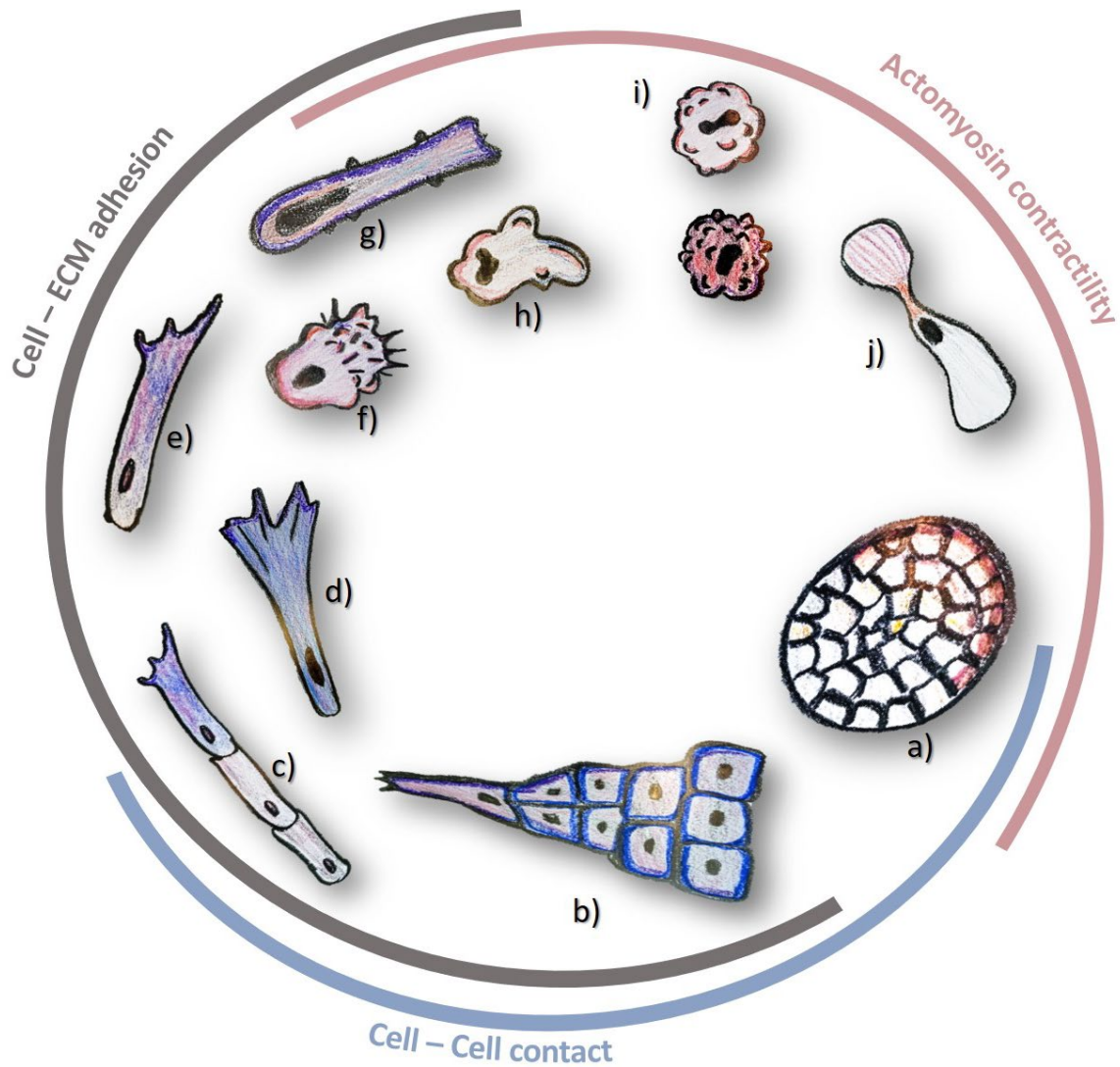


**Figure 6: Summary of cancer invasion modes.** A wide range of cancer invasion modes has been described, including many hybrid phenotypes. In a simplified model, the invasion modes can be segregated according to three main traits – intercellular contact, adhesion to the ECM and the level of actomyosin contractility. *a)* collective amoeboid invasion; *b)* collective invasion with leader and follower cells; *c)* collective strand invasion; *d-e)* mesenchymal invasion with broad leading edge (*d)* or thin protrusions (*e*); *f)* hybrid mode with filopodia and blebs; *g)* lobopodial invasion; *h)* pseudopodal amoeboid invasion; *i)* blebby amoeboid invasion, *j)* leader-bleb based amoeboid invasion.

### Plasticity governed by the cytoskeleton

There are striking morphological differences between mesenchymal cells and amoeboid cells pointing to the distinctive involvement of the cytoskeletal components and associated proteins in either invasion mode. All three cytoskeletal systems have been implicated in cell invasion plasticity.

There is a large difference in the dependence on MTs between mesenchymal and amoeboid invasion. During mesenchymal invasion, microtubules are required for persistent outgrowth of protrusions enabling cell elongation (Bouchet et al., 2016), while amoeboid cells are not dependent on a stable microtubule network. In fact, drugs inhibiting MT polymerization such as vincristine or nocodazole induce the amoeboid phenotype (Belletti et al., 2010; Eitaki et al., 2012). Moreover, microtubule-associated proteins affecting MT stability and/or polymerization can drive invasion plasticity. In lymphoma cells, microtubule-associated GEFH1 is released in response to activation of Stat3 signalling, resulting in RhoA activation and increased amoeboid invasion (Pan et al., 2018). The overexpression of an active form of stathmin 1, a microtubule destabilizing protein, led to a morphological switch to the rounded amoeboid-like phenotype in fibrosarcoma cells (Belletti et al., 2008). Accordingly, MT destabilization caused by the downregulation of mDia2 leads to amoeboid invasion (Hager et al., 2012). Expectedly, intermediate filament distribution affects invasion plasticity as well, for example, loss of vimentin enhanced amoeboid leader bleb-based migration of confined cancer cells (Lavenus et al., 2020).

Unsurprisingly, the transitions are mostly actin-dependent, driven by RhoGTPases. Multiple evidence shows that preferential activation of either Rho or Rac could be decisive for the establishment of either invasion mode. RhoA mediated contractility facilitates amoeboid invasion and activation of the Rho/ROCK pathway results in MAT (Rösel et al., 2008; Sahai and Marshall, 2003). The downregulation of pro-mesenchymal factors also promotes transition to the amoeboid phenotype, as documented in the case of silencing Rac1 activators DOCK3 (*dedicator of cytokinesis 3*) and NEDD9 (*Neural Precursor Cell Expressed, Developmentally Down-Regulated 9*) (Sanz-Moreno et al., 2008), or Smurf, which drives proteasomal degradation of RhoA (Sahai et al., 2007). On the other hand, when contractility is blocked, for example by ROCK inhibitors, or if Rac1 is activated, cells favour mesenchymal invasion (Sanz-Moreno et al., 2008). Similarly, downregulation of the Rho pathway by silencing the glycoprotein NG2 (*neuron-gial antigen 2*) also induced AMT (Paňková et al., 2012). The pro-amoeboid role of RhoA and pro-mesenchymal role of Rac1 were also documented by the expression of dominant negative and constitutively active mutants with preferential binding of GDP and GTP, respectively (MacKay and Kumar, 2014). Collectively, there is multiple evidence showing that manipulating cytoskeletal dynamics alters invasion phenotype plasticity.

### Plasticity governed by mechanical cues

It is apparent that mechanical cues largely contribute to invasion plasticity. Migrating cells respond to the physical properties of their surrounding environment, which is by no means possible to imitate in basic 2D culture conditions. Therefore, only 3D culture techniques should be considered for studying invasion plasticity. These include the use of fibrillar matrices, such as collagen, non-fibrillar protein gels such as Matrigel, engineered hydrogels, and more advanced options such as decellularized ECM or even patient-derived ECM.

There is growing evidence showing that the migration mode of cells is largely dictated by the characteristics of the surrounding environment, particularly by the rigidity and composition of the ECM, which determine its physical properties. Leukocyte motility is a prime example of ECM-regulated invasion plasticity. In low-density fibrillar environments, they utilize the amoeboid invasion mode, whereas in high-density collagen they switch to the protease-dependent, mesenchymal invasion strategy (Čermák et al., 2018; Van Goethem et al., 2010).

Mesenchymal and amoeboid cells have different requirements for the mechanical and chemical properties of the ECM, which determine its stiffness and pore size that in turn favour either mesenchymal invasion or amoeboid invasion (Geiger et al., 2019). If proteolytical degradation of the ECM is blocked by chemical inhibitors, mesenchymally invading cells can transit to the amoeboid phenotype, which enables navigation through the ECM without proteolytical degradation. However, amoeboid invasion is abrogated if pore sizes are smaller than  $7\mu\text{m}^2$ , which is limiting for nuclear passage (Wolf et al., 2003).

Another defining property of the ECM is the availability of adhesion sites in the ECM recognized by cell adhesion receptors. The cell-ECM adhesion is a requirement for mesenchymal migration, and the lack of the binding sites within the ECM, or lack of integrins, which mediate ECM adhesion, hinders mesenchymal migration. *In vitro*, this has been shown by the use of integrin blocking antibodies (Carragher et al., 2006; Wolf et al., 2003) or cultivation of cells under conditions that do not support the formation of cellular adhesions, such as mixed collagen-agarose gels, in which cells adopt a round morphology (Cambria et al., 2020; Ulrich et al., 2010). In confining conditions with no adhesion sites, cells adopt amoeboid phenotypes (Liu et al., 2015; Ruprecht et al., 2015). Accordingly, cells spontaneously undergo MAT during invasion into non-adhesive confining channels (Holle et al., 2019).

Overall, mesenchymal invasion is preferably used in environments with a higher density of ECM components, providing adhesion sites and demanding proteolytical degradation. On the other hand, amoeboid invasion is promoted in environments with low density, low adhesion or high confinement, in which cell deformability is advantageous.

### Plasticity governed by signalling within the tumour stroma

Cells constantly interact with the biochemical and mechanical nature of their surroundings. In tumours, the surrounding environment is referred to as the tumour microenvironment (TME), and consists, apart from cancer cells, of many non-cancer cells which are generally called stromal cells. There is rich dynamic and reciprocal interaction among these cells with cancer cells, promoting tumour growth and expansion (Lorusso and Rüegg, 2008). Moreover, the proximity of non-cancer cells can promote cancer invasion plasticity by direct interaction (Itoh et al., 2017), or indirectly, such as through re-modelling the surrounding matrix (Guiet et al., 2011).

Typically, the TME shows lower pH due to high metabolic activity of tumour cells, intermittent inflammatory-like conditions as a result of high cytokine production and deficiency in nutrients. Moreover, the size and dimensionality of the growing tumour mass invariantly lead to unequal exposure to resources, resulting in oxygen and nutrient deprivation. These characteristics of the TME modulate invasion phenotypes of cancer cells as they need to adapt to such conditions. For example, hypoxic conditions promote EMT by direct HIF1 (*hypoxia-inducible factor 1*) mediated gene expression changes of EMT inducers, such as Twist and Snail (Saxena et al., 2020), stimulate cancer cell invasion (Lewis et al., 2016) and promote phenotypic plasticity by inducing collective to amoeboid transition (Lehmann et al., 2017). This is in agreement with the finding that hypoxia induces RhoA and ROCK1 expression (Gilkes et al., 2014).

An important component of the tumour environment are cytokines that are secreted by both cancer cells, and non-cancer cells present in the tumour stroma, and crosstalk of fibroblasts with metastatic cells further enhances the production of pro-invasive cytokines (Li et al., 2009). Cytokine signalling generally triggers cell invasion and can impact invasion strategies of cancer cells by activating multiple signalling pathways, including Jak (*Janus kinase*)/Stat (*signal transducers and activators of transcription*), Smad, MAPK (*mitogen-activated protein kinase*) or Rho signalling (Odenthal et al., 2016). Increased cytokine signalling has been generally associated with amoeboid invasion. For example, TGF $\beta$  was shown to promote amoeboid invasion of melanoma cells (Cantelli et al., 2015), as well as Wnt11 (Rodriguez-Hernandez et al., 2020), while Wnt5a is associated with the amoeboid phenotype of lymphoma cells (Linke et al., 2017). Moreover, conditioned media containing chemokines including TGF $\beta$ , or interleukins (IL) IL6 and IL8 promoted the amoeboid phenotype of osteosarcoma cells (Petrovito et al., 2018). Accordingly, the downregulation of cytokines such as IL8, IL24 or TGF $\beta$  was detected after conversion to a pro-mesenchymal phenotype caused by overexpression of PEDF (*pigment epithelium-derived factor*), which is a secreted anti-inflammatory factor in melanoma cells (Ladhani et al., 2011; Orgaz et al., 2011).

### Inflammation in cancer invasion plasticity

There is increasing evidence that inflammation, inherently present in the tumour stroma, modulates the invasive behaviour of cells (Coussens and Werb, 2002; Solinas et al., 2010). Metastatic cancer has been referred to as “a wound that never heals” due to the resemblance of the tumour stroma to wounded tissue (Dvorak, 1986). There are multiple pathways involved in inflammatory signalling, but only those with a described link to cancer invasion modes will be discussed further.

Inflammation associated transcription factor NF $\kappa$ B (*nuclear factor kappa-light-chain-enhancer of activated B cells*) is activated mainly in response to secreted factors, such as TNF (*tumor necrosis factor*) or IL1 $\beta$ , and is implicated in regulating the expression of various cytokines. Interestingly, there is a direct link between Rho GTPases and the activation of NF $\kappa$ B (Tong and Tergaonkar, 2014), and it was shown that the cell shape and the stiffness of the ECM can influence NF $\kappa$ B signalling, favouring its activation in well-spread cells and cells on a stiff substrate (Sero et al., 2015). NF $\kappa$ B can promote mesenchymal traits by increased expression of proteolytic enzymes (Bond et al., 2001), but also has a direct link to amoeboid invasion. Amoeboid cells have been shown to secrete increased levels of cytokines, including high levels of IL1 $\beta$ , which leads to NF $\kappa$ B pathway activation that subsequently drives transcriptional upregulation of IL1 $\beta$ , promoting a self-driven pro-invasive circuit (Georgouli et al., 2019).

The Jak/Stat pathway has an utmost important role in inflammatory signalling and responds to a range of pleiotropic cytokines. Upon cytokine binding, receptors oligomerize and transmit signal through activation of Jak kinases that further activate transcription factors of the Stat family, which includes Stat1, Stat2 and Stat3, as well as less pronounced members, for example, Stat5 or Stat6. Stat3 is typically activated by cytokines of the IL6 family and various growth factors, while Stat1 and Stat2 respond to interferon (IFN) signalling by forming Stat1-Stat2 heterodimers and Stat1 homodimers in case of type I and type II IFN signalling, respectively (Rawlings et al., 2004). The response is tuned by the multiformity of Stat transcription complexes, which may be composed of homodimers or heterodimers (Delgoffe and Vignali, 2013). In addition, the complexes have differing roles if formed by phosphorylated or unphosphorylated Stats, which mediate the immediate (in terms of minutes) and long-term (in terms of hours) response, respectively (Yang and Stark, 2008).

The Stat3 pathway has been shown to promote amoeboid invasion through RhoA/ROCK enhanced actomyosin contractility (Sanz-Moreno et al., 2011). In this thesis, we present novel findings that show that also Stat1 and Stat2 are implicated in amoeboid invasion by sustaining an inflammatory state due to prolonged activity of ISGF3 (*interferon stimulated gene factor 3*), a complex composed of Stat1, Stat2 and adaptor protein IRF9 (*interferon regulatory factor 9*) (Gandalovičová et al., 2020).

## Migrastatic therapy

Due to the fact that metastatic dissemination to adjacent tissues accounts for the majority of solid tumour-related deaths, there is an ongoing strive to identify anti-invasive therapies. However, the large plasticity of cancer cell invasion makes this task more challenging than previously expected, and even decades after declaring the “war on cancer” there is a lack of anti-metastatic strategies. Recently, substances able to interfere with cancer migration modes have been termed migrastatics (Gandalovičová et al., 2017). Identification of such compounds that would either directly, or in combination, target all invasion modes would increase the chance of preventing drug escape mechanisms, as previously experienced in the case of protease inhibitors or integrin blocking antibodies that cells evaded through the process of MAT (Wolf et al., 2003). So far, multi-kinase inhibitors of ROCK and protein kinase A and B have been shown to suppress both amoeboid and mesenchymal invasion *in vitro* and *in vivo* (Sadok et al., 2015). A different study showed that dual targeting of the RhoA and Rac1 pathway hinders invasion and metastasis of breast cancer in a mouse model (Jones et al., 2017).

The need for anti-invasive therapy is also enhanced by the paradoxical observations that chemotherapy, despite targeting tumour proliferation, may promote metastatic behaviour of cells as an unsolicited bystander effect by selecting for more aggressive cells and by modulating signalling within the tumour stroma (D’Alterio et al., 2020). Yet still, clinical evaluation of anti-cancer drugs follows a cytotoxic, antiproliferative paradigm, although this does not evaluate anti-metastatic effects and may in fact lead to their enhancement, as mentioned above. Only recently have drugs that delay metastatic events been approved based on this endpoint (Fernandes et al., 2019). Unlike treatment with cytotoxic drugs, migrastatics are not expected to result in the selection of resistant clones as in the case of cytotoxic therapies, and even if so, these would not have a proliferative advantage, thus not becoming primarily widespread (Rosel et al., 2019). Overall, the naming and description of anti-metastatic drugs as migrastatics has already gained an international response, which will help unite the effort of individual labs into a worldwide effort.



## Search for invasion plasticity mechanisms- aims of this thesis

The lack of efficient antimetastatic drugs reflects our incomplete understanding of cells' invasive behaviour and justifies the need to conduct further research. Up till today, only a limited number of specific cancer cell markers have been described, out of which most are associated with a certain cancer type, such as prostate specific membrane antigen for prostate cancer or vascular endothelial growth factor for glioblastoma (Ghosh and Heston, 2004; Montano et al., 2016). The situation is even more discouraging in the case of pan-cancer markers of invasive cells, not to mention amoeboid or mesenchymal specific markers (Gerashchenko et al., 2019). The determination of the invasion mode is thus still mostly dependent on visual assessment of cell morphology and live-cell imaging, and thus assessment of the invasive potential of cancer from genetic profiling is largely remote.

Our goal was to study invasion plasticity in 3D environments to expand our existing knowledge of this phenomenon, as current publicly available datasets are limited.

The specific aims were to:

- 1) Identify and establish reliable *in vitro* model systems of invasion plasticity;
- 2) Characterize changes in gene expression and protein levels before and after the induction of invasion plasticity by high throughput methods;
- 3) Study and validate the significance of the identified signalling pathways in individual invasion modes.

## List of publications and author contribution

The individual findings and novel observations on invasive behaviour of cancer cells obtained throughout the years of my PhD studies were summarized in publications accepted to impact journals. Three publications integral to this thesis are listed below with a brief commentary on my contribution to each work and are included in their full version. Other publications that were published during my PhD studies are listed, but not discussed further.

*(Please note that studies published before 2021 are listed under my maiden name, Gandalovičová).*

## Publications included in this thesis

- 1) Tolde, O.\*; Gandalovičová, A.\*; Křížová, A.; Veselý, P.; Chmelík, R.; Rosel, D.; Brábek, J. Quantitative phase imaging unravels new insight into dynamics of mesenchymal and amoeboid cancer cell invasion. *Sci Rep.* **2018**, 13, 12020.

*\* these authors contributed equally*

As shared first author, I performed all amoeboid cell related live-cell imaging using digital holographic microscopy; imaging of mesenchymal cells was performed by dr. Ondřej Tolde. I largely contributed to image-post processing, figure preparation and manuscript writing of the amoeboid-related parts. In collaboration with Mgr. Aneta Křížová, who processed raw data, I carried out cell mass density analysis. I also took part in the revision process.

[\(link to online version\)](#)

- 2) Čermák, V.\*; Gandalovičová, A.\*; Merta, L.\*; Harant, K.; Rösel, D.; Brábek, J. High throughput Transcriptomic and Proteomic Profiling of Mesenchymal-Amoeboid Transition in 3D Collagen. *Sci. Data.* **2020**, 7, 160.

*\* these authors contributed equally*

As one of three first co-authors, I largely contributed to the publication by testing experimental systems of mesenchymal-amoeboid induction in 3D collagen, preparation of experimental stable cell lines, cell morphology analysis, live-cell imaging, and validation of results of proteomic studies by western blot. The preparation of RNA-sequencing libraries and raw-data processing was done by dr. Vladimír Čermák, RT-qPCR validation was carried out by dr. Ladislav Merta. I assisted with both manuscript preparation and the review process.

[\(link to online version\)](#)

- 3) Gandalovičová, A.; Šúchová, A.-M.; Čermák, V.; Merta, L.; Rösel, D.; Brábek, J. Sustained inflammatory signalling through Stat1/Stat2/IRF9 is associated with the amoeboid phenotype of melanoma cells. *Cancers.* **2020**, 12, 2450.

As first author, I performed the majority of experiments including gene enrichment analysis, preparation of stable cell lines, morphology and invasion experiments, analysis of signalling pathways by western blotting and RT-qPCR. I prepared the manuscript and figures, and contributed to the review process.

[\(link to online version\)](#)

## Other published articles

The following articles will not be discussed in detail in this thesis.

- 1) Gandalovičová, A.; Rösel, D.; Fernandes, M.; Veselý, P.; Heneberg, P.; Čermák, V.; Petruželka, L.; Kumar, S.; Sanz-Moreno, V.; Brábek, J. Migrastatics-Anti-metastatic and Anti-invasion Drugs: Promises and Challenges. *Trends Cancer*. **2017**, 3, 391-406.  
[\(link to online version\)](#)
- 2) Čermák, V.; Gandalovičová, A.; Merta, L.; Fučíková, J.; Špišek, R.; Rösel, D.; Brábek, J. RNA-seq of macrophages of amoeboid or mesenchymal migratory phenotype due to specific structure of environment. *Sci. Data*. **2018**, 5, 180198.  
[\(link to online version\)](#)
- 3) Strouhalova, K.; Přečková, M.; Gandalovičová, A.; Brábek, J.; Gregor, M.; Rosel, D. Vimentin Intermediate Filaments as Potential Target for Cancer Treatment. *Cancers*. **2020** 11, 184.  
[\(link to online version\)](#)
- 4) Merta, L.; Gandalovičová, A.; Čermák, V.; Dibus, M.; Gutschner, T.; Diederichs, S.; Rösel, D.; Brábek, J. Increased Level of Long Non-Coding RNA MALAT1 Is a Common Feature of Amoeboid Invasion. *Cancers*. **2020**, 12, 1136.  
[\(link to online version\)](#)
- 5) Čermák, V.; Škarková, A.; Merta, L.; Kolomazníková V.; Palušová, V.; Uldrijan, S.; Rösel, D.; Brábek, J. RNA-seq Characterization of Melanoma Phenotype Switch in 3D Collagen after p38 MAPK Inhibitor Treatment. *Biomolecules*. **2021**, 11(3):449  
[\(link to online version\)](#)
- 6) Janovec, V.; Ryabchenko, B.; Škarková, A.; Pokorná, K.; Rösel, D.; Brábek, J.; Weber, J.; Forstová, J.; Hirsch, I.; Huérfano, S. TLR4-Mediated Recognition of Mouse Polyomavirus Promotes Cancer-Associated Fibroblast-Like Phenotype and Cell Invasiveness. *Cancers*. **2021**, 13(9):2076  
[\(link to online version\)](#)
- 7) Kolouchova K, Groborz O, Cernochova Z, Skarkova A, Brabek J, Rosel D, Svec P, Starcuk Z, Slouf M, Hruby M. Thermo- and ROS-Responsive Self-Assembled Polymer Nanoparticle Tracers for 19F MRI Theranostics. *Biomacromolecules*. **2021** Apr 21. Online ahead of print.  
[\(link to online version\)](#)

Publication #1: Quantitative phase imaging unravels new insight into dynamics of mesenchymal and amoeboid cancer cell invasion

# SCIENTIFIC REPORTS



OPEN

## Quantitative phase imaging unravels new insight into dynamics of mesenchymal and amoeboid cancer cell invasion

Ondřej Tolde<sup>1,2</sup>, Aneta Gandalovičová<sup>1,2</sup>, Aneta Křížová<sup>3,4</sup>, Pavel Veselý<sup>3</sup>, Radim Chmelík<sup>3,4</sup>, Daniel Rosel<sup>1,2</sup> & Jan Brábek<sup>1,2</sup>

Observation and analysis of cancer cell behaviour in 3D environment is essential for full understanding of the mechanisms of cancer cell invasion. However, label-free imaging of live cells in 3D conditions is optically more challenging than in 2D. Quantitative phase imaging provided by coherence controlled holographic microscopy produces images with enhanced information compared to ordinary light microscopy and, due to inherent coherence gate effect, enables observation of live cancer cells' activity even in scattering milieu such as the 3D collagen matrix. Exploiting the dynamic phase differences method, we for the first time describe dynamics of differences in cell mass distribution in 3D migrating mesenchymal and amoeboid cancer cells, and also demonstrate that certain features are shared by both invasion modes. We found that amoeboid fibrosarcoma cells' membrane blebbing is enhanced upon constriction and is also occasionally present in mesenchymally invading cells around constricted nuclei. Further, we demonstrate that both leading protrusions and leading pseudopods of invading fibrosarcoma cells are defined by higher cell mass density. In addition, we directly document bundling of collagen fibres by protrusions of mesenchymal fibrosarcoma cells. Thus, such a non-invasive microscopy offers a novel insight into cellular events during 3D invasion.

Cancer cell invasion is the crucial step in the process of metastasis formation, which is responsible for 90% of deaths in patients with solid tumours<sup>1</sup>. It is the only hallmark, which distinguishes benign and malign tumours<sup>2</sup>. To invade through the surrounding extracellular environment, cancer cells can utilize collective or individual migration. Collective invasion occurs when cancer cells maintain cell-cell contacts and stay in proximity with leading cells that proteolytically degrade the surrounding matrix, making way for the cell cohort to move forward<sup>3</sup>. Alike for collective migration, individually invading cells utilizing the mesenchymal invasion mode are characterized by their dependence on pericellular proteolysis, which enables cells to form tunnels in the extracellular matrix (ECM) for movement<sup>4</sup>. They are typically elongated with many actin-rich protrusions and cell-ECM adhesions. Conversely, amoeboid invasion does not rely on cell-ECM adhesions or proteolytical degradation of the ECM, instead amoeboid cells generate force by enhanced actomyosin contractility<sup>5</sup> enabling them to squeeze through the pre-existing holes in the ECM. They are typically more rounded and exhibit membrane blebbing due to high hydrostatic pressure<sup>6,7</sup>.

Importantly, all modes of cancer cell invasiveness are interconvertible and could be employed by cancer cells in combination<sup>8–10</sup>. The ability of cancer cells to switch between modes of invasiveness is called plasticity and is an important issue related to the development of anti-invasive and anti-metastatic therapies<sup>11–14</sup>.

For the analysis of cancer cell malignant potential, manifested by invasiveness and plasticity, as well as for the analysis of the ability of various inhibitors to interfere with these processes, it is critical to observe the behaviour

<sup>1</sup>Department of Cell Biology, Charles University, Viničná 7, Prague, Czech Republic. <sup>2</sup>Biotechnology and Biomedicine Centre of the Academy of Sciences and Charles University (BIOCEV), Průmyslová 595, 252 42, Vestec u Prahy, Czech Republic. <sup>3</sup>Central European Institute of Technology, Brno University of Technology, Purkyňova 656/123, 612 00, Brno, Czech Republic. <sup>4</sup>Institute of Physical Engineering, Faculty of Mechanical Engineering, Brno University of Technology, Technická 2896/2, Brno, 616 00, Czech Republic. Ondřej Tolde and Aneta Gandalovičová contributed equally to this work. Correspondence and requests for materials should be addressed to J.B. (email: [jan.brabek@natur.cuni.cz](mailto:jan.brabek@natur.cuni.cz))

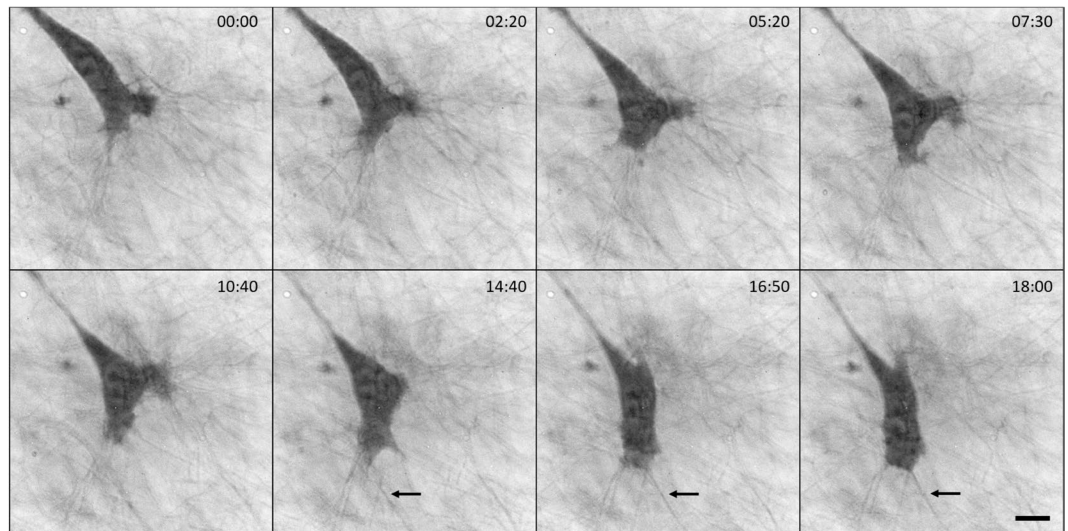


**Figure 1.** Migration of a mesenchymal cell within collagen matrix. Cells were embedded in 3D bovine collagen (1 mg/ml) and migration was observed by CCHM. Representative images with indicated times are shown. It can be noticed that the cell follows a thicker fibre (indicated by an arrow) once it gets to contact with it. The thickness of fibres was measured using ImageJ Plot Profile tool. The thick fibre has an average value  $0.66\ \mu\text{m}$ . The average value of the thinner fibres that are surrounding the cell in any direction or are in contact with the cell, is  $0.39\ \mu\text{m}$  (median  $0.37\ \mu\text{m}$ ;  $n = 30$ ). For full sequence see Suppl. Video V1. Scale bar:  $10\ \mu\text{m}$ .

of cancer cells in a 3D environment. The most frequently used biologically derived 3D matrices for *in vitro* analysis of cancer cell invasiveness are Matrigel and 3D collagen gels<sup>15</sup>. Beside these gel-based matrices, more complex life-like matrices derived from tissues are also used<sup>16–18</sup>.

However, there are general problems with lower optical transparency and light scattering in all these environments. These can be overcome by quantitative phase imaging (QPI) provided by coherence - controlled holographic microscopy (CCHM) due to inherent coherence gate effect (CGE), which makes possible imaging through a flowing turbid as well as static scattering medium. CGE is enabled by the spatially incoherent light<sup>19</sup> used in CCHM. CGE differentiates among ballistic and strongly scattered light to eliminate the strongly scattered photons from contributing to the final image as noise<sup>20–22</sup> (see Suppl. Fig. S1 and Supplementary text for details). Notably, the technique is non-invasive – no dyes or labels are used – and there is no halo artefact present, which typically disturbs imaging in Zernike phase contrast microscopy<sup>23</sup>. In addition, acquired images by CCHM are quantitative, making it possible to calculate cell dry mass in  $\text{pg}/\mu\text{m}^2$  from detected phase shifts<sup>24–26</sup>.

Here, we take advantage of CCHM to visualize in detail dynamics of cancer cell invasive behaviour, with focus on the interaction of cancer cells with collagen fibres, and utilize the quantitative information contained in the acquired images for analysis of cellular mass distribution and translocation.

## Results

**Establishment of a cell model for the study of amoeboid and mesenchymal migration.** To compare features of amoeboid and mesenchymal invasion, we took advantage of the possibility to induce the mesenchymal-amoeboid transition by activation of the RhoA-ROCK pathway<sup>27–29</sup>. We used HT1080 fibrosarcoma cells stably expressing doxycycline-inducible constitutively active RhoA (caRhoA). Upon expression of caRhoA, the primarily mesenchymal cells gain a rounded phenotype with numerous membrane blebs. Their migration in 3D collagen is unaffected in the presence of GM6001, a broad-spectrum matrix metalloproteinase inhibitor, unlike migration of control mesenchymal cells that is stalled in such conditions (Suppl. Fig. S2), which corresponds to earlier descriptions of amoeboid and mesenchymal migration, respectively<sup>4,30</sup>. Using this cell model, we employed CCHM microscopy to describe in detail features of amoeboid and mesenchymal invasion.

### Mesenchymal migrating cells interact with surrounding ECM: examples of ruffling, bundling, and blebbing.

Mesenchymal cell migration through tissue barriers requires pericellular remodelling of the ECM executed by cell-surface proteases, particularly membrane-type-1 matrix metalloproteinase (MT1-MMP). Invasive HT1080 fibrosarcoma cells were previously shown to coordinate mechanotransduction and fibrillar collagen remodelling by segregating the anterior force-generating leading edge containing  $\beta 1$ -integrin, MT1-MMP and F-actin from a posterior proteolytic zone executing fibre breakdown. During forward movement, sterically impeding fibres are selectively realigned<sup>31,32</sup>. To study the interaction of mesenchymal cells with collagen fibres, we employed CCHM for imaging of HT1080 cells embedded within a fibrillar collagen matrix. We observed that during migration a mesenchymal cell followed a thick collagen fibre and evidently pulled on it (see Fig. 1 and Supplementary Videos V1–V4). When the mesenchymal cells were imbedded in collagen of lower density (0.5 mg/ml), the pulling on collagen fibres was more prominent and had larger impact on the collagen architecture (Suppl. Video V3). In addition, we observed that cells' pseudopodia-like protrusions hold together several thinner fibres (Fig. 2, Suppl. Videos V4 and V5). We reckon this bundling of fibres is an active process serving to

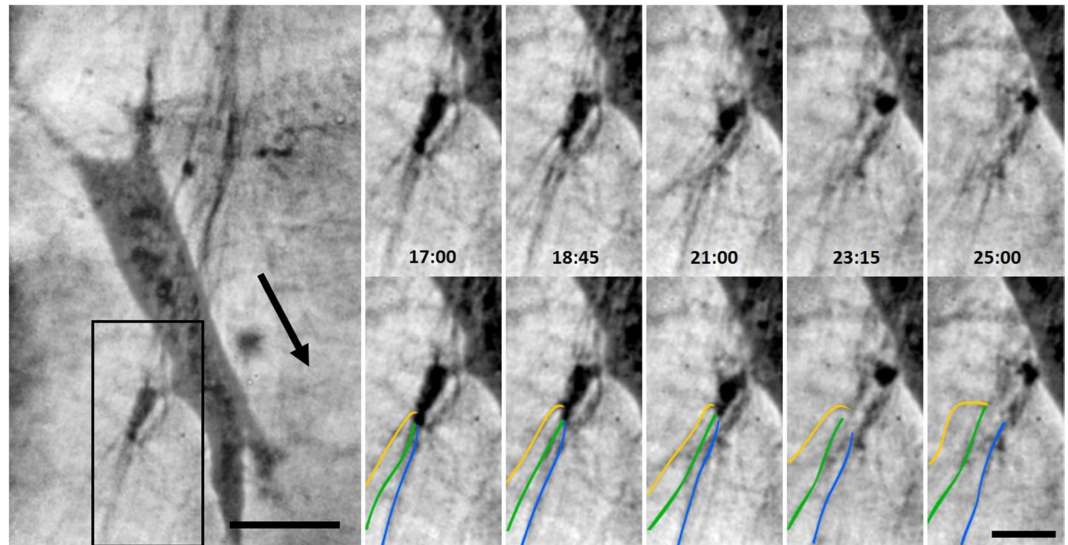


**Figure 2.** Bundling of collagen fibres by a mesenchymal cell. Cells were embedded within 3D bovine collagen (1 mg/ml) and images of migrating cells were acquired by CCHM. For better visualization of the fibre bundling, a situation when the cell retracts its pseudopodium, thus relaxing the fibres, is demonstrated. Left: Whole cell image, arrow indicates the direction of cell's movement. Scale bar:  $10\ \mu\text{m}$  Right: A sequence of representative images with indicated time intervals corresponding to the Suppl. Video V4. Upper and bottom row show the same images, in the bottom row the three separate fibres are marked by different colours. Several fibres are apparently clustered by the cell protrusion, and a prominent displacement of these fibres is well seen after the protrusion is retracted and the fibres return to their relaxed positions. Scale bar  $5\ \mu\text{m}$ . Contrast was adjusted to higher degree in the inset.

provide a more stable connection to the surrounding matrix, however further experiments would be needed for confirmation. CCHM also enabled observation of dynamic membrane ruffles at the cell front (Suppl. Fig. S3).

Furthermore, we occasionally observed dynamic membrane blebbing of cells utilizing the mesenchymal invasion mode. The blebbing was temporary and observed around nuclei of cells whose movement was restrained by the surrounding matrix (Fig. 3 and Suppl. Video V6), making an impression that this blebbing serves to push away surrounding matrix and enable nuclear translocation.

**Cell mass is polarized and defines leading protrusions in mesenchymal cells.** Next, we focused on cell mass distribution during mesenchymal migration. We computed mean mass densities of mesenchymal cells and their protrusions. The mean mass density within the cell body was significantly higher ( $0.85\ \text{pg}/\mu\text{m}^2$ ,  $p < 0.001$ ) than in the protrusions, reflecting mostly the high mass density of the nucleus and overall higher thickness of the cell body. Nevertheless, the leading protrusions have significantly higher ( $0.55\ \text{pg}/\mu\text{m}^2$ ,  $p < 0.04$ ) mean mass density compared to side protrusions and retracting protrusions ( $0.38\ \text{pg}/\mu\text{m}^2$  and  $0.32\ \text{pg}/\mu\text{m}^2$ , respectively) (Fig. 4). These results suggest that distribution of cell mass differs among individual protrusions to specify the leading protrusion, and in result defines the direction of invasion.

Moreover, postprocessing of images acquired by CCHM enables analysis of dynamic changes of cell mass distribution in migrating cells by calculating the dynamic phase differences (DPD) between consequent images (see Methods for more detail). The advantages of this method were demonstrated previously<sup>33</sup>. Analysis of cell mass differences during mesenchymal invasion highlighted the dynamics of membrane protrusions at the cell front and revealed a large influx of cell mass into the leading edge, clearly demonstrating the polarization of the cell, which corresponds to directionality of cell migration (Fig. 5).

**Various amoeboid cells phenotypes can be distinguished by cell mass distribution.** To study amoeboid cancer cell behaviour in 3D collagen, we induced expression of constitutively active RhoA in HT1080 cells, which resulted in the gain of the amoeboid phenotype. It is well known that various amoeboid phenotypes can be employed, depending on the level of actomyosin contractility and adhesion<sup>34,35</sup>. By visualizing 3D migration of HT1080 cells with caRhoA using CCHM, we noticed that blebbing intensity is not constant and can be transiently replaced by formation of pseudopodia, denoting that various amoeboid states are acquired. We further describe these amoeboid phenotypes in more detail.

We observed enhanced dynamic blebbing in amoeboid cells partly limited in movement, presumably due to ECM constriction. This phenotype resembles the blebby-amoeboid phenotype, during which numerous small membrane blebs form due to increased intracellular pressure. As observed by DPD, mass distribution inside the cell body during migration is less polarized compared to mesenchymal cells (Fig. 6 and Suppl. Video V7).

Blebbing intensity decreases when the cells switch to pseudopodal-amoeboid migration. Cells of this amoeboid phenotype are less rounded with several pseudopodia, resulting in a more motile state. Correspondingly, cell mass distribution is more polarized compared to blebby-amoeboid cells, with evident influx of cell mass into the

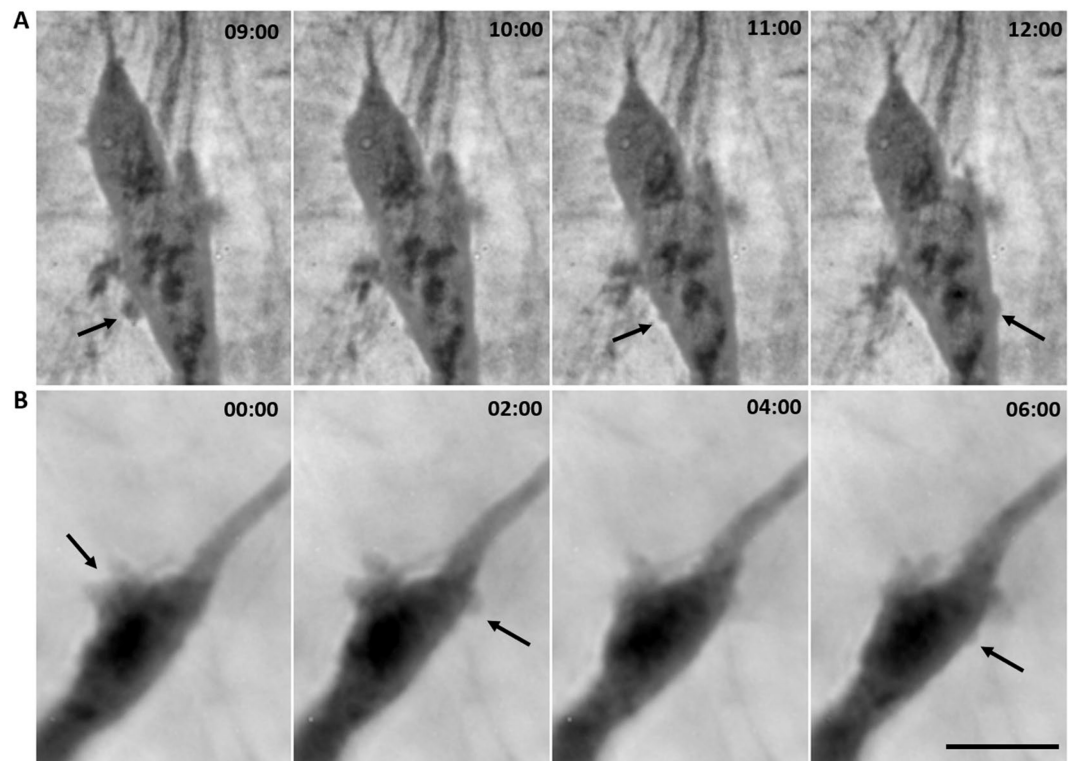


**Figure 3.** Perinuclear blebbing during mesenchymal invasion. Mesenchymal cells embedded in 3D bovine collagen (1 mg/ml) were imaged using CCHM. Arrows point towards membrane blebs formed around the nucleus. **(A)** Image sequence taken from Suppl. Video V6, which shows the dynamics of blebbing. For full sequence see Suppl. Video V4. **(B)** A second example of perinuclear blebbing during mesenchymal invasion. Scale bar: 10  $\mu\text{m}$ .

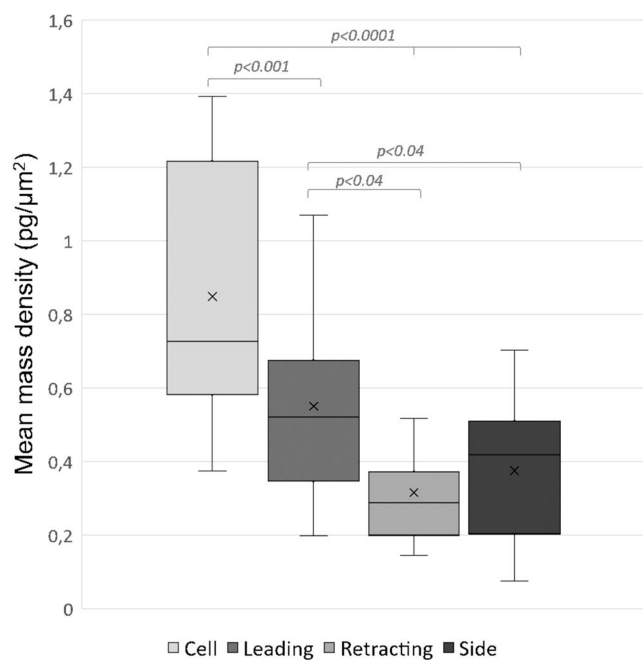


**Figure 4.** Analysis of mean mass density in protrusions of migrating mesenchymal cells. Images of mesenchymal cells embedded in 3D bovine collagen (1 mg/ml) were analysed to compute mean mass densities in whole cells and individual protrusions. Quantification results are expressed as box and whiskers (minimum to maximum) of 10 different cells. Cells were measured two to five times with time interval between measurements long enough for cells to substantially changed their morphology. Cell body (n = 22), leading (n = 20), retracting (n = 16), side (n = 50). Statistical significance was determined by one-way ANOVA followed by Tukey's post-hoc test.



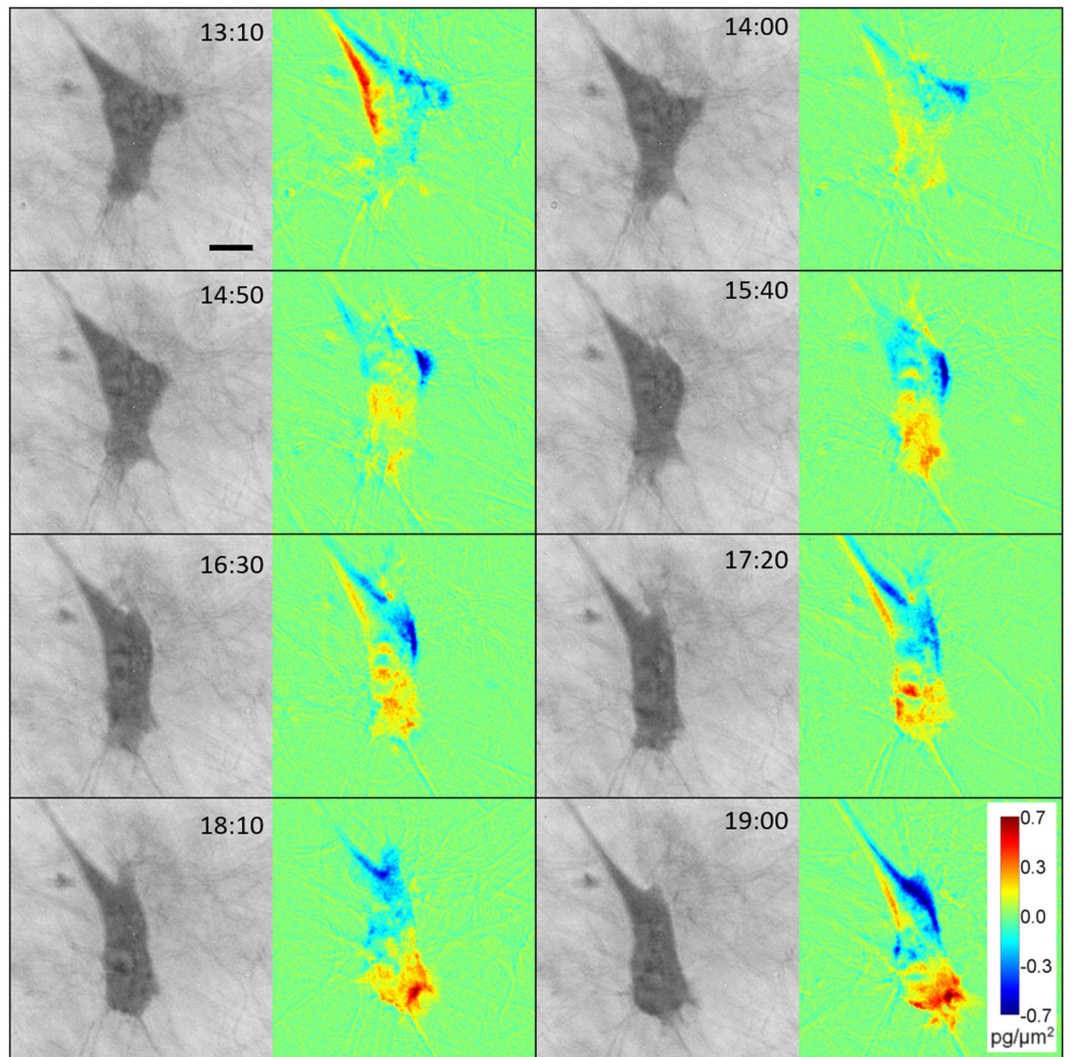


**Figure 5.** Analysis of cell mass during mesenchymal cell migration. Image sequence acquired by CCHM of a migrating mesenchymal cell. For full sequence see Suppl. Video V1. DPD show mass fluctuations between preceding and following images. The sequence demonstrates polarized cell mass distribution in a motile mesenchymal cell with a large influx of cell mass at cell front. Scale bar: 10  $\mu\text{m}$ .

leading front of the cell (Fig. 7). Moreover, as demonstrated for leading protrusions of mesenchymal cells, higher mean mass density also defines the leading pseudopodium during pseudopodal-amoeboid invasion. In fact, the mean mass density differentiates the leading pseudopodium from the lateral pseudopodium earlier than its size or weight individually (Suppl. Fig. S4). Furthermore, we directly observed that pseudopodal-amoeboid cells can promote transient contacts with surrounding fibres (Fig. 8).

To further characterize the two amoeboid phenotypes, we computed mean mass densities of individual cells, blebs and pseudopodia from acquired image sequences (Fig. 9). The mean mass density of blebby-amoeboid cells is significantly higher than of pseudopodal-amoeboid cells (1.45  $\text{pg}/\mu\text{m}^2$  and 1.18  $\text{pg}/\mu\text{m}^2$ , respectively;  $p < 0.001$ ). This corresponds to the more rounded cell body of blebby-amoeboid and more elongated body of pseudopodal-amoeboid cells. Interestingly, the mean mass density of amoeboid pseudopodia is 0.51  $\text{pg}/\mu\text{m}^2$ , which is very similar to pseudopodia of mesenchymal cells (0.55  $\text{pg}/\mu\text{m}^2$ ). The mean mass densities of blebs were not significantly different in case of blebby-amoeboid cells and pseudopodal-amoeboid cells (0.41  $\text{pg}/\mu\text{m}^2$  and 0.33  $\text{pg}/\mu\text{m}^2$ , respectively) and were 2.8x lower than mean mass densities in cell bodies in both cases. Overall, the variance of mean mass densities in blebs was much lower (coefficient of variation ( $C_v$ ) 30%) compared to variance of bleb area ( $C_v$ , 65%) or weight ( $C_v$ , 92%).

The plasticity of amoeboid cells is provided by high deformability of the cell body, which is limited by stiffness of the cell nucleus<sup>36,37</sup>. Therefore, we were interested in cell mass distribution within an amoeboid cell that undergoes large deformation of its body and nucleus while overcoming a constriction in the ECM (Suppl. Video V8). To pass through the narrow constriction, the cell initially formed a large membrane bleb protruding through the pore in the collagen matrix. The bleb later transformed into a stable pseudopodium, which increased in size until the remaining cell body was able to proceed. As demonstrated by DPD, the translocation of the nucleus is limiting for translocation of the whole cell, since the largest influx of cell mass occurs after the nucleus is able to pass (Fig. 10).

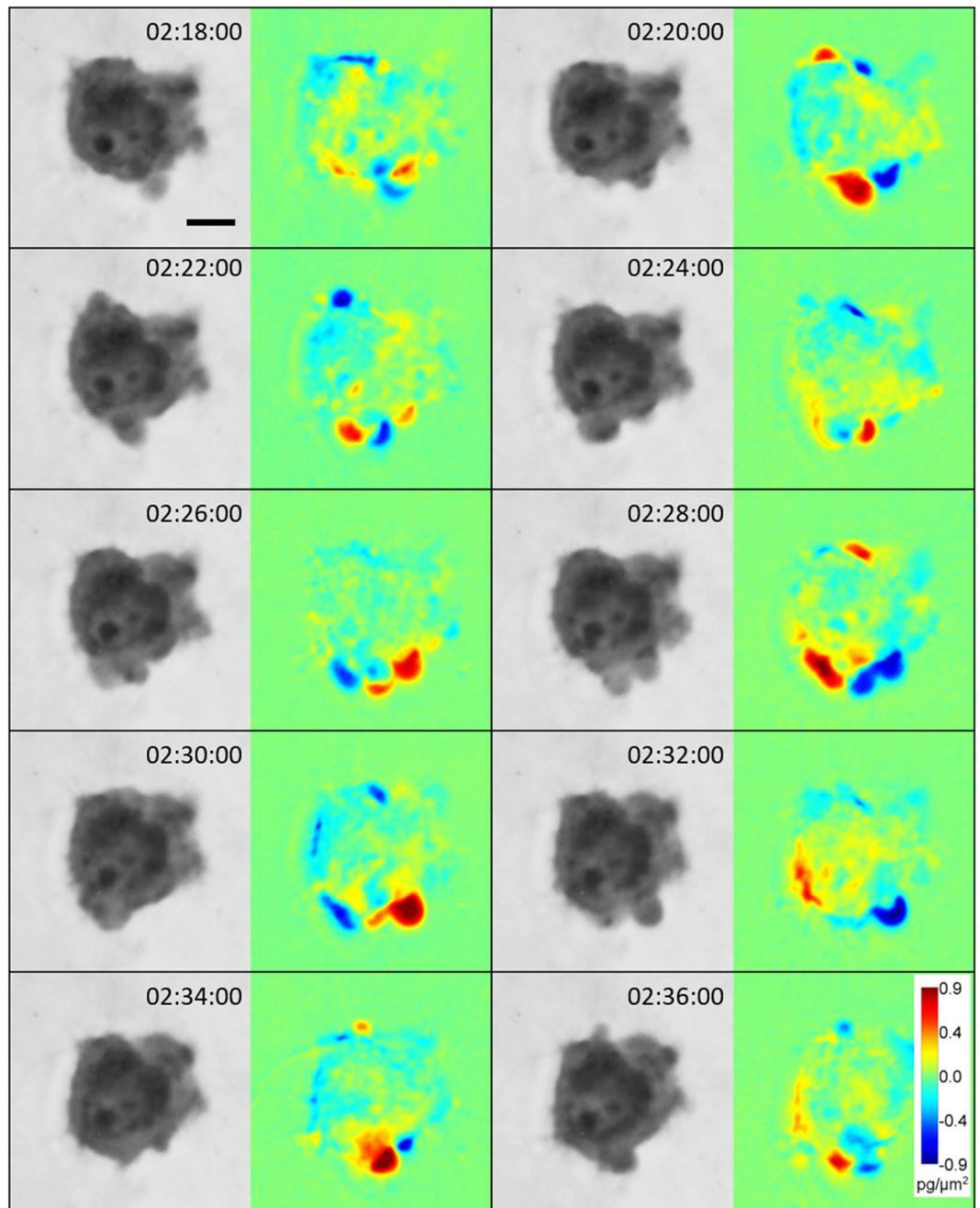


**Figure 6.** Dynamic cell blebbing observed in blebby-amoeboid cells. Image sequence acquired by CCHM of an amoeboid cell constricted in 3D rat-tail collagen (1 mg/ml), which led to enhanced blebbing. DPD show mass fluctuations between preceding and following images. It is clearly visible that the cell mass is unpolarized. For full sequence, see Suppl. Video V7. Scale bar: 10  $\mu\text{m}$ .

Taken together, our results demonstrate the ability of CCHM to not only visualize features of cell invasion in detail, but also directly analyse cell mass densities and distribution.

### Discussion and Conclusions

Noninvasive quantitative phase imaging through scattering media is an important task in biomedical research and draws the *in vitro* model applications nearer to real situations in living organisms. Detailed visualization of live cells in 3D collagen as reported here was enabled by coherence gate effect, which is characteristic of quantitative phase imaging in the spatially incoherent light. Taking advantage of the CCHM we investigated in detail the features of cancer cells utilizing either the amoeboid or mesenchymal invasion mode and analysed cell mass distribution changes within the migrating cancer cell.

First, we observed the dynamic interaction of cancer cells with surrounding fibres. We directly documented migration of a mesenchymal cell toward a thicker fibre in 3D collagen. The tendency of cells to follow thicker

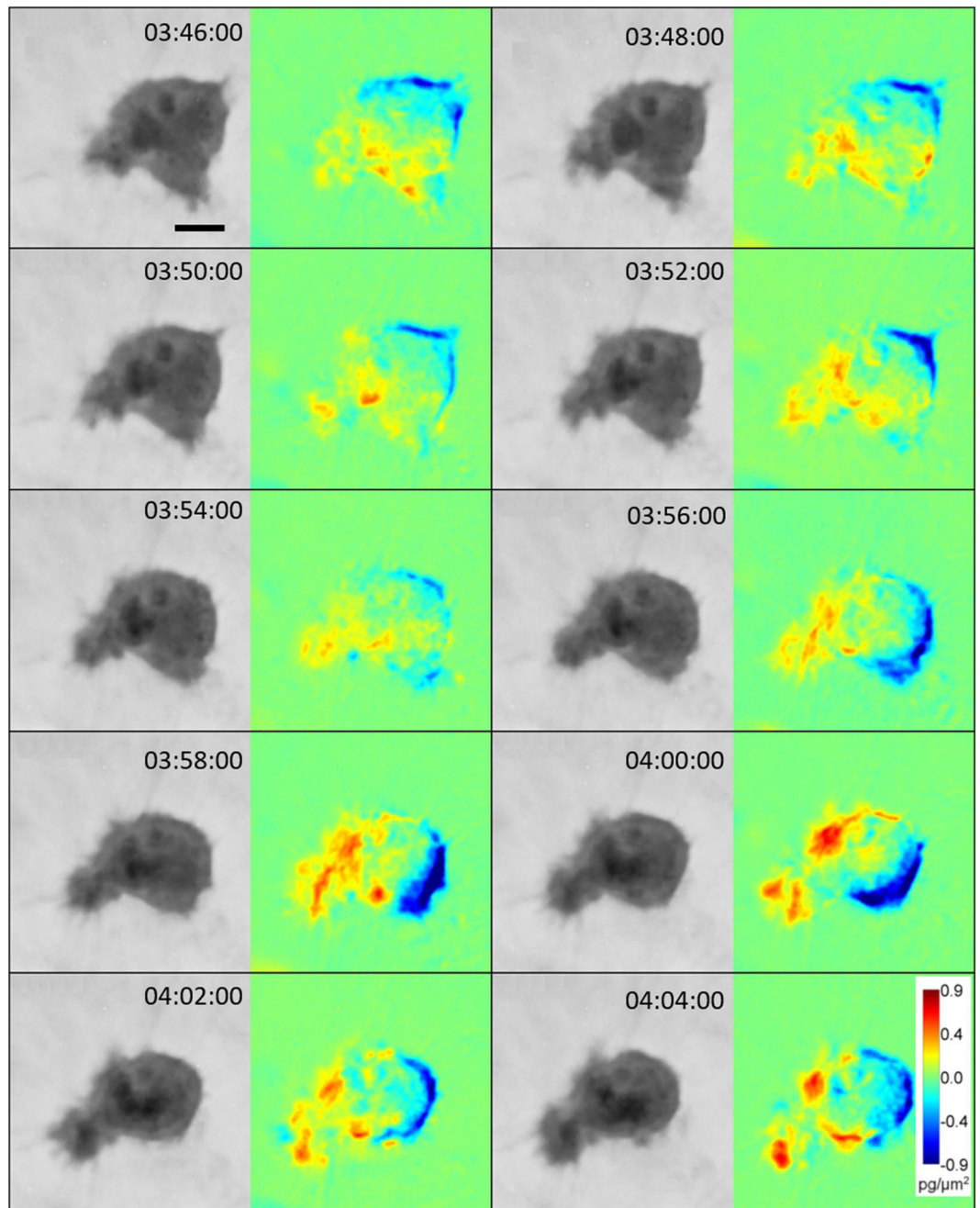


**Figure 7.** Analysis of cell mass during pseudopodal-amoeboid cell migration. Image sequence acquired by CCHM of a migrating amoeboid cell. For full sequence see Suppl. Video V7. DPD show mass fluctuations between preceding and following images. The sequence demonstrates polarized cell mass distribution in a pseudopodal-amoeboid cell, similar to cell mass polarization in mesenchymal cells (see Suppl. Fig. S3). Compare with unpolarized mass distribution during dynamic blebbing (Fig. 6). Scale bar: 10  $\mu\text{m}$ .

fibres was shown previously<sup>17,38,39</sup>, moreover it was speculated that thick collagen fibres serve as a migration high-ways for cancer cells within tissues<sup>40</sup>. An interesting observation visualized by CCHM was bundling of several collagen fibres together by pseudopodia-like protrusions of a mesenchymal cell (Fig. 2). We can speculate that the bundling serves to ensure a more stable connection to the surrounding matrix by providing focal/fibrillar adhesion sites or by alternative strategies, such as forming clathrin/adaptor protein 2 lattices<sup>41</sup>.

Further, we observed dynamic filopodia at the leading edge of mesenchymal cells (Suppl. Fig. S3). Filopodia can act alone or in combination with blebs, lobopodia or lamellipodia in 2D and 3D environments<sup>42</sup>. We assume that these dynamic filopodia are components of membrane ruffles - structures initially described in detail in 2D, but proven to form in 3D environments as well using other microscopy techniques<sup>42-44</sup>. Peripheral ruffles assemble at the leading edge of motile cells, where filopodia act to sense the local microenvironment<sup>45</sup>. It was shown that activated  $\beta 1$  integrins are localized to the tips of filopodia along the leading edge<sup>46</sup>, as well as other

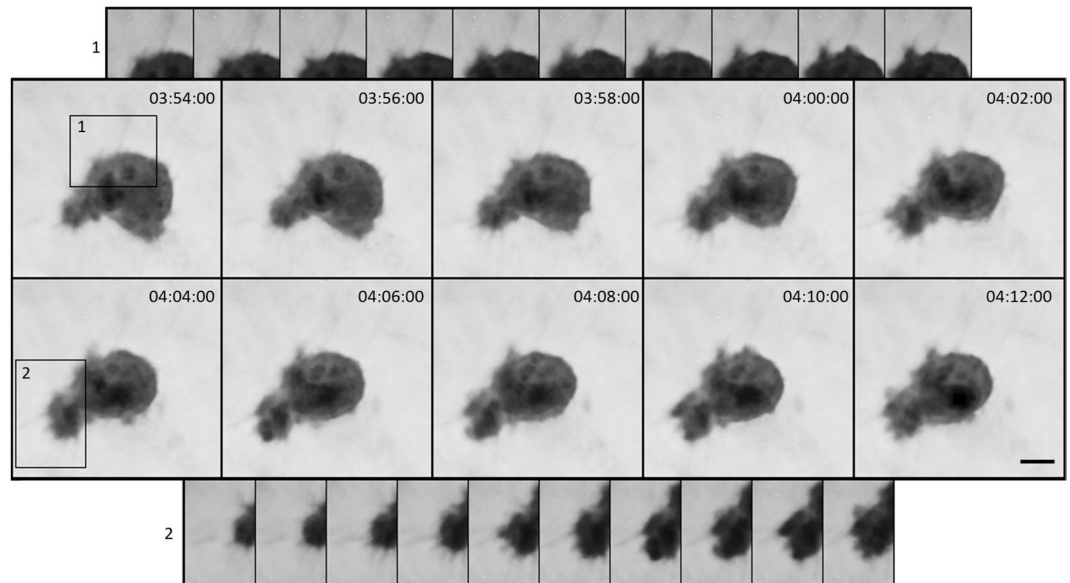


**Figure 8.** Interaction of an amoeboid cell with collagen fibres. Image sequence acquired by CCHM of a migrating amoeboid cell embedded in 3D rat-tail collagen (1 mg/ml). Transient contacts with surrounding fibres are visible in both inset 1 and 2. Notice that filopodia-like structures can form at the same site as blebs. Contrast was adjusted to higher degree in the insets. For full sequence, see Suppl. Video V7. Scale bar: 10  $\mu\text{m}$ .

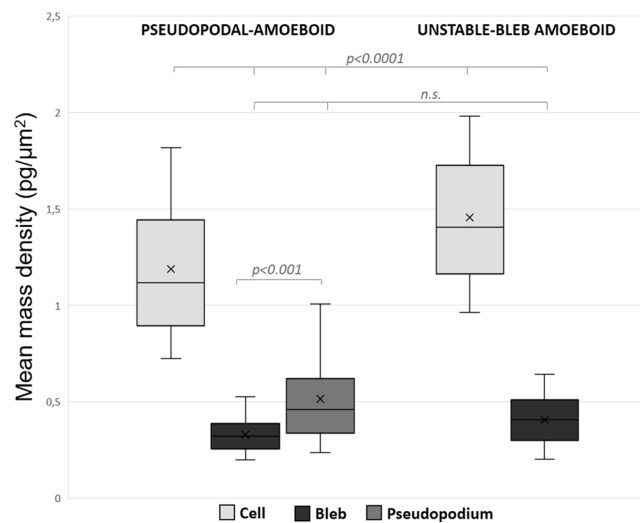


**Figure 9.** Amoeboid cell bleb measurements. Images of amoeboid cells embedded in 3D rat-tail collagen (1 mg/ml) acquired by CCHM were analysed to compute mean mass densities of cell bodies, pseudopodia and blebs in context of the observed amoeboid phenotypes. Overall, 10 cells and their pseudopodia and blebs were measured repeatedly with time interval between measurements long enough for cells to substantially changed their morphology. Cell body (n = 10), pseudopodium (n = 15), bleb (n = 88). Quantification results are expressed as box and whiskers (minimum to maximum). Statistical significance was determined by one-way ANOVA followed by Tukey's post-hoc test.

components of focal adhesions<sup>47</sup>. Actin-based movement of primed integrins along the leading edge suggests a “sticky fingers” mechanism to probe for new adhesion sites and direct migration<sup>46</sup>. Thus, we assume that formation of 3D ruffles, as visualized by CCHM, share a similar function as their 2D equivalents.

Notably, cell-ECM contact was observed also in case of amoeboid migration (Fig. 8), which is often considered to be independent of ECM adhesions<sup>48–50</sup>. Adhesions of amoeboid cells differ from those of mesenchymal cells - they are often depleted of integrins and instead formed by alternative adhesive molecules such as cell surface receptors<sup>49</sup>. Our observations of transient cell-ECM fibres contacts correspond with previous reports that show that amoeboid cells employ only short-lived contacts with collagen fibres that do not result in fibre cleavage<sup>4</sup> and enable rapidly adaptive migration<sup>51</sup>.

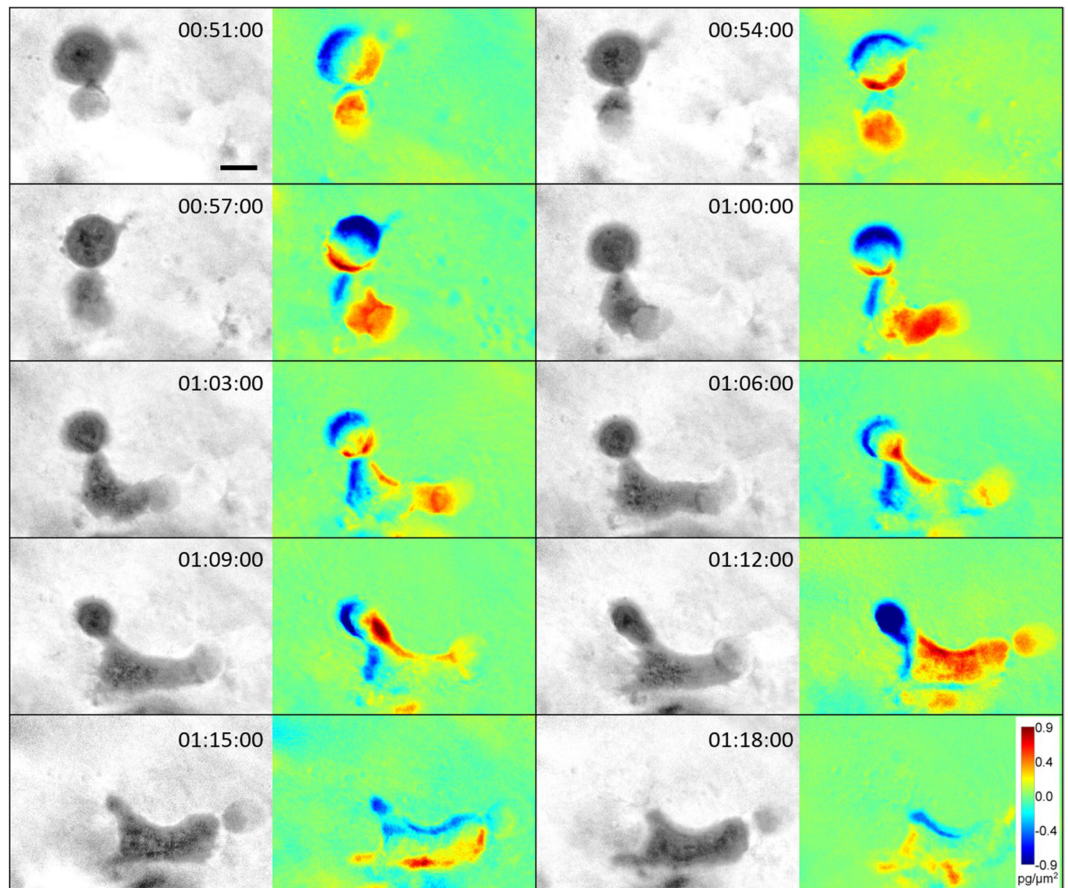


**Figure 10.** Analysis of cell mass of an amoeboid cell during translocation through a narrow pore. Image sequence acquired by CCHM of an amoeboid cell translocating through a narrow pore in 3D rat-tail collagen (1 mg/ml). To invade through the pore, the cell dynamically deforms its cell body and nucleus. DPD depict mass fluctuations between preceding and following images. As shown by DPD, the largest influx of cell mass occurs between time 01:12:00 and 01:15:00, corresponding to the time of nuclear translocation. For full sequence see Suppl. Video V8. Scale bar: 10  $\mu\text{m}$ .

Imaging typical features of mesenchymal and amoeboid cells unveiled that these elements can be shared among all individually invading cancer cells. As mentioned above, we observed cell-ECM contact, typical of mesenchymal cells, also in amoeboid cells. Moreover, we repeatedly observed dynamic membrane blebbing of amoeboid cells and, surprisingly also mesenchymal cells, at sites where ECM constrictions impede further movement (Figs 3, 6, Suppl. Video V6 and V7). We hypothesize that the purpose of this enhanced blebbing is to push away surrounding material to unravel a path wide enough for the stiffest part of the cell to translocate- its nucleus. Because this phenomenon was observed also in mesenchymal cells that produce ECM-degrading enzymes, we assume that under certain conditions, temporally enhanced blebbing is preferred over ECM proteolysis. This phenomenon was already observed in migrating macrophages<sup>52</sup>, but to what extent it facilitates cancer cell invasion remains to be clarified.

The quantitative character of CCHM images allows to measure mean cell mass densities. We show the method is applicable for measurements of cells inside a 3D environment and can be used to determine mean mass densities of individual cell regions. Other methods utilized for cell mass measurements, such as cantilever mass sensors or microfluidic channels, only perform whole cell measurements<sup>53-55</sup>.

For analysis of cell mass translocation during cancer cell invasion, we applied DPD method that reveals influx or decrease of mass from subsequent images. In migrating mesenchymal cells, cell mass increases towards the leading edge and overall maintains this polarized distribution during invasion (Fig. 5). We also show that mean mass densities are higher in leading protrusions than side or retracting protrusions, which can serve to define the direction of invasion (Fig. 4).

On the other hand, amoeboid cells display dynamic changes in cell mass distribution. During blebby-amoeboid invasion, the cell mass translocation is largely unpolarized inside the cell (Fig. 6 and Suppl. Video V7). The gain of a pseudopodal-amoeboid phenotype results in more polarized cell mass, with mean mass density increasing in the leading protrusion (Fig. 7, Suppl. Fig. S4 and Suppl. Video V7). This indicates that increased cell mass redistribution to the leading protrusion is a characteristic common for both mesenchymal and amoeboid cells.

Notably, mean mass density in blebs does not change considerably with increasing bleb size and maintains a value approximately 2.8x lower than the mean mass density of the whole cell in case of both blebby- and pseudopodal- amoeboid migration (Fig. 9). We also demonstrate, that cell mass is unequally distributed during invasion of a cell through a narrow pore until the nucleus itself is able to pass (Fig. 10).

These results confirm the potential of CCHM to reveal novel characteristics of cancer cell invasion and contribute to our understanding of invasive mechanisms. Nevertheless, QPI techniques have already yielded several findings of cellular behaviour<sup>56</sup>. For example, dynamic phase differences were employed for the visualization of changes in distribution of cell dry mass upon nutritional stress<sup>57</sup>, an approach, which was later elaborated as an evaluation method<sup>33</sup>. QPI also permits to differentiate between cell death caused by apoptosis and oncosis<sup>58</sup> or reveal necrosis<sup>59</sup>. Further, it enabled to observe entosis as a way of cancer cell survival under stress<sup>60</sup>. CCHM analysis of primary cells derived from head and neck squamous cell carcinoma biopsy proposed a dynamic phenotype of carcinoma cells to be a criterion for the recognition of cancer while still alive in primary culture<sup>61</sup>. Such recognition was achieved by exploitation of the possibility to simultaneously measure cell migration and growth by evaluating gain of cell dry mass. A different study demonstrates that digital holographic microscopy can distinguish the metastatic potential of melanoma cells<sup>62</sup>.

Recently, a new category of agents focused on cancer metastasis prevention was proposed and named migrastatics<sup>14</sup>. The search for migrastatics will require to test the effect of candidate agents on the behaviour of cells in 3D environments. According to results obtained from both 2D cultures<sup>61</sup> and here in 3D, we propose CCHM as a suitable approach for the early stages of potential migrastatic drugs assessment, mainly due to its ability to clearly visualize cell invasion without any need of labelling.

However, high-throughput analysis of cell invasive behaviour requires the establishment of an automated evaluation method<sup>63</sup>. Automatic classification of cells based on QPI has already shown to be possible in 2D environments<sup>64</sup>. The quest is now to enable similar evaluation in 3D. With the incorporation of DPD method and development of proper machine learning algorithms, it is considered feasible. Our results suggest that mesenchymal cells maintain polarized cell mass during migration, whereas amoeboid cells switch among the less-polarized (blebby-amoeboid) and more-polarized (pseudopodal-amoeboid) states. Moreover, amoeboid cells form numerous membrane blebs in both states, while mesenchymal cells form blebs only temporally. Thus, an algorithm able to include both QPI and DPD parameters could differentiate among the various invasion modes given images with sufficient time resolution are provided. In addition, DPD enables to easily determine the direction of cell movement by analysis of mass polarization and can monitor the migratory process, represented by cycles of high and low mass changes during rear retraction (Suppl. Fig. S5).

Altogether, we took advantage of the coherence gate effect produced by coherence - controlled holographic microscopy to study invasive behaviour of cancer cells in 3D collagen. Observations presented here using CCHM demonstrate that cancer cells can temporally and dynamically utilize characteristics of both the amoeboid and mesenchymal phenotype and adjust their modes of invasion according to current conditions. It is evident that CCHM is a valuable tool for studying the plasticity of cancer cell invasion.

## Methods

**Cells, culture and material.** Human fibrosarcoma cells HT1080 and HT1080 with constitutively active RhoA (RhoA G14V) stable cell line were routinely cultured in standard conditions (37°C, humidified atmosphere with 5% CO<sub>2</sub>) in full DMEM medium (Life Technologies) with 4.5 g/l L-glucose, L-glutamine, and pyruvate, supplemented with 10% fetal bovine serum (Sigma Aldrich) and 0.1% ciprofloxacin (Sigma Aldrich). The HT1080 RhoA G14V stable cell line was prepared and provided by Vladimír Čermák, PhD.

**Microscopy.** Quantitative phase imaging (QPI) was performed using Q-PHASE (TESCAN Brno, s.r.o.) a multimodal holographic microscope based on CCHM technology. A halogen lamp and interference filter with a central wavelength 650 nm and 10 nm FWHM were employed as a light source. For observations Nikon Plan 10×/0.3, Nikon Plan Fluor 20×/0.5 and Nikon Plan Apo 40×/0.95 objectives were used. The hologram was taken by a single shot with a CCD camera (XIMEA MR4021MC). Quantitative phase image was computed in real time by implemented Q-PHASE control software. For more information see Supplementary text.

**3D collagen matrix.** Cells were trypsinized, centrifuged and resuspended at concentration  $1 \times 10^6$  cells/ml in phenol red free DMEM supplemented with 10% FBS. Buffered solution (composed of 1x DMEM, 0.375% NaHCO<sub>3</sub>, 8.5 mM NaOH, 15 mM Hepes, 0.1% ciprofloxacin and 1 mM folic acid final concentration) was mixed with ddH<sub>2</sub>O and collagen (Cultrex; rat tail or Biochrom; bovine; both 4 mg/ml) depending on final collagen concentration. Cell suspension was added in ratio 1:10. For the analysis of mesenchymal invasion we used 1 mg/ml bovine collagen solution (unless stated otherwise), which led to clearly visible thicker fibres. Rat-tail collagen 1 mg/ml was employed for the analysis of amoeboid invasion.

The mixture was placed either in a  $\mu$ -Slide Angiogenesis well (Ibidi) or a custom-made chamber created from Mattek dishes. Gel solidification was performed at 37°C for at least 1 hour, after which the Ibidi  $\mu$ -Slide or custom-made chamber was filled entirely with medium (phenol red free DMEM supplemented with 10% FBS, 10 mM BES buffer, and 7.5 mM Hepes buffer) and covered with a cover slip (22 × 40 mm), or chamber lid, respectively, to avoid the formation of a meniscus that would disrupt the interference and quality of the phase image. Prior to observation, the chambers were transferred to the Q-PHASE microscope placed in a box tempered to 37°C.

**Image processing.** Images and live cell videos were obtained using Q-PHASE control software (TESCAN Brno, s.r.o.). These quantitative phase images contain information about cell dry mass density in each pixel. The total mass of the cell is given as a sum of pixel values in the area of the cell, the mean cell mass density is calculated

as a sum of individual pixel values in the cell divided by the area of the cell. For the analysis of mean mass density values of different regions, acquired images were analysed in ImageJ. Each region of interest (cell, bleb, protrusion) was marked manually and measured. Mean values in  $\text{pg}/\mu\text{m}^2$  were plotted into graphs.

For step by step analysis of cell mass changes, the difference in mass distribution between two images was calculated by dynamic phase differences (DPD)<sup>33</sup>. Briefly, DPD visualizes the difference between selected subsequent images, which is calculated by subtracting the previous from the following image. The resulting plus difference indicates proportionally the mass gain in red colour, while the minus difference depicts mass loss in blue colour. Small differences are indicated as noise around zero value, which is illustrated in light green colour. Because the changes of cell mass are distinctly higher than those of the surrounding collagen, they appear in red or blue colours, whereas the collagen milieu is represented in light green colour.

For presentation purposes only, the contrast of quantitative phase images was enhanced by non-linear filtration in ACC (Adaptive Contrast Control © software by SOFO).

Post processing for visualisation of membrane ruffles was performed by ImageJ. Pseudo-coloured images were prepared using a macro. In brief, pixels with grey value above a manually set threshold were copied to a new channel and coloured using LUT. Subsequently, a threshold was used for marking the pixels on the cell's periphery and obtained masks were saved as binary images. The assembly and colouring of layers were performed in Photoshop.

**Statistical analysis.** Statistical analysis of significance was done in Prism 6 software (GraphPad Software, Inc.). For analysis of mean mass densities one-way ANOVA followed by Tukey's post-hoc test was used. Coefficients of variation were calculated standardly as ratio of standard deviation to mean value and are expressed as percentage.

## References

- Sleeman, J. & Steeg, P. S. Cancer metastasis as a therapeutic target. *Eur. J. Cancer* **46**, 1177–1180 (2010).
- Lazebnik, Y. What are the hallmarks of cancer? *Nat. Rev. Cancer* **10**, 232–233 (2010).
- Friedl, P., Locker, J., Sahai, E. & Segall, J. E. Classifying collective cancer cell invasion. *Nat. Cell Biol.* **14**, 777–783 (2012).
- Wolf, K. *et al.* Compensation mechanism in tumor cell migration: mesenchymal-amoeboid transition after blocking of pericellular proteolysis. *J. Cell Biol.* **160**, 267–277 (2003).
- Rösel, D. *et al.* Up-regulation of Rho/ROCK signaling in sarcoma cells drives invasion and increased generation of protrusive forces. *Mol. Cancer Res.* **6**, 1410–20 (2008).
- Lämmermann, T. & Sixt, M. Mechanical modes of 'amoeboid' cell migration. *Curr. Opin. Cell Biol.* **21**, 636–44 (2009).
- Charras, G. T., Coughlin, M., Mitchison, T. J. & Mahadevan, L. Life and times of a cellular bleb. *Biophys. J.* **94**, 1836–53 (2008).
- Panková, K., Rösel, D., Novotný, M. & Brábek, J. The molecular mechanisms of transition between mesenchymal and amoeboid invasiveness in tumor cells. *Cell. Mol. Life Sci.* **67**, 63–71 (2010).
- Friedl, P. & Wolf, K. Tumour-cell invasion and migration: diversity and escape mechanisms. *Nat. Rev. Cancer* **3**, 362–74 (2003).
- Clark, A. G. & Vignjevic, D. M. Modes of cancer cell invasion and the role of the microenvironment. *Curr. Opin. Cell Biol.* **36**, 13–22 (2015).
- Friedl, P. Preshaping and plasticity: shifting mechanisms of cell migration. *Curr. Opin. Cell Biol.* **16**, 14–23 (2004).
- Micuda, S., Rosel, D., Ryska, A. & Brabek, J. ROCK inhibitors as emerging therapeutic candidates for sarcomas. *Curr. Cancer Drug Targets* **10**, 127–134 (2010).
- Rosel, D., Brabek, J., Vesely, P. & Fernandes, M. Drugs for solid cancer: the productivity crisis prompts a rethink. *Onco. Targets. Ther.* **6**, 767–777 (2013).
- Gandalovičová, A. *et al.* Migrastatics—Anti-metastatic and Anti-invasion Drugs: Promises and Challenges. *Trends in Cancer* **3**, 391–406 (2017).
- Edmondson, R., Broglie, J. J., Adcock, A. F. & Yang, L. Three-Dimensional Cell Culture Systems and Their Applications in Drug Discovery and Cell-Based Biosensors. *Assay Drug Dev. Technol.* **12**, 207–218 (2014).
- Tolde, O., Rösel, D., Vesely, P., Folk, P. & Brábek, J. The structure of invadopodia in a complex 3D environment. *Eur. J. Cell Biol.* **89**, 674–80 (2010).
- Tolde, O., Rosel, D., Janostiak, R., Vesely, P. & Brabek, J. Dynamics and morphology of focal adhesions in complex 3D environment. *Folia Biol. (Praha)*. **58**, 177–184 (2012).
- Cukierman, E., Pankov, R., Stevens, D. R. & Yamada, K. M. Taking cell-matrix adhesions to the third dimension. *Science* **294**, 1708–1712 (2001).
- Leith, E. N. *et al.* Imaging through scattering media using spatial incoherence techniques. *Opt. Lett.* **16**, 1820–1822 (1991).
- Lostak, M., Chmelik, R., Slaba, M. & Slaby, T. Coherence-controlled holographic microscopy in diffuse media. *Opt. Express* **22**, 4180–4195 (2014).
- Kollarova, V., Collakova, J., Dostal, Z., Vesely, P. & Chmelik, R. Quantitative phase imaging through scattering media by means of coherence-controlled holographic microscope. *J. Biomed. Opt.* **20**, 111206 (2015).
- Chmelik, R. *et al.* The Role of Coherence in Image Formation in Holographic Microscopy. *Prog. Opt.* **59**, 267–335 (2014).
- Pastorek, L., Venit, T. & Hozak, P. Holography microscopy as an artifact-free alternative to phase-contrast. *Histochem. Cell Biol.* **149**, 179–186 (2018).
- Davies, H. G. & Wilkins, M. H. F. Interference Microscopy and Mass Determination. *Nature* **169**, 541 (1952).
- Barer, R. Interference microscopy and mass determination. *Nature* **169**, 366–367 (1952).
- Zangle, T. A. & Teitell, M. A. Live-cell mass profiling: an emerging approach in quantitative biophysics. *Nat. Methods* **11**, 1221–1228 (2014).
- Taddei, M. L. *et al.* Mesenchymal to amoeboid transition is associated with stem-like features of melanoma cells. *Cell Commun. Signal.* **12**, 24 (2014).
- MacKay, J. L. & Kumar, S. Simultaneous and independent tuning of RhoA and Rac1 activity with orthogonally inducible promoters. *Integr. Biol. (Camb)*. **6**, 885–894 (2014).
- Rodriguez-Hernandez, I., Cantelli, G., Bruce, F. & Sanz-Moreno, V. Rho, ROCK and actomyosin contractility in metastasis as drug targets. *F1000Research* **5**, F1000 Faculty Rev-783 (2016).
- Wyckoff, J. B., Pinner, S. E., Gschmeissner, S., Condeelis, J. S. & Sahai, E. ROCK- and myosin-dependent matrix deformation enables protease-independent tumor-cell invasion *in vivo*. *Curr. Biol.* **16**, 1515–23 (2006).
- Wolf, K. *et al.* Multi-step pericellular proteolysis controls the transition from individual to collective cancer cell invasion. *Nat. Cell Biol.* **9**, 893–904 (2007).
- van Helvert, S. & Friedl, P. Strain Stiffening of Fibrillar Collagen during Individual and Collective Cell Migration Identified by AFM Nanoindentation. *ACS Appl. Mater. Interfaces* **8**, 21946–21955 (2016).

33. Krizova, A. *et al.* Dynamic phase differences based on quantitative phase imaging for the objective evaluation of cell behavior. *J. Biomed. Opt.* **20**, 111214 (2015).
34. Petrie, R. J. & Yamada, K. M. Multiple mechanisms of 3D migration: the origins of plasticity. *Curr. Opin. Cell Biol.* **42**, 7–12 (2016).
35. Friedl, P. & Wolf, K. Plasticity of cell migration: a multiscale tuning model. *J. Cell Biol.* **188**, 11–9 (2010).
36. Wolf, K. *et al.* Physical limits of cell migration: Control by ECM space and nuclear deformation and tuning by proteolysis and traction force. *J. Cell Biol.* **201**, 1069–1084 (2013).
37. McGregor, A. L., Hsia, C.-R. & Lammerding, J. Squish and squeeze—the nucleus as a physical barrier during migration in confined environments. *Curr. Opin. Cell Biol.* **40**, 32–40 (2016).
38. Wang, W. *et al.* Single cell behavior in metastatic primary mammary tumors correlated with gene expression patterns revealed by molecular profiling. *Cancer Res.* **62**, 6278–6288 (2002).
39. Condeelis, J. & Segall, J. E. Intravital imaging of cell movement in tumours. *Nat. Rev. Cancer* **3**, 921–930 (2003).
40. Egeblad, M., Rasch, M. G. & Weaver, V. M. Dynamic interplay between the collagen scaffold and tumor evolution. *Curr. Opin. Cell Biol.* **22**, 697–706 (2010).
41. Elkhatab, N. *et al.* Tubular clathrin/AP-2 lattices pinch collagen fibers to support 3D cell migration. *Science* **356** (2017).
42. Petrie, R. J. & Yamada, K. M. At the leading edge of three-dimensional cell migration. *J. Cell Sci.* **125**, 5917–5926 (2012).
43. Paul, N. R. *et al.* alpha5beta1 integrin recycling promotes Arp2/3-independent cancer cell invasion via the formin FHOD3. *J. Cell Biol.* **210**, 1013–1031 (2015).
44. Doyle, A. D., Carvajal, N., Jin, A., Matsumoto, K. & Yamada, K. M. Local 3D matrix microenvironment regulates cell migration through spatiotemporal dynamics of contractility-dependent adhesions. *Nat. Commun.* **6**, 8720 (2015).
45. Chhabra, E. S. & Higgs, H. N. The many faces of actin: matching assembly factors with cellular structures. *Nat. Cell Biol.* **9**, 1110–1121 (2007).
46. Galbraith, C. G., Yamada, K. M. & Galbraith, J. A. Polymerizing actin fibers position integrins primed to probe for adhesion sites. *Science* **315**, 992–995 (2007).
47. Schafer, C. *et al.* One step ahead: role of filopodia in adhesion formation during cell migration of keratinocytes. *Exp. Cell Res.* **315**, 1212–1224 (2009).
48. Lämmermann, T. *et al.* Rapid leukocyte migration by integrin-independent flowing and squeezing. *Nature* **453**, 51–5 (2008).
49. Schmidt, S. & Friedl, P. Interstitial cell migration: integrin-dependent and alternative adhesion mechanisms. *Cell Tissue Res.* **339**, 83–92 (2010).
50. Paňková, D. *et al.* NG2-mediated Rho activation promotes amoeboid invasiveness of cancer cells. *Eur. J. Cell Biol.* **91**, 969–977 (2012).
51. Friedl, P., Borgmann, S. & Brocker, E. B. Amoeboid leukocyte crawling through extracellular matrix: lessons from the Dictyostelium paradigm of cell movement. *J. Leukoc. Biol.* **70**, 491–509 (2001).
52. Ma, M. & Baumgartner, M. Filopodia and membrane blebs drive efficient matrix invasion of macrophages transformed by the intracellular parasite *Theileria annulata*. *Plos One* **8**, e75577 (2013).
53. Park, K. *et al.* Measurement of adherent cell mass and growth. *Proc. Natl. Acad. Sci. USA* **107**, 20691–20696 (2010).
54. Cermak, N. *et al.* High-throughput measurement of single-cell growth rates using serial microfluidic mass sensor arrays. *Nat. Biotechnol.* **34**, 1052–1059 (2016).
55. Martinez-Martin, D. *et al.* Inertial picobalance reveals fast mass fluctuations in mammalian cells. *Nature* **550**, 500–505 (2017).
56. Lee, K. *et al.* Quantitative Phase Imaging Techniques for the Study of Cell Pathophysiology: From Principles to Applications. *Sensors (Basel)*. **13**, 4170–4191 (2013).
57. Janeckova, H., Vesely, P. & Chmelik, R. Proving tumour cells by acute nutritional/energy deprivation as a survival threat: a task for microscopy. *Anticancer Res.* **29**, 2339–2345 (2009).
58. Balvan, J. *et al.* Multimodal holographic microscopy: distinction between apoptosis and oncosis. *Plos One* **10**, e0121674 (2015).
59. Collakova, J. *et al.* Coherence-controlled holographic microscopy enabled recognition of necrosis as the mechanism of cancer cells death after exposure to cytopathic turbid emulsion. *J. Biomed. Opt.* **20**, 111213 (2015).
60. Balvan, J. *et al.* Oxidative Stress Resistance in Metastatic Prostate Cancer: Renewal by Self-Eating. *Plos One* **10**, e0145016 (2015).
61. Gal, B. *et al.* Distinctive behaviour of live biopsy-derived carcinoma cells unveiled using coherence-controlled holographic microscopy. *Plos One* **12**, e0183399 (2017).
62. Calin, V. L. *et al.* Evaluation of the metastatic potential of malignant cells by image processing of digital holographic microscopy data. *FEBS Open Bio* **7**, 1527–1538 (2017).
63. Driscoll, M. K. & Danuser, G. Quantifying modes of 3D cell migration. *Trends Cell Biol.* **25**, 749–759 (2015).
64. Strbkova, L., Zicha, D., Vesely, P. & Chmelik, R. Automated classification of cell morphology by coherence-controlled holographic microscopy. *J. Biomed. Opt.* **22**, 1–9 (2017).

## Acknowledgements

This work was funded by Czech Science Foundation grants 18-15684J and 18-01396S, by the Ministry of Education, Youth and Sports of CR within the LQ1604 National Sustainability Program II (Project BIOCEV-FAR) and LQ1601 (Project CEITEC 2020), by the project “BIOCEV” (CZ.1.05/1.1.00/02.0109). We acknowledge the support by the MEYS CR (CZ.02.1.01/0.0/0.0/16\_013/0001775 Czech-BioImaging) and the support by Imaging Methods Core Facility at BIOCEV, institution supported by the Czech-BioImaging large RI project (LM2015062 funded by MEYS CR) for their support with obtaining imaging data presented in this paper. We acknowledge Mr. Jaroslav Klíma, CEO TESCANA ORSAY HOLDING, a.s. for bestowing Q-PHASE for our testing.

## Author Contributions

O.T. and A.G. equally contributed to data acquisition and analysis and wrote the main text. A.K. performed D.P.D. analysis and prepared the figures. R.C., J.B., D.R. and P.V. conceived the experiments and contributed to data analysis. All authors contributed to and reviewed the manuscript.

## Additional Information

**Supplementary information** accompanies this paper at <https://doi.org/10.1038/s41598-018-30408-7>.

**Competing Interests:** A.K. is an employee of TESCANA Brno, s.r.o., R.C. is a co-author of patents related to Q-Phase, but both declare this has not affected their work. All other authors declare no conflict of interest.

**Publisher's note:** Springer Nature remains neutral with regard to jurisdictional claims in published maps and institutional affiliations.





**Open Access** This article is licensed under a Creative Commons Attribution 4.0 International License, which permits use, sharing, adaptation, distribution and reproduction in any medium or format, as long as you give appropriate credit to the original author(s) and the source, provide a link to the Creative Commons license, and indicate if changes were made. The images or other third party material in this article are included in the article's Creative Commons license, unless indicated otherwise in a credit line to the material. If material is not included in the article's Creative Commons license and your intended use is not permitted by statutory regulation or exceeds the permitted use, you will need to obtain permission directly from the copyright holder. To view a copy of this license, visit <http://creativecommons.org/licenses/by/4.0/>.

© The Author(s) 2018

## SUPPLEMENTARY INFORMATION

# Quantitative phase imaging unravels new insight into dynamics of mesenchymal and amoeboid cancer cell invasion

Ondřej Tolde <sup>1,2#</sup>, Aneta Gandalovičová <sup>1,2#</sup>, Aneta Křížová <sup>3,4</sup>, Pavel Veselý <sup>3</sup>, Radim Chmelík <sup>3,4</sup>, Daniel Rosel <sup>1,2</sup> and Jan Brábek <sup>1,2</sup>

<sup>1</sup>Department of Cell Biology, Charles University, Viničná 7, Prague, Czech Republic

<sup>2</sup>Biotechnology and Biomedicine Centre of the Academy of Sciences and Charles University (BIOCEV), Průmyslová 595, 252 42, Vestec u Prahy, Czech Republic

<sup>3</sup>Central European Institute of Technology, Brno University of Technology, Purkyňova 656/123, 612 00, Brno, Czech Republic

<sup>4</sup>Institute of Physical Engineering, Faculty of Mechanical Engineering, Brno University of Technology, Technická 2896/2, Brno 616 00, Czech Republic

# These authors contributed equally to the work.

\*Correspondence: jan.brabek@natur.cuni.cz (Jan Brábek)

### Supplementary text:

#### CCHM setup

In layman's terms, coherence gate effect permits only the use of image information carrying photons, which are the ballistic (un-scattered) or snake-like (slightly scattered) photons for image formation by interference. Each of them originates from single emitting atom making the single illuminating ray until it is split (BS in Fig. S1) into the reference and object rays, the coherent twins (yellow and blue rays respectively, in Fig. S1). Thus, they can contribute to building the final image only by interfering with the twin partner provided they meet at detector level (D in Fig. S1) within the coherence volume. The coherence volume is very small in partially coherent systems compared to its large size in coherent (laser driven) systems in which every ray can interfere with any other ray. Strongly scattered rays (red rays in Fig. S1) cannot contribute to image formation as they miss the coherence volume and so their twin reference partners for interference get lost. In result, no disturbance of the final image by noise generated by strongly scattered rays, as it happens in coherent systems, occurs.

Supplementary Figures with legends

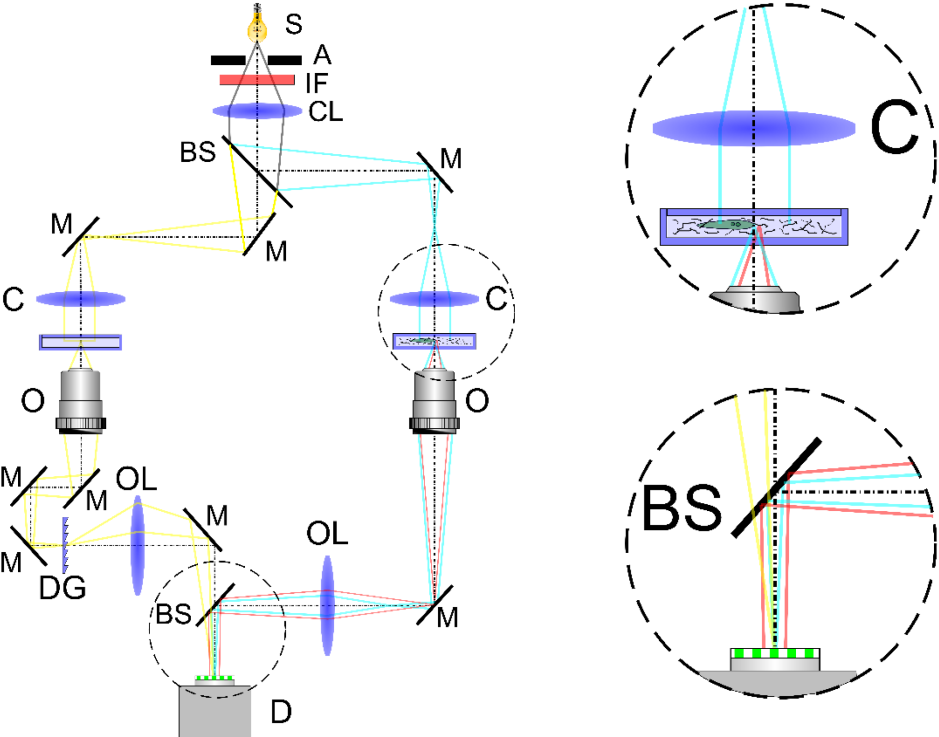


**Figure S1. Detailed description of coherence-controlled holographic microscope quantitative phase imaging with coherence gate effect.**

The light from source S passes through an aperture A and interference filter IF. The beam splitter BS divides it into two separated optical paths - the object arm (blue) and the reference arm (yellow) of the interferometer. Both arms consist of condenser C, objective O and output lens OL. The sample with scattering medium is placed in the object arm, only the reference object without scattering medium is in the reference arm. The diffraction grating DG is located in the reference arm. The reference beam and the object beam that include only ballistic (un-scattered) light recombine in the output plane and create an interference fringes pattern. The primary beam, reference beam and corresponding object beam are depicted in black, yellow and blue colour, respectively. Green interference fringes are produced by combination of yellow reference beam with blue ballistic object beam. Strongly scattered light (red colour in the figure) does not contribute to the interference because it has no corresponding (mutually coherent) reference beam to interfere with (see detail at the bottom right). Camera D captures the interference fringes pattern as holograms. The upper detail shows the formation of strongly scattered light at an ECM fibre.

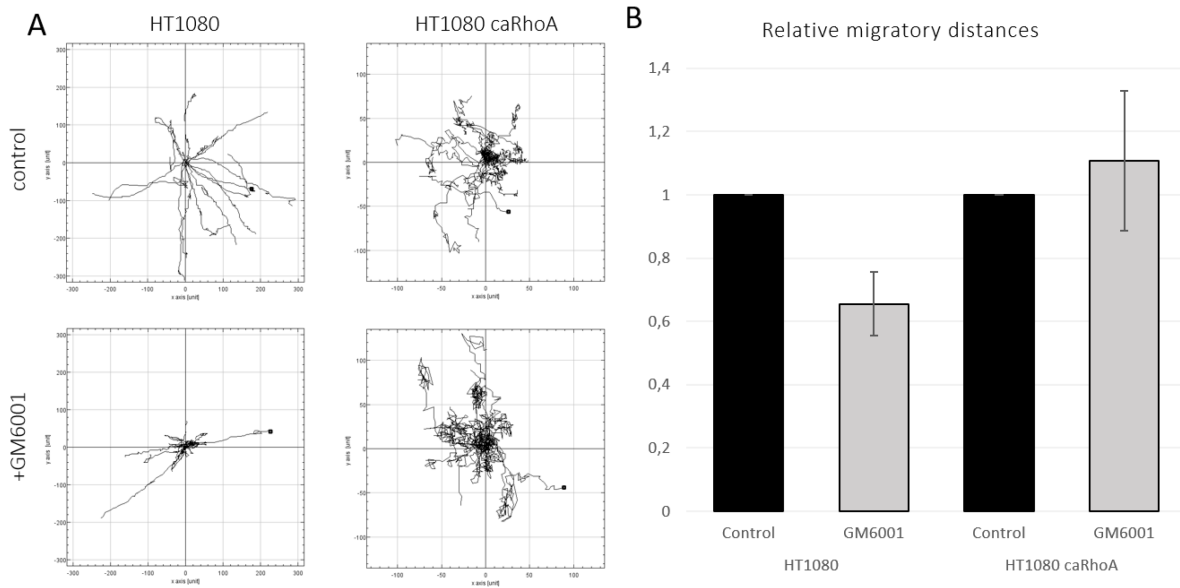


**Figure S2. Migratory distances of HT1080 cells of the mesenchymal and amoeboid phenotype.**

HT1080 cells and HT1080 cells expressing constitutively active RhoA were embedded in rat-tail collagen (1mg/ml) with or without GM6001. 12 hours later, migration of cells of the mesenchymal phenotype (HT1080) and amoeboid phenotype (HT1080 caRhoA) was monitored by wide-field microscopy for 15h. Three independent experiments were evaluated. A) Track plots were generated using Chemotaxis Tool in ImageJ. For each condition, one representative track plot is shown. B) Quantification of relative migratory distances.

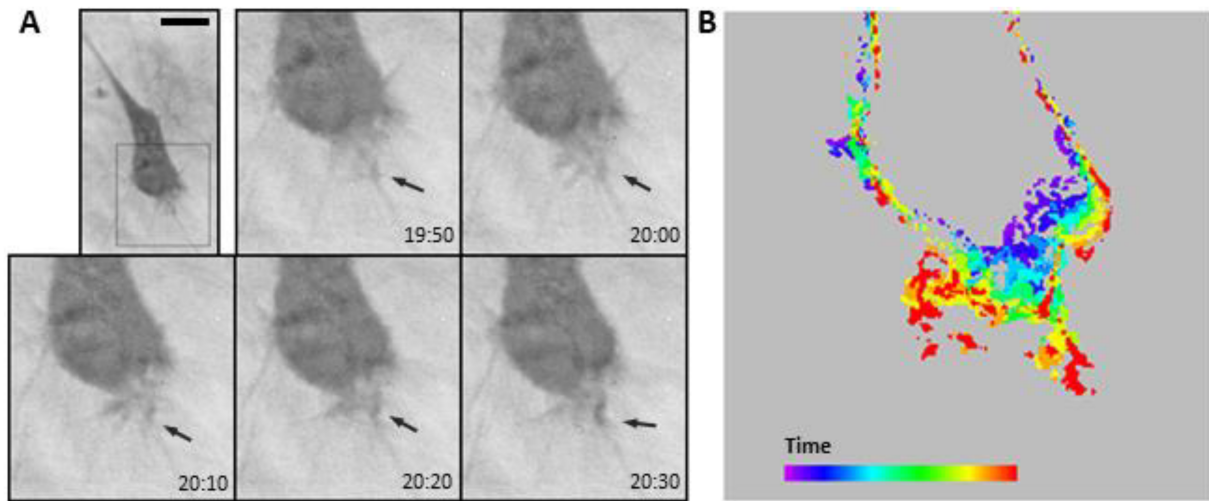


**Figure S3. Membrane ruffles in 3D collagen.** Image sequence acquired by CCHM of a migrating mesenchymal cell showing membrane ruffles at the cell's front. A: Representative images are taken from Supplementary video V1 with time points corresponding to the video. Arrows points towards presumed membrane ruffles, an enrichment of filopodia at the cell's leading edge. B: The dynamics of membrane filopodia protrusions at the cell's front visualized in colours. The rainbow colours represent cell periphery at different time points (14 in total) in chronological order, with violet representing the periphery from the earliest frame and red the latest. Pseudo-coloured representation highlights the most dynamic areas of cell periphery that correspond to the filopodia ruffles indicated in A. Scale bar: 10  $\mu\text{m}$

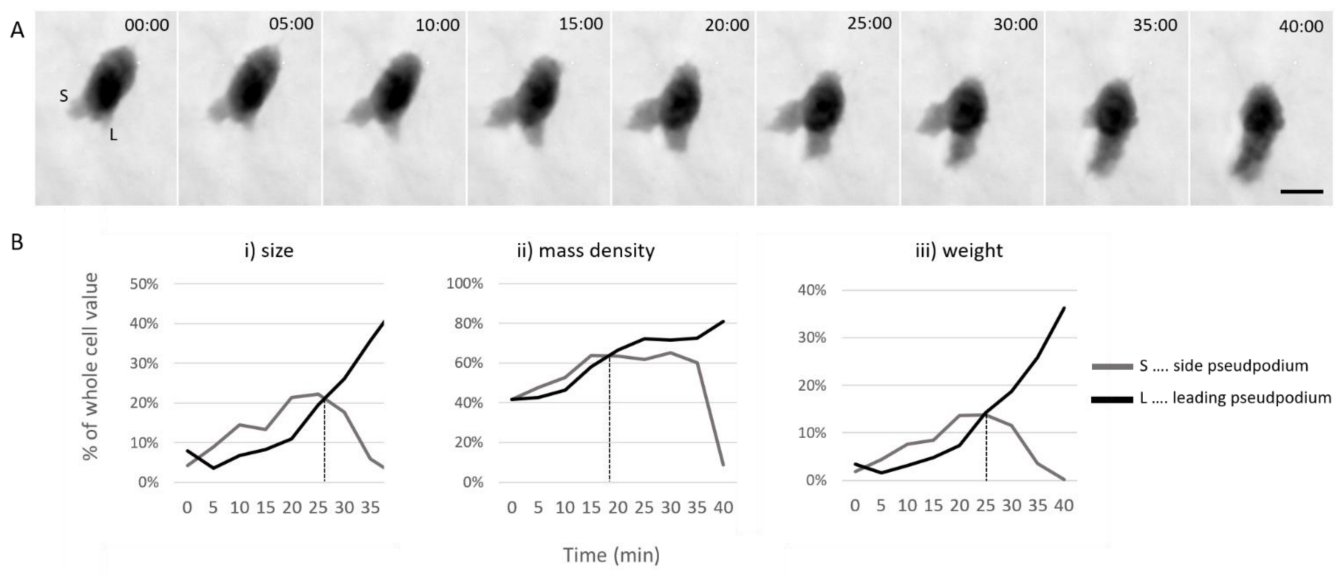


**Figure S4. Analysis of mean cell mass in pseudopodia during amoeboid cell migration.** Images acquired by CCHM of an amoeboid cell embedded in 3D collagen matrix were analysed to compute mean cell mass densities in whole cells and each pseudopodium. A: Analysed image sequence. B: The values for each pseudopodium are plotted as percentage of the values measured in the whole cell. The size (i) and weight (ii) differentiates the leading pseudopodium (L) from the side pseudopodium (S) at time 25 min, mean mass density (ii) already at time 20 min. Scale bar: 10  $\mu\text{m}$ .

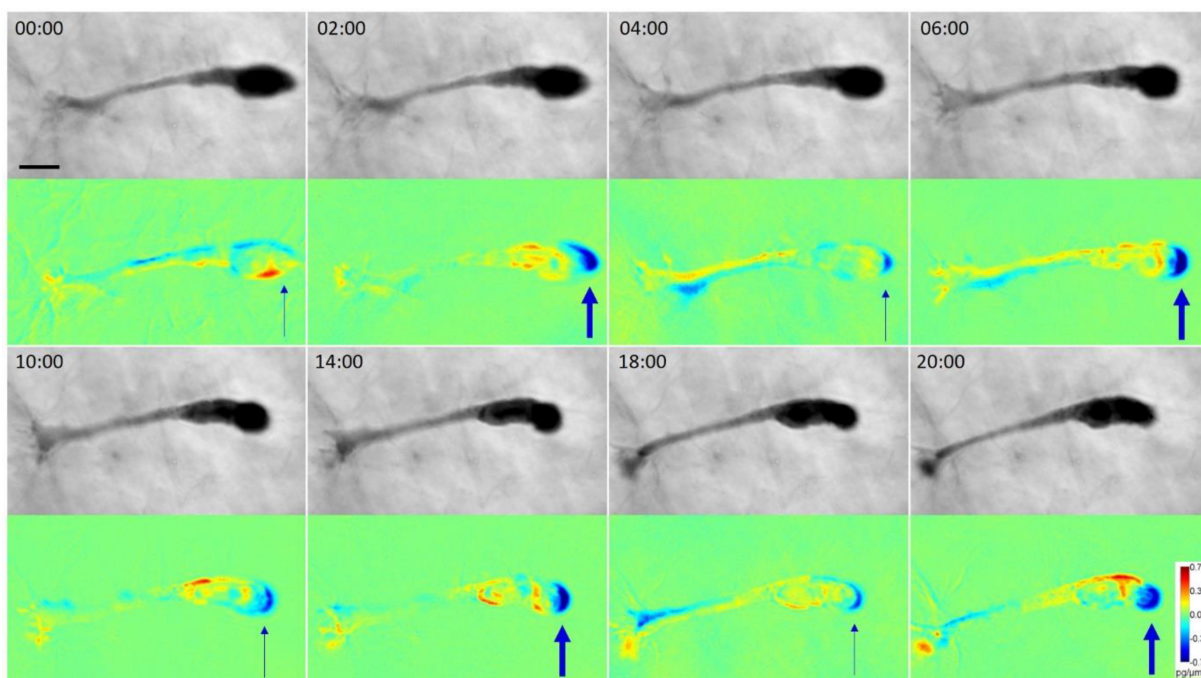


**Figure S5: Cell migration dynamics demonstrated by DPD.** Dynamic phase differences were calculated for an image sequence of a migrating mesenchymal cell. It can be noticed that the cell undergoes cycles of rear retraction, here clearly depicted by dark blue colour. The rear retraction succeeds a less dynamic phase with lower mass translocation, here shown as thin and thick arrows. Scale bar: 10  $\mu\text{m}$ .

## Supplementary videos

**Supplementary video V1. A migration of mesenchymal cell within collagen matrix.** Cells were embedded within bovine collagen gel (1mg/ml) and observed using CCHM. Grey values were adjusted for best fibre contrast.

**Supplementary video V2. A migration of mesenchymal cell within collagen matrix.** Cells were embedded within bovine collagen gel (1mg/ml) and observed using CCHM. Grey values were adjusted for best fibre contrast. This video shows a similar situation as Suppl. Video V1.

**Supplementary video V3. A migration of mesenchymal cell within low density collagen matrix.** Cells were embedded in 0.5 mg/ml bovine collagen. The cell movement within low density collagen affects the overall architecture of collagen fibre matrix to higher degree than in higher density collagen (compare with video V1, V2). Grey values were adjusted for best fibre contrast.

**Supplementary video V4. Clustering of collagen fibres by a mesenchymal cell.** Cells were embedded within bovine collagen gel (1mg/ml) and observed using CCHM. Note that the vesicular material (black spots) is directed towards the very front pseudopodium, and a temporal appearance of blebs around nucleus where is the cell constricted (see also Supplementary video V6).

**Supplementary video V5. Clustering of collagen fibres by a mesenchymal cell.** This video is a detail from video V4. For details see text and Fig. 2.

**Supplementary video V6. Perinuclear blebbing during mesenchymal invasion.** This video is a detail from video V4. Membrane blebbing can be observed around the nucleus at sites of constriction.

**Supplementary video V7. Cell mass distribution during amoeboid invasion.** An amoeboid cell embedded in rat-tail collagen (1 mg/ml) was observed using CCHM. DPD were calculated during post-processing. The left and right part show the actual and subsequent image, respectively, DPD are shown in the middle.

**Supplementary video V8. Translocation of an amoeboid cell through a narrow pore.** An amoeboid cell embedded in rat-tail collagen (1 mg/ml) was observed using CCHM. This video demonstrates the dynamic cell body deformation during invasion through a narrow pore.





Publication #2: High throughput Transcriptomic and Proteomic Profiling of Mesenchymal-Amoeboid Transition in 3D Collagen



OPEN

DATA DESCRIPTOR

# High-throughput transcriptomic and proteomic profiling of mesenchymal-amoeboid transition in 3D collagen

Vladimír Čermák<sup>1,2,4</sup>, Aneta Gandalovičová<sup>1,2,4</sup>, Ladislav Merta<sup>1,2,4</sup>, Karel Harant<sup>2,3</sup>, Daniel Rösel<sup>1,2</sup> & Jan Brábek<sup>1,2</sup>  

The plasticity of cancer cell invasion represents substantial hindrance for effective anti-metastatic therapy. To better understand the cancer cells' plasticity, we performed complex transcriptomic and proteomic profiling of HT1080 fibrosarcoma cells undergoing mesenchymal-amoeboid transition (MAT). As amoeboid migratory phenotype can fully manifest only in 3D conditions, all experiments were performed with 3D collagen-based cultures. Two previously described approaches to induce MAT were used: doxycycline-inducible constitutively active RhoA expression and dasatinib treatment. RNA sequencing was performed with ribo-depleted total RNA. Protein samples were analysed with tandem mass tag (TMT)-based mass spectrometry. The data provide unprecedented insight into transcriptome and proteome changes accompanying MAT in true 3D conditions.

## Background & Summary

Cancer is the result of deregulation of cellular processes, namely of cell proliferation, differentiation, survival/apoptosis, metabolism and migration<sup>1</sup>. Aberrant invasive behaviour of cancer cells can result in metastasis, a process responsible for tumour dissemination and related mortality, accounting for approx. 90% deaths from cancer. Using ancient, evolutionary conserved mechanisms, cancer cells invade the extracellular matrix (ECM) either as cell clusters or sheets, described as collective invasion, or alternatively, migrate as individual cells<sup>2</sup>. When migrating individually, cells can adopt either the protease-dependent mesenchymal mode or the protease-independent amoeboid mode. In general, mesenchymally invading cells display a fibroblast-like morphology with a distinct leading and trailing edge<sup>3</sup>. They form actin-rich protrusions that engage in stable cell-ECM contacts mediated mostly by integrins<sup>4</sup>. Mesenchymal cells further form invasive structures, such as invadopodia and podosomes, that produce proteolytically active enzymes, most commonly matrix metalloproteinases<sup>5,6</sup>. The secretion of such enzymes serves to digest the surrounding ECM and form tracks large enough for cell body translocation<sup>7</sup>.

Unlike mesenchymal invasion, amoeboid invasion does not fully depend on proteolytic digestion and formation of stable cell-ECM adhesions. The cells rather take advantage of pre-existing pores in the ECM and dynamically change their cell body to squeeze through<sup>8,9</sup>. Amoeboid cells may display enhanced actomyosin contractility due to persistent activation of the RhoA/ROCK pathway, leading to increased hydrostatic pressure that drives formation of membrane blebs<sup>10,11</sup>. However, a few different subtypes of the amoeboid migratory phenotype have been described and diverse theories explaining the physical mechanism of cell translocation in amoeboid cells have been suggested<sup>12</sup>. So far, no specific biochemical marker of the phenotype has been shown to be a universal feature of amoeboid cells arising from different cell types. Importantly, cancer cell invasion is responsive to surrounding conditions and transitions between the individual modes can occur. The mesenchymal-amoeboid (MAT) or amoeboid-mesenchymal (AMT) transitions can be induced by modulating the activity of key signalling hubs, such as the Rho GTPases, or by targeting necessary mechanisms of either invasion mode<sup>13,14</sup>. The plasticity of invasion is presumably the main reason why clinically usable anti-metastatic treatment strategies are

<sup>1</sup>Department of Cell Biology, Charles University, Viničná 7, Prague, Czech Republic. <sup>2</sup>Biotechnology and Biomedicine Centre of the Academy of Sciences and Charles University (BIOCEV), Průmyslová 595, 25242, Vestec u Prahy, Czech Republic. <sup>3</sup>Proteomics Core Facility, Faculty of Science, Charles University, Prague, Czech Republic. <sup>4</sup>These authors contributed equally: Vladimír Čermák, Aneta Gandalovičová, Ladislav Merta. ✉e-mail: [jan.brabek@natur.cuni.cz](mailto:jan.brabek@natur.cuni.cz)

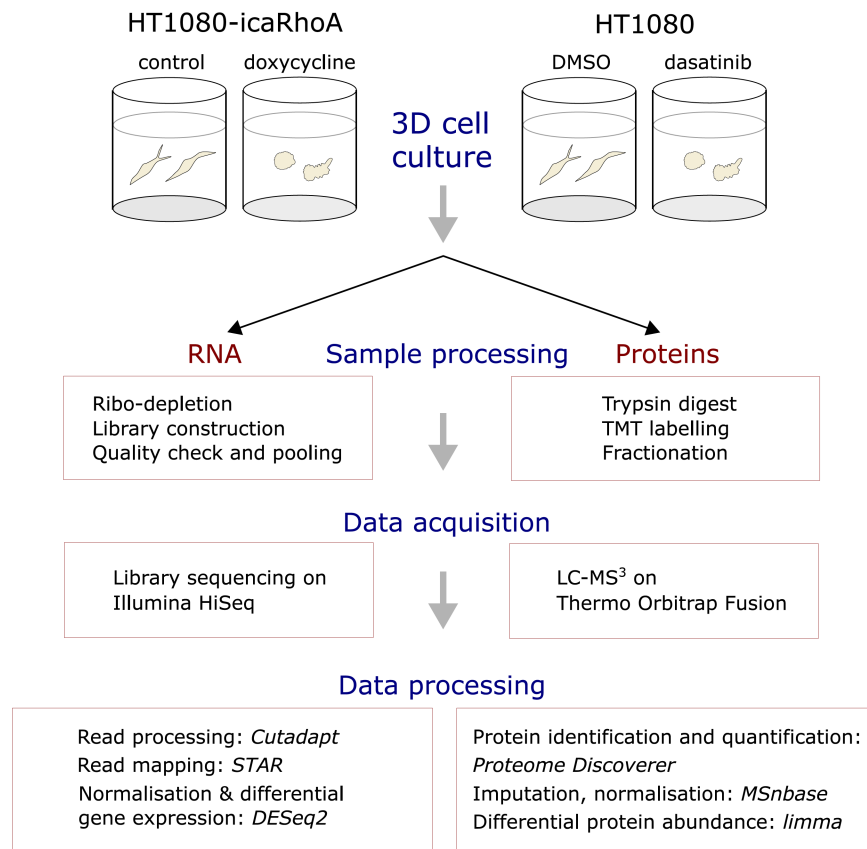


**Fig. 1** Schematic overview and experimental design of the study.

still unavailable<sup>15</sup>. Despite the large effort to reveal signalling underlying invasive behaviour of cells, understanding of cancer cell invasion plasticity is still insufficient, mainly due to the scarcity of results obtained from more *in vivo*-like 3D cell culture conditions. To date, there are only three published works reporting gene expression profiling of amoeboid cells<sup>16–18</sup>. While these data provided the first insight into the transcriptome of amoeboid cells, they were not obtained from three-dimensional (3D) cultures, an essential requirement to get the most relevant results.

To gain more insight into molecular level adaptation of cancer cells to the amoeboid state, we performed large scale transcriptomic and proteomic profiling of HT1080 fibrosarcoma cells after MAT in 3D cell culture (Fig. 1). In order to discern treatment-specific effects, we used two experimental treatments that are sufficiently effective in inducing MAT and compatible with cell viability in 3D collagen gels. The first treatment was doxycycline-inducible constitutively active RhoA (icaRhoA) gene expression; RhoA-ROCK pathway is known to play a key role in amoeboid migration<sup>13,19</sup> and constitutively active RhoA expression has been shown to induce amoeboid morphology in glioblastoma cells and effective MAT in HT1080<sup>3,20</sup>. The second, very different treatment was that with dasatinib, a Src kinase inhibitor, that has been previously also shown to induce MAT<sup>21,22</sup>. The cells were kept for 48 hours in 3D collagen without or with the MAT-inducing treatment and then the whole samples including the collagen and any extracellular material were homogenized and further processed for RNA sequencing or mass spectrometry analysis. Total RNA was depleted of rRNA, converted into a stranded cDNA library and sequenced with Illumina HiSeq sequencer. Protein lysates were trypsin-digested, TMT-labelled, fractionated and analysed on Thermo Orbitrap Fusion mass spectrometer.

Overall, our work provides data for an unprecedented comparison of parallel mesenchymal and amoeboid transcriptomes and proteomes obtained from 3D conditions to reveal new details of the transition regulation, the impact of the transition on biological properties of the cells in terms of gene expression and protein abundance, and possibly discover potential new therapeutic opportunities.

## Methods

**Cells, DNA constructs and transfection.** HT1080 cells were maintained in DMEM (4.5 g/l glucose, pyruvate) supplemented with 10% fetal bovine serum and 50 µg/ml gentamicin (all from Sigma) at 37 °C in humidified atmosphere with 5% CO<sub>2</sub>. The cultures were regularly tested for mycoplasma contamination. 3D cell culture experiments were performed with rat tail collagen (SERVA) at concentration 1 mg/ml and DMEM supplemented with 1% fetal bovine serum, 15 mM HEPES and 50 µg/ml gentamicin. Stably transfected cells were prepared by lentiviral transduction using the second-generation packaging system (pLVX constructs, Tet-On Advanced Gene expression system, Clontech). The DNA transfections were performed with polyethylenimine (Polysciences, Inc.). All populations of stably transfected cells were further enriched for the respective encoded fluorescence with a

cell sorter. Cells bearing inducible constructs were transiently induced with doxycycline before the sorting. In all experiments, cells stably transfected with the doxycycline-inducible EGFP-RhoA G14V fusion construct were treated with 250 ng/ml doxycycline (Sigma). In dasatinib experiments, HT1080 cells stably expressing LifeAct-mCherry exogene<sup>23</sup> (further referenced just as HT1080) were treated with 1  $\mu$ M dasatinib (LC Laboratories) in DMSO or equivalent volume of DMSO only (0.1% final concentration). All plasmids used in the study were constructed in the lab with standard molecular cloning procedures; details as well as the plasmids themselves are available upon request.

**Time-lapse microscopy in 3D collagen matrix.** To record cell invasion in 3D collagen, control and doxycycline- and dasatinib-treated cells with or without protease inhibitor GM6001 (10  $\mu$ M) were imaged every 5 minutes using JuLI FL, an in-incubator microscope (NanoEnTek Inc.). For digital holographic microscopy, cells were embedded in collagen as stated above and left to adjust to 3D conditions for at least 12 hours. Images were acquired automatically in 80–90 second intervals. Cells were imaged using QPHASE (TESCAN Brno, s.r.o.) a multimodal holographic microscope based on CCHM technology as described previously<sup>3</sup>.

**Cell morphology in 3D collagen matrix.** 100,000 cells were seeded in 250  $\mu$ l of collagen matrix in a 48-well plate. Hoffman modulation contrast microscopy images were taken 48 hours later from approx. 20 planes along z-axis. Cell morphology was assessed by measuring the ratio of the maximum length and maximum width manually using Fiji software<sup>24</sup>. At least 300 cells were analysed for each condition.

**RNA extraction and sequencing.** One million HT1080 cells were cultured in a 500  $\mu$ l 3D collagen gel for 48 hours in a 24-well plate. Gels from two wells were transferred into one 2 ml tube and homogenized with Tissue Tearor (BioSpec Products) in 600  $\mu$ l of RNA extraction solution (60% v/v water-saturated phenol, 3.25 M guanidine thiocyanate, 400 mM sodium acetate buffer pH 4.0, 0.4% w/v N-lauroylsarcosine, 160 mM 2-mercaptoethanol) plus 100  $\mu$ l of 6.1 M sodium chloride. 200  $\mu$ l of chlorophorm was added to approx. 1 ml of the lysate and the mixture was vortexed vigorously for 10 seconds. After 30-minute centrifugation at 18,000 g at 4 °C, the polar upper phase was transferred to a new tube, volume adjusted to 800  $\mu$ l with RNase-free water, RNA was precipitated with 600  $\mu$ l of isopropanol and recovered by centrifugation at 18,000 g for 30 min at 4 °C. The RNA pellet was washed three times with 600  $\mu$ l of 75% ethanol and air-dried. Next, the RNA was treated with DNase I to remove any possible genomic DNA contamination. To this end, the pellet was directly dissolved in 100  $\mu$ l of solution containing 4 units of DNase I (Thermo Fisher Scientific) in manufacturer-provided reaction buffer and incubated at 37 °C for 30 min. After that, the RNA was re-purified with RNeasy Protect Mini Kit (Qiagen) according to the manufacturer's instructions and eluted in 50  $\mu$ l of RNase-free water. Stranded, Illumina HiSeq-compatible library was constructed with ScriptSeq Complete (Human/Mouse/Rat) library preparation kit (Epicentre) according to the manufacturer's instructions. The quality and size distribution of sequencing libraries was analysed with Agilent BioAnalyzer 2100. An equimolar pool of 6 sample libraries was sequenced on one whole lane of Illumina HiSeq 2000/2500 series sequencer in high output, paired mode (2  $\times$  100 cycles in case of the inducible caRhoA cells and 2  $\times$  125 cycles in case of the DMSO/dasatinib treated cells). Raw reads were trimmed of adapter sequences with Cutadapt<sup>25</sup> (version 1.15), quality-checked with fastqc and mapped to human genome version GRCh38.91 with the STAR short read aligner<sup>26</sup> version 2.5.4b with default settings and output extended with read counts per gene. Complete adapter-trimmed fastq data are available from the ArrayExpress database at EMBL-EBI under accession number E-MTAB-6823<sup>27</sup>. The samples and related files are summarized in Table 1.

**High-throughput proteomic profiling.** One million HT1080 cells were cultured in a 500  $\mu$ l 3D collagen gel for 48 hours in a 24-well plate. Gels from two wells were transferred into one 2 ml tube, mixed with equal volume of 2x TEAB buffer (200 mM triethylammonium bicarbonate pH 8.5, 4% sodium deoxycholate, both from Sigma) and homogenized with Tissue Tearor (BioSpec Products). After 15-minute centrifugation at 18,000 g at 4 °C, supernatant was transferred into a new tube and kept frozen at –80 °C before further processing. Protein samples were trypsin-digested, TMT-labeled, fractionated and analysed on Orbitrap Fusion mass spectrometer (Thermo Fisher Scientific) as described previously<sup>28–30</sup>. Specifically, sample volume containing 100  $\mu$ g of proteins was precipitated by four volumes of cold acetone (overnight at –20 °C). After centrifugation the pellets were washed with 80% acetone and let dry. Samples were resuspended in 100 mM TEAB (Triethylammonium bicarbonate, Thermo #90114) reduced with 5 mM TCEP (Tris(2-carboxyethyl)phosphine hydrochloride, Sigma #4706) for 30 min at 60 °C and alkylated with 10 mM MMTS (S-Methyl methanethiosulfonate, Sigma #64306) for 10 min at room temperature. Proteins were digested with trypsin (trypsin:protein ratio 1:50) overnight at 37 °C. TMT label was added according to manufacturer protocol. After 60 min, the labelling reaction was stopped by addition of hydroxylamine. All samples were pooled and vacuum dried. Samples were desalted on Michrom C18 Opti Trap Macro (Optimize Technologies 10-04818-TN). Peptides were fractionated as follows. 100  $\mu$ l volume of a sample containing approx. 250  $\mu$ g of peptides was injected onto a C18 column (kinetex 1.7  $\mu$ m, EVOC18, 150  $\times$  2.1 mm) and separated with linear gradient from 0% A (20 mM ammonium formate, 2% acetonitrile pH 10) to 50% B (20 mM ammonium formate, 80% acetonitrile pH 10) in 32 min with flow rate 300  $\mu$ l/min 32 fractions were collected and pooled into 8 fractions. Resulting fractions were dried and resuspended in 20  $\mu$ l of 1% TFA. Nano reversed phase column (EASY-Spray column, 50 cm  $\times$  75  $\mu$ m ID, PepMap C18, 2  $\mu$ m particles, 100 Å pore size) was used for LC/MS analysis. Mobile phase buffer A was composed of water, 2% acetonitrile and 0.1% formic acid. Mobile phase buffer B was composed of 80% acetonitrile in water and 0.1% formic acid. Samples were loaded onto the trap column (AcclaimPepMap300, C18, 5  $\mu$ m, 300 Å wide pore, 300  $\mu$ m  $\times$  5 mm) at a flow rate of 15  $\mu$ l/min. Loading buffer was composed of water, 2% acetonitrile and 0.1% trifluoroacetic acid. Peptides were eluted with gradient of B from 2% to 60% over 240 min at a flow rate of 300 nl/min. Eluting peptide cations were

Sample	Cells	Treatment	Protocols	ENA	BioSD
1	HT1080-icaRhoA	none	P-MTAB-75206 to P-MTAB-75211	ERS2515967	SAMEA4695791
2	HT1080-icaRhoA	doxycycline	P-MTAB-75206 to P-MTAB-75211	ERS2515964	SAMEA4695788
3	HT1080-icaRhoA	none	P-MTAB-75206 to P-MTAB-75211	ERS2515968	SAMEA4695792
4	HT1080-icaRhoA	doxycycline	P-MTAB-75206 to P-MTAB-75211	ERS2515966	SAMEA4695790
5	HT1080-icaRhoA	none	P-MTAB-75206 to P-MTAB-75211	ERS2515969	SAMEA4695793
6	HT1080-icaRhoA	doxycycline	P-MTAB-75206 to P-MTAB-75211	ERS2515965	SAMEA4695789
7	HT1080-LifeAct-mCherry	DMSO	P-MTAB-75206 to P-MTAB-75211	ERS2515962	SAMEA4695786
8	HT1080-LifeAct-mCherry	dasatinib	P-MTAB-75206 to P-MTAB-75211	ERS2515960	SAMEA4695784
9	HT1080-LifeAct-mCherry	DMSO	P-MTAB-75206 to P-MTAB-75211	ERS2515963	SAMEA4695787
10	HT1080-LifeAct-mCherry	dasatinib	P-MTAB-75206 to P-MTAB-75211	ERS2515958	SAMEA4695782
11	HT1080-LifeAct-mCherry	DMSO	P-MTAB-75206 to P-MTAB-75211	ERS2515961	SAMEA4695785
12	HT1080-LifeAct-mCherry	dasatinib	P-MTAB-75206 to P-MTAB-75211	ERS2515959	SAMEA4695783

**Table 1.** Summary of RNA sequencing data.

Sample	Cells	Treatment	PRIDE RAW file
R1	HT1080-icaRhoA	none	D1_170107152223
R2	HT1080-icaRhoA	doxycycline	D2_170107195536
R3	HT1080-icaRhoA	none	D3_170108002847
R4	HT1080-icaRhoA	doxycycline	D4_170107104914
R5	HT1080-icaRhoA	none	D5_170108050200
R6	HT1080-icaRhoA	doxycycline	D6_170108093514
D1	HT1080-LifeAct-mCherry	DMSO	R1_170110145546
D2	HT1080-LifeAct-mCherry	dasatinib	R2_170110192857
D3	HT1080-LifeAct-mCherry	DMSO	R3_170111000208
D4	HT1080-LifeAct-mCherry	dasatinib	R4_170111043519
D5	HT1080-LifeAct-mCherry	DMSO	R5_170111090830
D6	HT1080-LifeAct-mCherry	dasatinib	R6_170111134141

**Table 2.** Summary of mass spectrometry proteomic data.

converted to gas-phase ions by electrospray ionization and analyzed on a Thermo Orbitrap Fusion (Q-OT-qIT, Thermo) mass spectrometer. Spectra were acquired with 4 seconds duty cycle. Full MS spectra were acquired in orbitrap within mass range 350–1,400 m/z with resolution 120,000 at 200 m/z and maximum injection time 50 ms. Most intense precursors were isolated by quadrupole with 1.6 m/z isolation window and fragmented using CID with collision energy set to 30%. Fragment ions were detected in ion trap with scan range mode set to normal and scan rate set to rapid with maximum injection time 50 ms. Fragmented precursors were excluded from fragmentation for 60 seconds. For quantification information of a TMT label 10 most intense fragments were isolated (simultaneous precursor selection) and fragmented in HCD on 65% energy, maximum accumulation time 140 ms, and fragments were measured in orbitrap on 60 K resolution. Raw data were processed in Proteome Discoverer 2.1. TMT reporter ions ratios were used for estimation of relative amount of each protein. Searches were done with the Human Uniprot reference database and a common contaminant database. Modification were set: peptide N terminus, lysine (unimod #737) and cysteine (unimod #39) as static, and methionine oxidation (unimod #1384) and protein N-terminus acetylation (unimod #1) as variable. Raw data are available from the PRIDE database<sup>31</sup> under identifier PXD010425<sup>32</sup>. The samples and related files are summarized in Table 2.

**Immunoblotting.** One million cells were cultured in a 500  $\mu$ l 3D collagen gel for 48 hours in a 24-well plate. Gels from two wells were transferred to tubes containing 500  $\mu$ l of 2x SDS lysis buffer (2% SDS, 20% glycerol, 120 mM Tris, pH = 6.8) and homogenized using Tissue Tearor (BioSpec Products). After 10-minute centrifugation (18,000 rcf, 10 °C) 900  $\mu$ l of the solution was transferred to a fresh tube and protein concentration in the lysate was determined using the DCTM Protein Assay (Bio-Rad Laboratories). The lysates in each series were adjusted to the same protein concentration with 1x SDS lysis buffer. DTT (final concentration 50 mM) and bromophenol blue (final concentration 30  $\mu$ M) were added, and the samples were incubated at 95 °C for 10 min. Samples were separated on 10% or 12% SDS-polyacrylamide gels and transferred onto nitrocellulose membrane. Non-specific binding was blocked by incubation of the membranes for 60 min at room temperature in Tris-buffered saline (TBS) containing 4% BSA or 5% non-fat dry milk. The membranes were incubated with a primary antibody in 4 °C overnight, washed three times in Tris-buffered saline with Tween-20 (TBST) and incubated for 75 min with HRP-conjugated secondary antibody at room temperature. Membranes were washed with TBST two times, with TBS one time and developed using Amersham<sup>TM</sup> Imager 600 (GE Healthcare) and

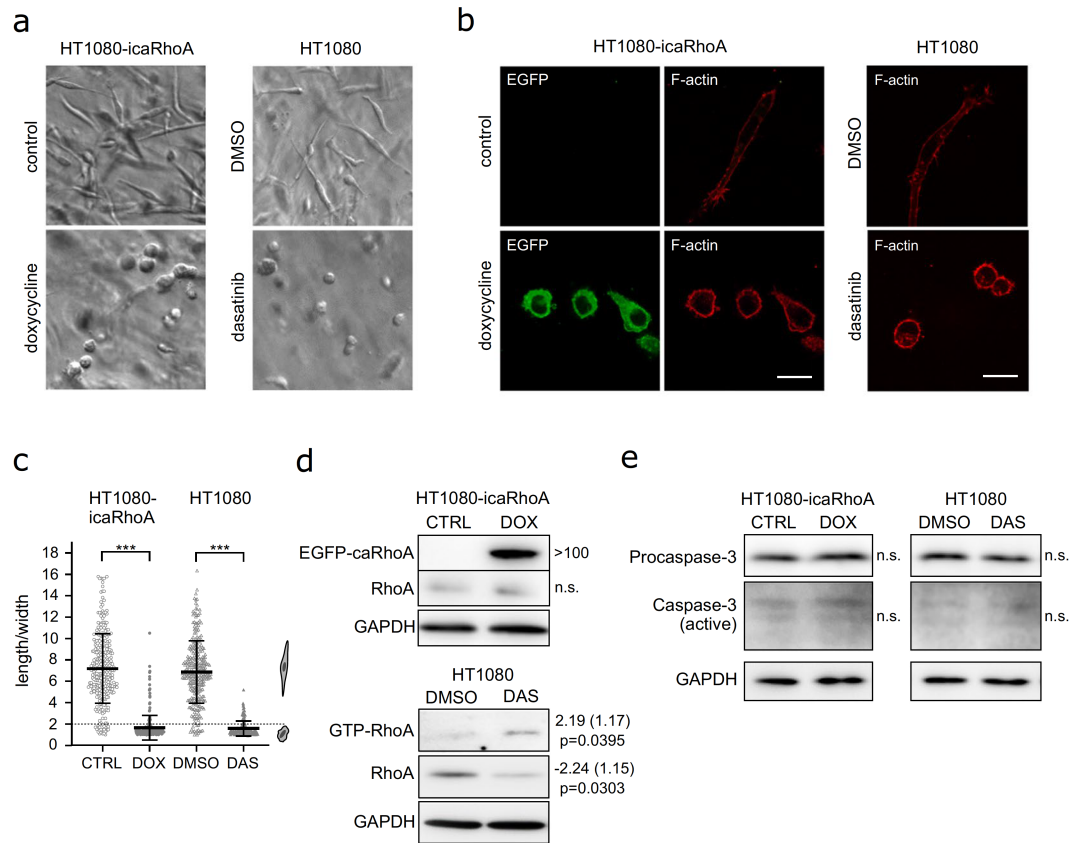


**Fig. 2** Characterization of HT1080 cells induced to undergo MAT. **(a)** Representative wide-field images of cells in 3D collagen without or with induction of MAT. **(b)** Confocal microscopy of cells stained with fluorescently labeled phalloidin. **(c)** Quantification of cell morphology in 3D collagen (Student's t-test, p-values: \*\*\* $p < 0.001$ , \*\* $p < 0.01$ , \* $p < 0.05$ ). **(d)** Immunoblotting detection of RhoA protein in cell lysates. In cells treated with DMSO or dasatinib, the active, GTP-bound RhoA was separated using GST-Rhotekin 1 RBD pulldown. Numbers next to blots indicate average fold change, standard error (both geometric) and p-value of paired t-test. **(e)** Immunoblotting detection of Caspase-3 in cell lysates. All results come from 48-hour experiments. Scale bar 20  $\mu\text{m}$  in all cases. Abbreviations: CTRL – control, DOX – doxycycline, DAS – dasatinib, n.s. – not significant.

SuperSignal™ Femto Maximum Sensitivity Substrate (Thermo Fisher Scientific) or Western Bright TMECL (Advansta) HRP substrates. For probing the total protein level after a phosphoprotein detection and for loading control (GAPDH) detection, membranes were stripped in stripping buffer (200 mM NaOH) at 42 °C for 10 min. The primary antibodies used were as follows: GAPDH (Thermo Fisher Scientific MA5-15738), Caspase-3 (Cell Signaling Technology #9662), Fra-1 (Developmental Studies Hybridoma Bank PCR-FOSL1-1E3), C/EBP $\beta$  (Abcam Ab32358), RhoA (Cell Signaling Technology #2117), GDF15 (Thermo Fisher Scientific PA5-17065) and MX1 (Cell Signaling Technology #37849). Quantification of band signals was performed using Multi Gauge software (Fujifilm, Tokyo, Japan). Band intensities of specific proteins were normalized to the GAPDH protein signal. Log-transformed signal values from at least three experiments were analyzed with paired Student's t-test. The results were presented as geometric means of fold change values with respect to control samples and the uncertainty was expressed as geometric standard errors.

**Activated RhoA detection.** One million cells were cultured in a 500  $\mu\text{l}$  3D collagen gel for 48 hours in a 24-well plate. Gels from two wells were transferred to tubes containing 500  $\mu\text{l}$  of 2x Triton-X100 lysis buffer (2% Triton X-100, 100 mM Tris, 300 mM NaCl, pH = 7.1, protease inhibitors) and homogenized using Tissue Tearor (BioSpec Products) on ice. After 10-minute centrifugation (18,000 g, 10 °C) 800  $\mu\text{l}$  of the solution was transferred to a fresh tube, protein concentration in the lysate was determined using the DCTM Protein Assay (Bio-Rad Laboratories) and adjusted to the same value in each series with 1x Triton X-100 lysis buffer. 50  $\mu\text{l}$  of the lysate was transferred to a fresh tube (total lysate control) and the rest was incubated with rhotekin-bound GST-beads at 4 °C for 45 min. Beads were separated by brief centrifugation and washed two times with 1x Triton X-100 lysis buffer. Finally, beads were resuspended in 1x Laemmli sample buffer (0.35 M Tris-HCl, pH = 6.8, 10% SDS, 40% glycerol, 0.012% bromophenol blue) with DTT (50 mM) and incubated at 95 °C for 10 minutes. Samples were further processed according to the immunoblotting protocol described above.

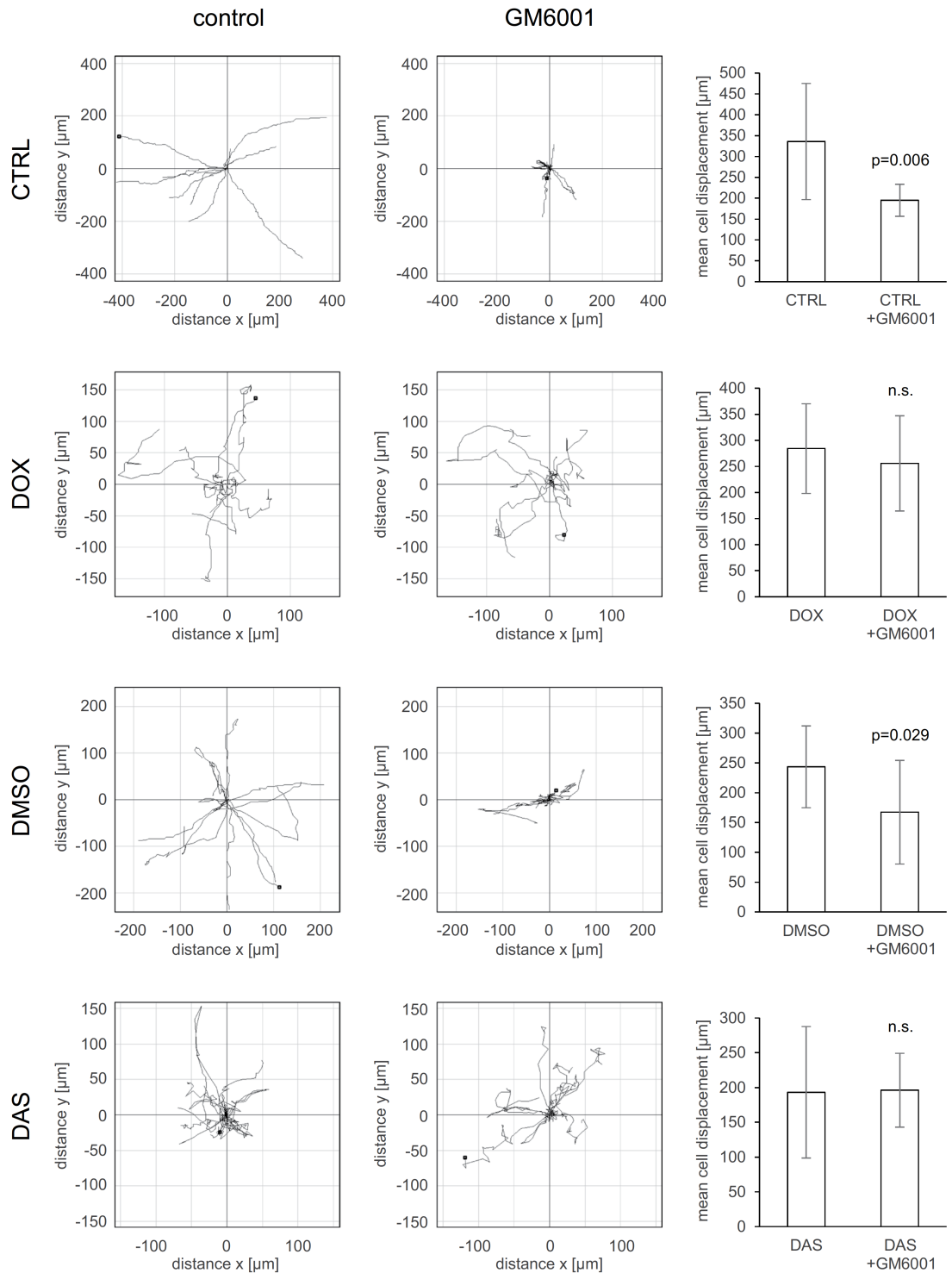


**Fig. 3** Quantitative analysis of cell migration. HT1080-icaRhoA cells and HT1080 cells were embedded in rat-tail collagen (1 mg/ml) with or without GM6001. 12 hours later, migration of cells of the mesenchymal phenotype (HT1080-icaRhoA CTRL, HT1080 DMSO) and amoeboid phenotype (HT1080-icaRhoA DOX, HT1080 DAS) was monitored by wide-field microscopy for 15 hours. Track plots were generated using Chemotaxis Tool in ImageJ. Differences in the mean length of the tracks were analysed with two-tailed Student's t-test,  $\alpha = 0.05$ ,  $n = 9\text{--}13$ . Error bars – standard deviation. Representative results of three independent experiments.

**Statistical analysis.** To estimate differential gene expression from RNA sequencing data a workflow based on the STAR aligner and DESeq2 R package was used as described previously<sup>18</sup>. Mass spectrometry data pre-processed with Proteome Discoverer 2.1 were imported into R environment and normalized with the MSnbase package<sup>33</sup>. Differences in protein levels were estimated with moderated t-test statistics using the limma package<sup>34</sup>.

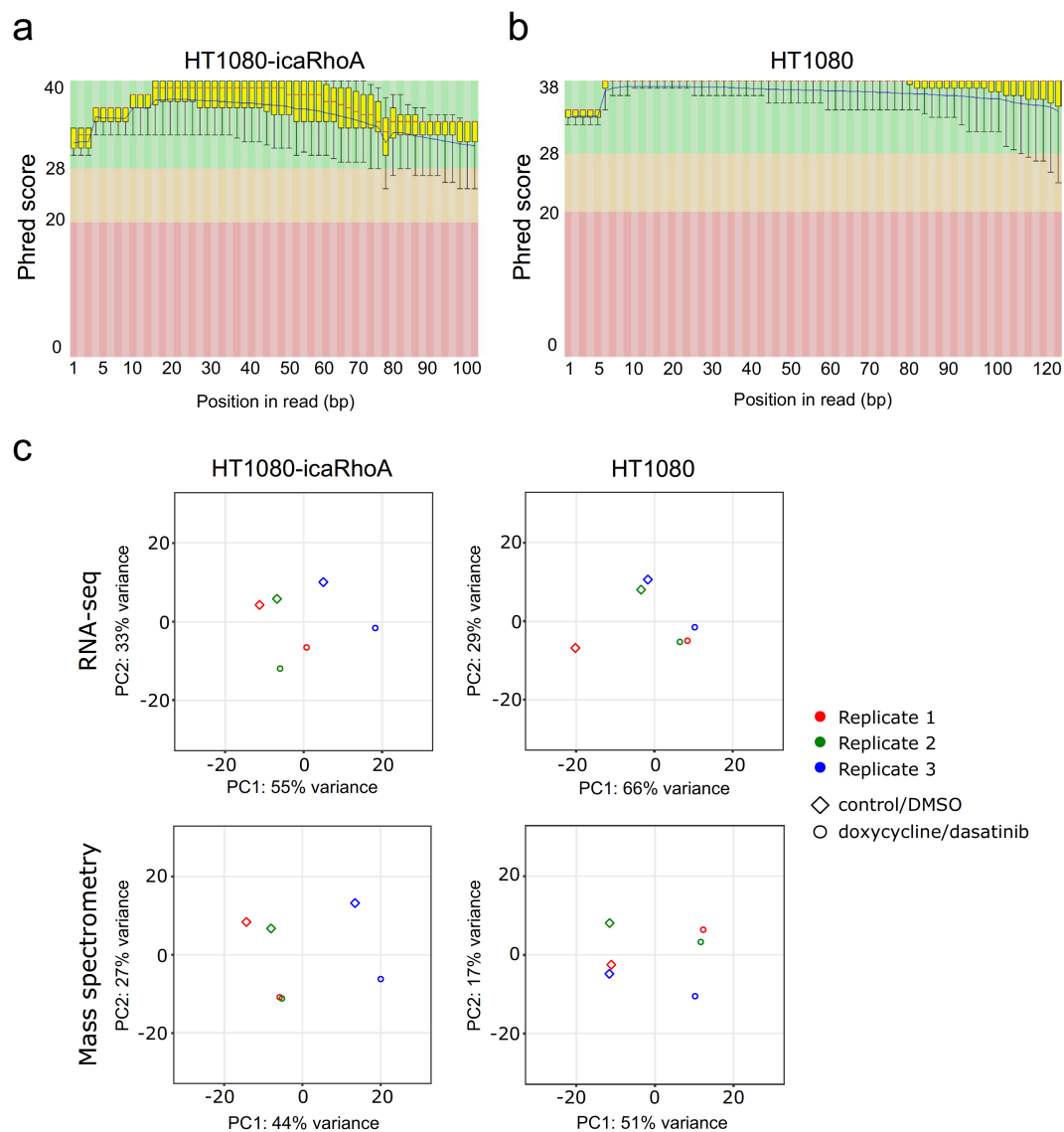


**Fig. 4** Transcriptomic and proteomic profiling of HT1080 cells of mesenchymal and amoeboid migratory phenotype. **(a)** Per base sequence quality of RNA sequencing reads expressed as Phred score by position, HT1080-icaRhoA control sample 1, first reads. **(b)** Same as **(a)**, HT1080 DMSO control sample 1. **(c)** Principal component analysis of gene expression and protein abundance profiles. The normalized expression abundance of mRNAs and proteins was used. Point shapes indicate treatment; point colours mark individual pairs of biological replicates.

### Data Records

Time-lapse movies documenting migratory phenotypes of the cells, uncropped immunoblot images, other supporting data referenced in the text, and complete results of differential transcript and protein level analyses were deposited in the Figshare<sup>35</sup> repository. Adapter-trimmed RNA sequencing data have been deposited in the ArrayExpress database at EMBL-EBI<sup>27</sup>. Raw proteomic data have been deposited in the PRIDE database via the ProteomeXchange Consortium<sup>32</sup>. Besides the described data, the PRIDE record contains also a series of data-sets obtained from HT1080-icaRhoA cells cultured on 2D collagen (three pairs of doxycycline-untreated/treated cells).

### Technical Validation

Induction of icaRhoA in otherwise mesenchymally migrating HT1080 fibrosarcoma induced effective MAT, i.e. cell rounding, membrane blebbing and amoeboid migration resistant to extracellular protease inhibitor (GM6001) in 3D collagen in the vast majority of the cell population (Figs. 2a–c, 3 and additional files available from Figshare<sup>35</sup>; time-lapse Movies 1 and 2). Treatment of HT1080 cells with 1  $\mu$ M dasatinib produced very similar effects (Figs. 2a–c, 3 and time-lapse Movies 1 and 3 plus the files “Src activity in MAT-induced cells” all available from Figshare<sup>35</sup>). We also tested the effect of other Src inhibitors and found that they were much weaker MAT



Sample	Cells	Treatment	Reads pairs total	Average read input length	% mapped	% multi-mapped	% too short
1	HT1080-icaRhoA	none	36,639,825	192	89.90	5.40	4.20
2	HT1080-icaRhoA	doxycycline	36,165,871	189	90.55	4.92	3.88
3	HT1080-icaRhoA	none	30,919,393	189	90.62	4.95	3.85
4	HT1080-icaRhoA	doxycycline	36,664,126	193	88.91	5.75	4.93
5	HT1080-icaRhoA	none	36,506,595	189	89.58	3.89	6.23
6	HT1080-icaRhoA	doxycycline	37,336,035	191	92.32	3.18	4.20
7	HT1080-LifeAct-mCherry	DMSO	39,167,799	245	95.18	2.83	1.85
8	HT1080-LifeAct-mCherry	dasatinib	35,644,171	235	90.21	6.67	2.84
9	HT1080-LifeAct-mCherry	DMSO	41,488,195	232	90.54	6.32	2.88
10	HT1080-LifeAct-mCherry	dasatinib	42,412,264	235	91.89	4.98	2.92
11	HT1080-LifeAct-mCherry	DMSO	42,742,403	232	88.94	7.72	3.02
12	HT1080-LifeAct-mCherry	dasatinib	45,846,680	231	89.71	6.87	3.08

**Table 3.** RNA sequencing raw data and mapping metrics.

inducers than dasatinib (see the file “Src inhibitors comparison” available from Figshare<sup>35</sup>). The different potential of the Src inhibitors to induce MAT could be attributed to their different effect on Src structure and localization<sup>36</sup>. The induction of the EGFP-RhoA G14V fusion protein in HT1080-icaRhoA cells was verified with immunoblotting (Fig. 2d). Activation of RhoA – an expected feature of the amoeboid phenotype – in dasatinib-treated cells was confirmed with GST-Rhotekin 1 Rho binding domain (RBD)-based pulldown assay (Fig. 2d, see also the file “RhoA activity in MAT-induced cells” available from Figshare<sup>35</sup>). To verify that the observed membrane blebbing is not due to initiation of apoptosis, we detected Caspase-3 in protein lysates from the cells in 3D collagen. While we easily detected the non-cleaved pro-form in all samples, only a faint signal of the active, cleaved form of Caspase-3 could be detected after a very long blot exposure in all samples with no significant differences (Fig. 2e).

RNA sequencing of control and MAT-induced samples (three pairs of independent biological replicates for each treatment) yielded 31–46 million paired-end reads per sample. Raw reads trimmed of adapter sequences were quality-checked with FastQC software<sup>37</sup>. FastQC’s plots of Phred scores (the standard measure of position reading confidence) by position (Fig. 4a,b) showed typical high-quality profiles with decreasing quality towards the ends of reads. Note that the inducible caRhoA series samples were sequenced with  $2 \times 100$  cycles while the dasatinib treatment series samples were sequenced later with improved version of the sequencing chemistry enabling longer read length ( $2 \times 125$  cycles). The mapping metrics of STAR aligner showed an average paired read length of 191 bases for inducible caRhoA samples and 235 bases for dasatinib treatment series samples. In average, the aligner uniquely mapped 90.7% of the fragments to human genome, 5.3% fragments were multi-mapped, and 3.7% fragments were excluded as too short. The complete mapping metrics is listed in Table 3.

Mass spectrometry sample quality was checked with the aid of Preview<sup>TM</sup> software, version 2.2.9 from Protein Metrics Inc. The effectiveness of tryptic digestions was verified before TMT labelling. Next, we checked for completeness of the labelling procedure. All checks were done as short 30-minute gradient with roughly 250 ng peptide injections. Missing cleavage was under 10% of all peptides and approx. 95% of all N termini and 100% of all lysines were successfully labelled with TMT tags. We identified 5,687 proteins in the icaRhoA series samples and 6,477 proteins in the dasatinib series samples. Among them there were 101 and 105 bovine proteins, respectively, coming from the fetal bovine serum used in the cell culture. For further analysis, we excluded these bovine proteins and all proteins with more than one missing intensity value in the sample series leading to 4,637 and 5,880 proteins, respectively usable for differential protein abundance analysis.

Principle component analysis of normalized gene expression and protein abundance profiles showed that the treatments, but also the biological replication are sources of significant variation (Fig. 4c). The paired character of the data thus has to be reflected in a linear model design formula in order to obtain the most accurate results from the statistical analyses of differential gene expression or differential protein abundance.

Differential gene expression analysis with DESeq<sup>238</sup> identified 894 out of 12,030 genes (7.4%) significantly changed (with adjusted P-value < 0.1) after induction of caRhoA. Dasatinib treatment changed the expression of 996 out of 12,637 (8.1%) genes. Differential protein abundance with limma R package<sup>34</sup> revealed 410 out of 4,637 (8.8%) proteins significantly changed with adjusted P-value < 0.2 after induction of caRhoA. Dasatinib treatment changed the abundance of 674 out of 5,880 with adjusted P-value < 0.05 (11.5%) proteins. Note that we used a stricter adjusted P-value cut-off on the dasatinib data as the biological replicates were more uniform providing smaller P-values overall (with the opposite for the icaRhoA data). The differential gene and protein expression analysis results are summarized with volcano plots in Fig. 5a. Complete results are available from Figshare<sup>34</sup> as “differential\_expression\_analyses.xlsx” spreadsheet file. The file also presents lists of genes and proteins concordantly affected by both MAT-inducing treatments in separate sheets. Joint hierarchical clustering of affected genes across both treatment sample series showed a high similarity in the overall impact of MAT on gene expression (Fig. 5b).

To validate the results of the high-throughput analyses, we performed immunoblotting experiments with independent biological samples (different from those used for the high-throughput analyses) to measure differences in protein abundance of four proteins – C/EBP $\beta$ , GDF15, MX1 and Fra-1 that were selected from those identified with both transcriptomic and proteomic profiling to be concordantly affected by both experimental

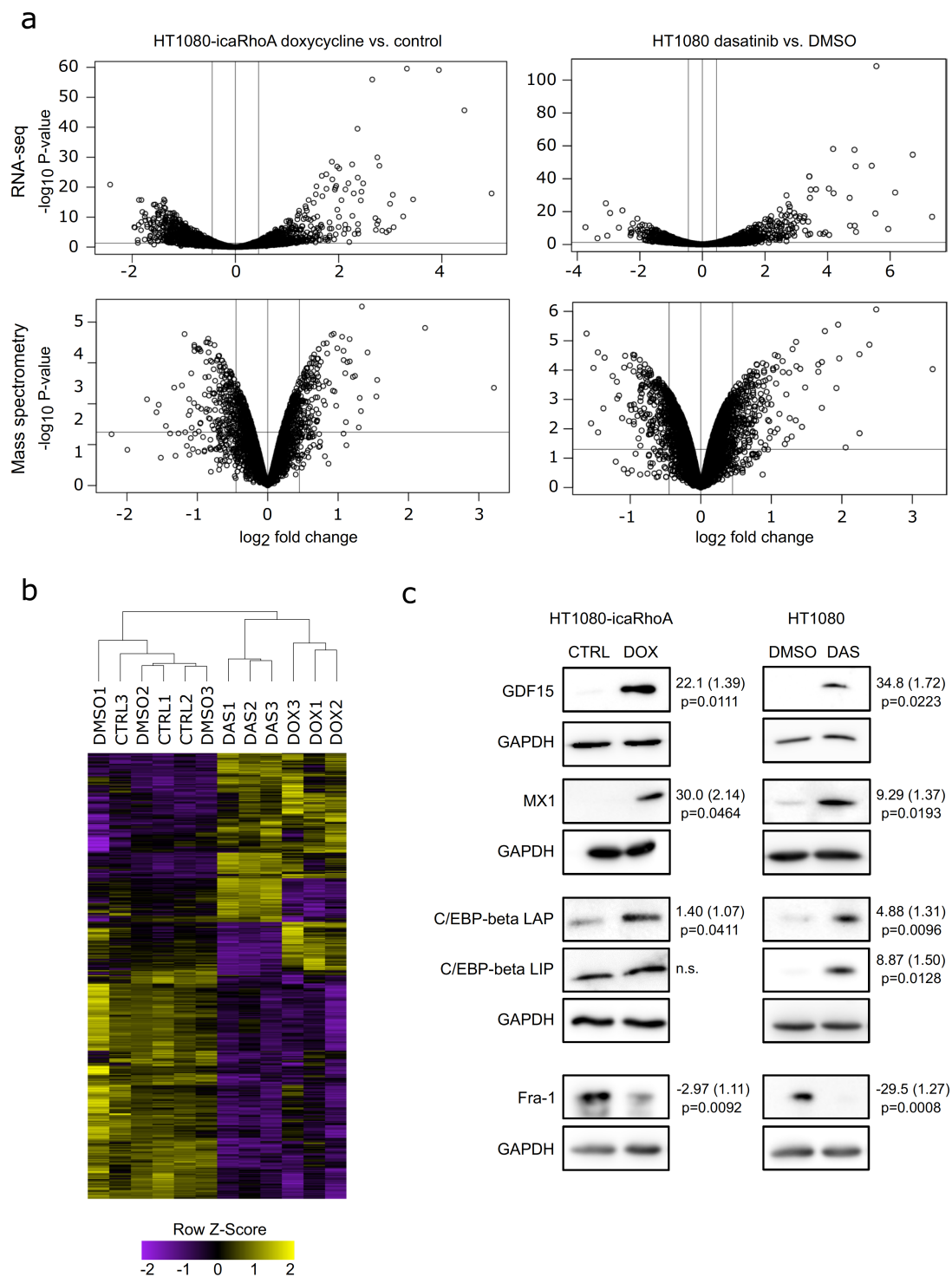


**Fig. 5** Analysis and validation of transcriptomic and proteomic results. **(a)** Volcano plots of transcripts and proteins affected by MAT in each treatment group. Vertical lines mark  $-1.5$  and  $1.5$ -fold change, respectively. Horizontal line marks statistical test P-value  $0.05$ . **(b)** Unsupervised hierarchical clustering of genes that are differentially expressed after MAT in both treatment groups ( $P < 0.05$ ). The yellow colour scale represents a higher expression level, and the purple colour scale represents a lower expression level. **(c)** Immunoblotting validation of differential protein abundance analysis results. GAPDH was used as a loading control in all experiments. Representative results of three independent experiments. Numbers next to blots indicate average fold change, standard error (both geometric) and p-value of paired t-test.

treatments (see “Targets selected for verification” on Figshare<sup>35</sup> for the detected fold changes and corresponding adjusted P-values). The blots confirmed reproducible differences in all four proteins in agreement with the data (Fig. 5c).

Taken together, we present a valuable transcriptomic and proteomic dataset characterizing fibrosarcoma cell response to induced migration mode switching. The dataset provides a useful resource for better understanding of the mechanisms of cancer metastatic spreading. The experimental model presented here has some limitations. Both treatments used in this work to induce MAT have their specific MAT-unrelated effects. The phenotypes induced by the treatments might be not identical. The mechanisms underlying the transition in HT1080 cells might be, at least in some details, different from those described in other cell types, particularly in melanoma cells. However, we believe that only continuing accumulation of data obtained from different cell contexts and with different experimental approaches will bring a better and more general understanding of the amoeboid migratory phenotype and its importance for cancer metastasis.

### Code availability

The scripts used in data processing are available from Figshare<sup>35</sup> (see “Code used in data processing”).

Received: 19 August 2019; Accepted: 21 April 2020;

Published online: 27 May 2020

### References

- Hanahan, D. & Weinberg, R. A. Hallmarks of cancer: the next generation. *Cell* **144**, 646–674 (2011).
- Vaškovičová, K. *et al.* Invasive cells in animals and plants: searching for LECA machineries in later eukaryotic life. *Biol. Direct* **8**, 8 (2013).
- Tolde, O. *et al.* Quantitative phase imaging unravels new insight into dynamics of mesenchymal and amoeboid cancer cell invasion. *Sci. Rep.* **8**, 12020 (2018).
- Parsons, J. T., Horwitz, A. R. & Schwartz, M. A. Cell adhesion: integrating cytoskeletal dynamics and cellular tension. *Nat. Rev. Mol. Cell Biol.* **11**, 633–643 (2010).
- Tolde, O., Rösel, D., Veselý, P., Folk, P. & Brábek, J. The structure of invadopodia in a complex 3D environment. *Eur. J. Cell Biol.* **89**, 674–680 (2010).
- Nabeshima, K., Inoue, T., Shimao, Y. & Sameshima, T. Matrix metalloproteinases in tumor invasion: role for cell migration. *Pathol. Int.* **52**, 255–64 (2002).
- Friedl, P. & Wolf, K. Tube Travel: The Role of Proteases in Individual and Collective Cancer Cell Invasion. *Cancer Res.* **68**, 7247–7249 (2008).
- Wyckoff, J. B., Pinner, S. E., Gschmeissner, S., Condeelis, J. S. & Sahai, E. ROCK- and myosin-dependent matrix deformation enables protease-independent tumor-cell invasion *in vivo*. *Curr. Biol.* **16**, 1515–1523 (2006).
- Wolf, K. *et al.* Compensation mechanism in tumor cell migration: mesenchymal-amoeboid transition after blocking of pericellular proteolysis. *J. Cell Biol.* **160**, 267–277 (2003).
- Lämmermann, T. *et al.* Rapid leukocyte migration by integrin-independent flowing and squeezing. *Nature* **453**, 51–55 (2008).
- Charras, G. T. A short history of blebbing. *J. Microsc.* **231**, 466–478 (2008).
- Agarwal, P. & Zaidel-Bar, R. Diverse roles of non-muscle myosin II contractility in 3D cell migration. *Essays in Biochemistry* **63**, 497–508 (2019).
- Panková, K., Rösel, D., Novotný, M. & Brábek, J. The molecular mechanisms of transition between mesenchymal and amoeboid invasiveness in tumor cells. *Cell. Mol. Life Sci.* **67**, 63–71 (2010).
- Pandya, P., Orgaz, J. L. & Sanz-Moreno, V. Modes of invasion during tumour dissemination. *Mol. Oncol.* **11**, 5–27 (2017).
- Gandalovičová, A. *et al.* Migrastatics—Anti-metastatic and Anti-invasion Drugs: Promises and Challenges. *Trends in Cancer* **3**, 391–406 (2017).
- Sanz-Moreno, V. *et al.* ROCK and JAK1 Signaling Cooperate to Control Actomyosin Contractility in Tumor Cells and Stroma. *Cancer Cell* **20**, 229–245 (2011).
- Taddei, M. L. *et al.* Mesenchymal to amoeboid transition is associated with stem-like features of melanoma cells. *Cell Commun. Signal.* **12**, 24 (2014).
- Čermák, V. *et al.* RNA-seq of macrophages of amoeboid or mesenchymal migratory phenotype due to specific structure of environment. *Sci. Data* **5**, 180198 (2018).
- Kosla, J. *et al.* Metastasis of aggressive amoeboid sarcoma cells is dependent on Rho/ROCK/MLC signaling. *Cell Commun. Signal.* **11**, 51 (2013).
- MacKay, J. L. & Kumar, S. Simultaneous and independent tuning of RhoA and Rac1 activity with orthogonally inducible promoters. *Integr. Biol.* **6**, 885–894 (2014).
- Ahn, J., Sanz-Moreno, V. & Marshall, C. J. The metastasis gene NEDD9 product acts through integrin 3 and Src to promote mesenchymal motility and inhibit amoeboid motility. *J. Cell Sci.* **125**, 1814–1826 (2012).
- Logue, J. S., Cartagena-Rivera, A. X. & Chadwick, R. S. c-Src activity is differentially required by cancer cell motility modes. *Oncogene* **37**, 2104–2121 (2018).
- Riedl, J. *et al.* Lifeact: a versatile marker to visualize F-actin. *Nat. Methods* **5**, 605–607 (2008).
- Schindelin, J. *et al.* Fiji: an open-source platform for biological-image analysis. *Nat. Methods* **9**, 676–682 (2012).
- Martin, M. Cutadapt removes adapter sequences from high-throughput sequencing reads. *EMBnet.journal* **17**, 10–12 (2011).
- Dobin, A. *et al.* STAR: ultrafast universal RNA-seq aligner. *Bioinformatics* **29**, 15–21 (2013).
- Čermák, V., Gandalovičová, A., Merta, L., Rösel, D. & Brábek, J. Transcriptomic profiling of HT1080 fibrosarcoma cells of mesenchymal or amoeboid migratory phenotype. *ArrayExpress* <https://identifiers.org/arrayexpress:E-MTAB-6823> (2019).
- Erbán, T., Harant, K., Chalupnikova, J., Kocourek, F. & Stara, J. Beyond the survival and death of the deltamethrin-threatened pollen beetle *Meligethes aeneus*: An in-depth proteomic study employing a transcriptome database. *J. Proteomics* **150**, 281–289 (2017).
- Wang, Y. *et al.* Reversed-phase chromatography with multiple fraction concatenation strategy for proteome profiling of human MCF10A cells. *Proteomics* **11**, 2019–26 (2011).
- McAlister, G. C. *et al.* MultiNotch MS3 enables accurate, sensitive, and multiplexed detection of differential expression across cancer cell line proteomes. *Anal. Chem.* **86**, 7150–8 (2014).
- Vizcaíno, J. A. *et al.* 2016 update of the PRIDE database and its related tools. *Nucleic Acids Res.* **44**, D447–56 (2016).
- Harant, K., Čermák, V., Rösel, D. & Brábek, J. Proteomic profiling of HT1080 fibrosarcoma cells of mesenchymal or amoeboid migratory phenotype. *PRIDE Archive* <https://identifiers.org/pride.project:PX010425> (2020).
- Gatto, L. & Lilley, K. S. MSnbase—an R/Bioconductor package for isobaric tagged mass spectrometry data visualization, processing and quantitation. *Bioinformatics* **28**, 288–9 (2012).
- Ritchie, M. E. *et al.* limma powers differential expression analyses for RNA-sequencing and microarray studies. *Nucleic Acids Res.* **43**, e47–e47 (2015).
- Čermák, V. *et al.* Mesenchymal-Amoeboid Transition in HT1080 Cells. *figshare* <https://doi.org/10.6084/m9.figshare.c.4623947.v4> (2020).

36. Koudelková, L. *et al.* Novel FRET-Based Src Biosensor Reveals Mechanisms of Src Activation and Its Dynamics in Focal Adhesions. *Cell Chem. Biol.* **26**, 255–268.e4 (2019).
37. Andrews, S. FastQC: a quality control tool for high throughput sequence data. [Online]. Available online at: <http://www.bioinformatics.babraham.ac.uk/projects/fastqc/> (2010).
38. Love, M. I., Huber, W. & Anders, S. Moderated estimation of fold change and dispersion for RNA-seq data with DESeq2. *Genome Biol.* **15**, 550 (2014).

### Acknowledgements

The work was supported by the Kellner Family Foundation Principal Investigator Grant, Center for Tumor Ecology (reg. no. CZ.02.1.01/0.0/0.0/16\_019/0000785) supported by the Operational Programme Research, Development and Education, and by the Charles University, projects GA UK No. 712217 and 1292217. The work was also funded in part by Czech Science Foundation grant 19-08410S. A part of the study was performed with the equipment for metabolomics and cell analyses (Grant no. CZ.1.05/2.1.00/19.0400) supported by the Research and Development for Innovations Operational Program, co-financed by the European regional development fund and the state budget of the Czech Republic. We acknowledge the BIOCEV Gene Core facility. We also acknowledge The Johns Hopkins University/CDI Laboratories and the Developmental Studies Hybridoma Bank (DSHB) for providing the anti-Fra-1 antibody.

### Author contributions

V.Č. and A.G. designed and performed experiments, analysed the data, and contributed to manuscript writing. L.M. executed experiments and data analyses. K.H. performed the mass spectrometry proteomic analysis. D.R. and J.B. conceived the study and supervised the work.

### Competing interests

The authors declare no competing interests.

### Additional information

**Correspondence** and requests for materials should be addressed to J.B.

**Reprints and permissions information** is available at [www.nature.com/reprints](http://www.nature.com/reprints).

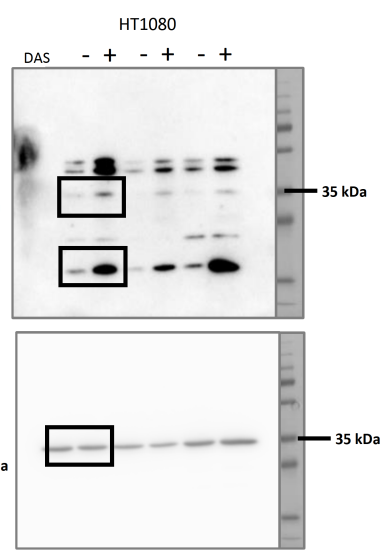
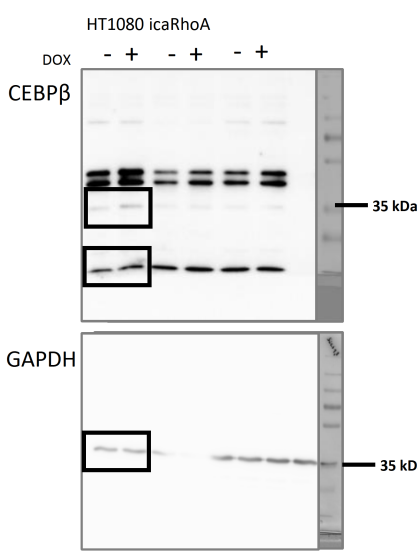
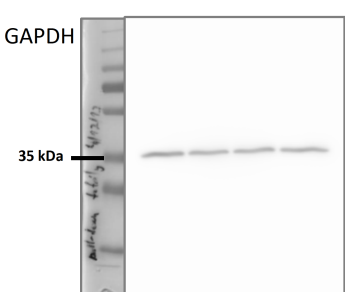
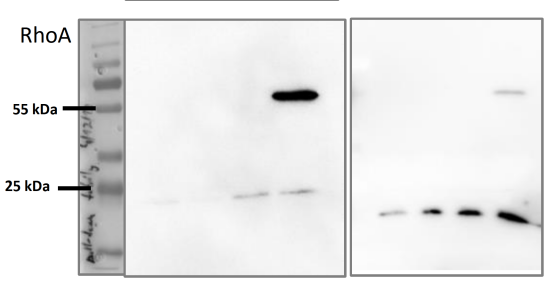
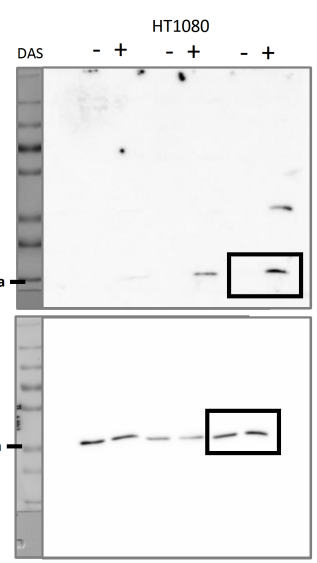
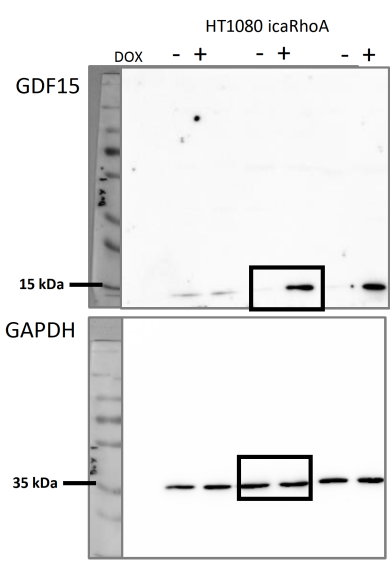
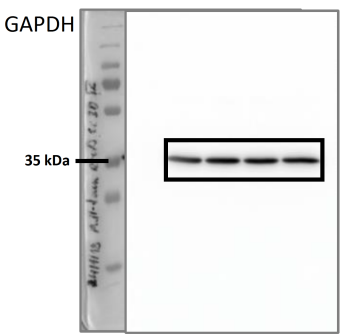
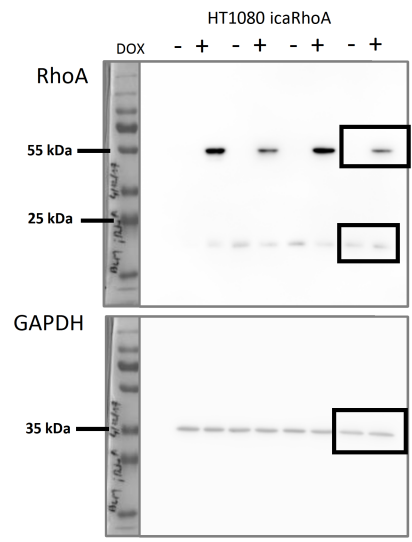
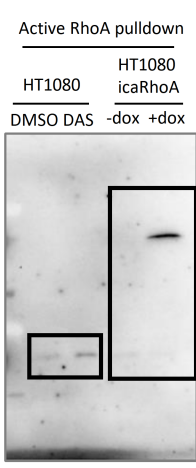
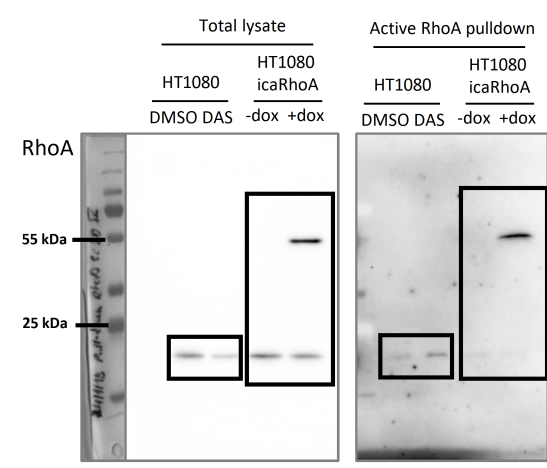
**Publisher's note** Springer Nature remains neutral with regard to jurisdictional claims in published maps and institutional affiliations.

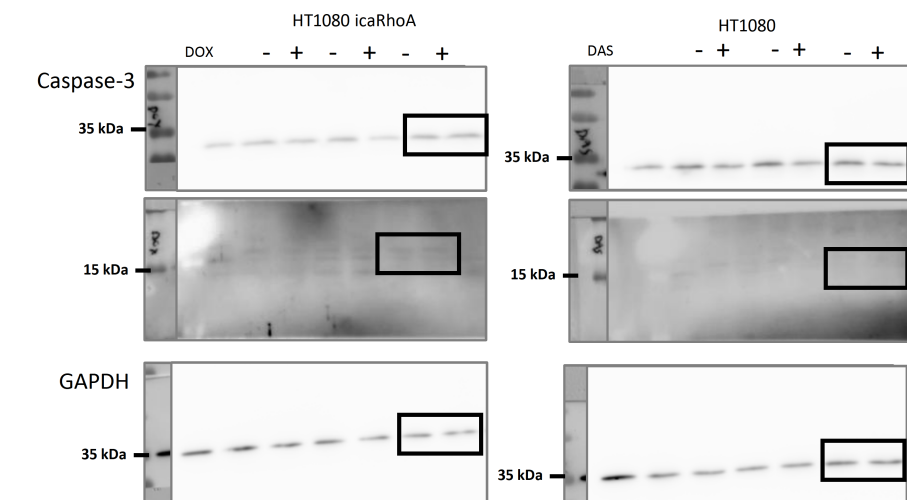
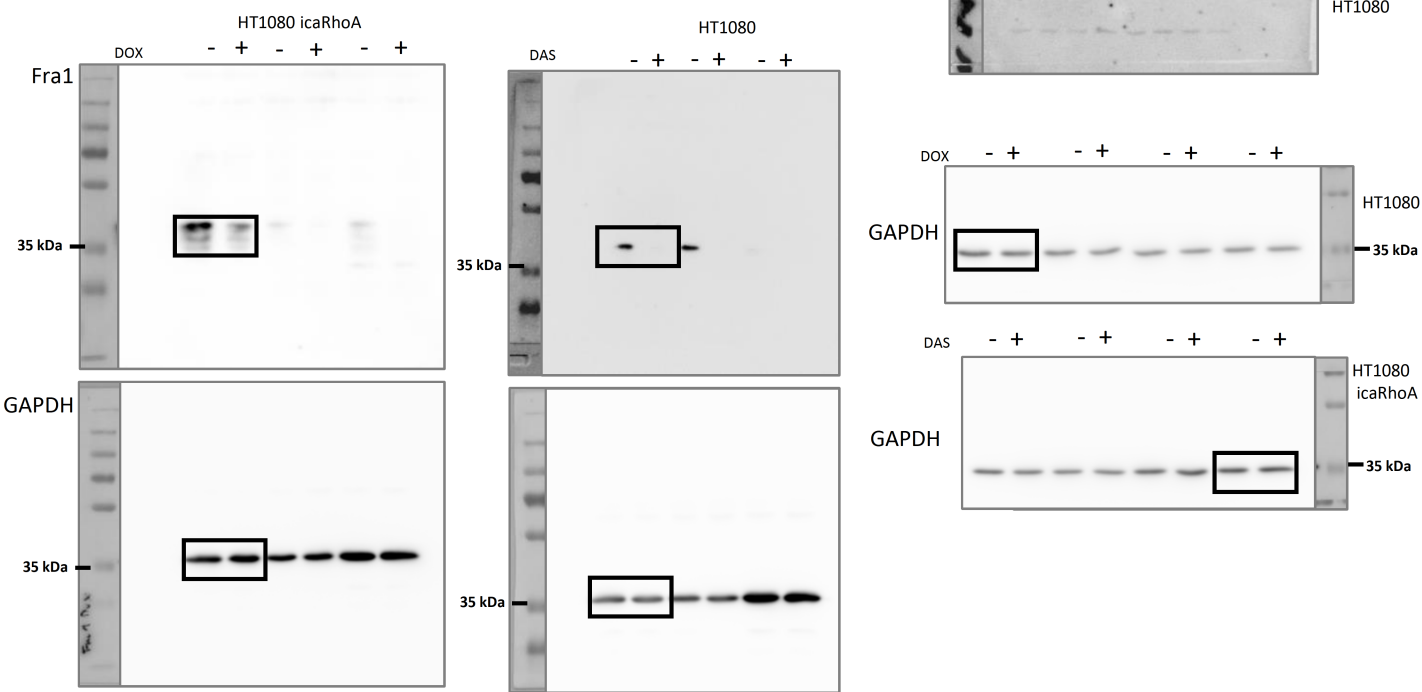
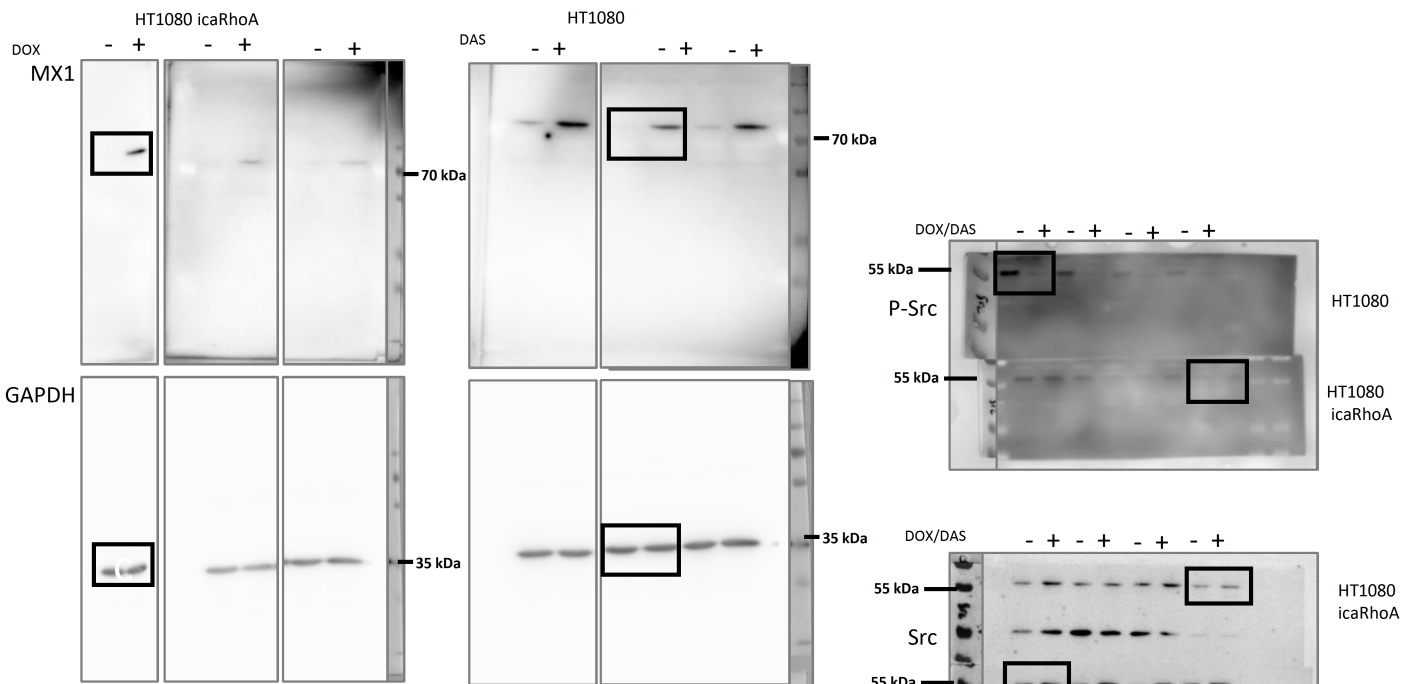


**Open Access** This article is licensed under a Creative Commons Attribution 4.0 International License, which permits use, sharing, adaptation, distribution and reproduction in any medium or format, as long as you give appropriate credit to the original author(s) and the source, provide a link to the Creative Commons license, and indicate if changes were made. The images or other third party material in this article are included in the article's Creative Commons license, unless indicated otherwise in a credit line to the material. If material is not included in the article's Creative Commons license and your intended use is not permitted by statutory regulation or exceeds the permitted use, you will need to obtain permission directly from the copyright holder. To view a copy of this license, visit <http://creativecommons.org/licenses/by/4.0/>.

The Creative Commons Public Domain Dedication waiver <http://creativecommons.org/publicdomain/zero/1.0/> applies to the metadata files associated with this article.

© The Author(s) 2020









Publication #3: Sustained inflammatory signalling through Stat1/Stat2/IRF9 is associated with the amoeboid phenotype of melanoma cells

Article

# Sustained Inflammatory Signalling through Stat1/Stat2/IRF9 Is Associated with Amoeboid Phenotype of Melanoma Cells

Aneta Gandalovičová <sup>1,2</sup>, Anna-Marie Šúchová <sup>1,2</sup>, Vladimír Čermák <sup>1,2</sup>, Ladislav Merta <sup>1,2</sup>, Daniel Rösel <sup>1,2</sup> and Jan Brábek <sup>1,2,\*</sup>

<sup>1</sup> Department of Cell Biology, Charles University, 12843 Prague, Czech Republic;

aneta.gandalovicova@natur.cuni.cz (A.G.); amsuchova@gmail.com (A.-M.Š.);

vladimir.cermak@natur.cuni.cz (V.Č.); ladislav.merta@natur.cuni.cz (L.M.); rosel@natur.cuni.cz (D.R.)

<sup>2</sup> Biotechnology and Biomedicine Centre of the Academy of Sciences and Charles University (BIOCEV), 25242 Vestec, Czech Republic

\* Correspondence: jan.brabek@natur.cuni.cz or brabek@natur.cuni.cz

Received: 19 August 2020; Accepted: 26 August 2020; Published: 28 August 2020



**Simple Summary:** Treatment of metastatic cancer is complicated by the ability of cancer cells to utilize various invasion modes when spreading through the body. Here, we studied the transition of melanoma cells between the round, amoeboid and elongated, mesenchymal invasion modes. Our results show that inflammatory signalling, which is commonly upregulated in the tumour microenvironment, is associated with the amoeboid phenotype of cancer cells. Treatment of melanoma cells with interferon beta promotes the amoeboid invasion modes and individual invasion. This suggests that inflammation associated signalling contributes to cancer cell invasion plasticity.

**Abstract:** The invasive behaviour of cancer cells underlies metastatic dissemination; however, due to the large plasticity of invasion modes, it is challenging to target. It is now widely accepted that various secreted cytokines modulate the tumour microenvironment and pro-inflammatory signalling can promote tumour progression. Here, we report that cells after mesenchymal–amoeboid transition show the increased expression of genes associated with the type I interferon response. Moreover, the sustained activation of type I interferon signalling in response to IFN $\beta$  mediated by the Stat1/Stat2/IRF9 complex enhances the round amoeboid phenotype in melanoma cells, whereas its downregulation by various approaches promotes the mesenchymal invasive phenotype. Overall, we demonstrate that interferon signalling is associated with the amoeboid phenotype of cancer cells and suggest a novel role of IFN $\beta$  in promoting cancer invasion plasticity, aside from its known role as a tumour suppressor.

**Keywords:** plasticity; melanoma; amoeboid; inflammation; interferon; invasion; mesenchymal

## 1. Introduction

Cancer mortality is mostly due to the invasive potential of tumour cells and their ability to establish secondary tumours—i.e., metastases. However, the metastatic behaviour of cells and associated invasion plasticity are largely heterogenous, making them difficult to target. Thus, further understanding of these processes is important for the development of migrastatic therapies [1,2].

The cancer cells' invasive behaviour is largely dictated by the tumour microenvironment (TME), comprising various cell types that mutually interact. Typically, this promotes the production of various secreted molecules that can alter the behaviour of cells in the tumour stroma and create an inflammatory-like environment, which is considered a tumour hallmark [3,4]. Moreover, the physical



properties of the extracellular matrix (ECM), such as pore size or density, determine the invasive ability of cells [5,6].

In response to these cues, cancer cells adapt their invasive behaviour by switching among invasion modes [7,8]. Cells can invade collectively in the form of whole sheets, strands or cell clusters by undergoing partial epithelial–mesenchymal transition while maintaining cell–cell junctions [9]. Additionally, cells can also disrupt intercellular adhesions and invade individually, using either the mesenchymal or amoeboid mode. Mesenchymally invading cells make use of proteolytic degradation of the ECM and integrin-based cell–ECM adhesions, which results in their typical elongated shape with cell protrusions at the leading edge [10,11]. In turn, amoeboid cells are mostly seen as round cells with membrane blebs, that dynamically deform the cell body to squeeze through pores within the ECM [12,13]. Importantly, cells can switch among these modes in response to conditions of the TME, such as matrix density or reciprocal signalling within the stroma, referred to as mesenchymal–amoeboid transition (MAT) and amoeboid–mesenchymal transition (AMT) [14,15].

To understand the plasticity of cancer invasion, approaches to induce MAT and AMT have been investigated [8,14,16,17]. Modifying the activity of Rho GTPases, which are key regulators of the invasion modes, can drive both AMT and MAT. RhoA activation promotes the amoeboid phenotype, while the use of ROCK inhibitors induces cell elongation and mesenchymal invasion. Accordingly, the upregulation of IL6/Stat3 or IL-1 $\alpha$ /NF- $\kappa$ B signalling, leading to RhoA activation, has been implicated in promoting and maintaining the amoeboid phenotype in melanoma cells [18,19].

Pro-inflammatory signalling has been associated with phenotypic plasticity in melanoma [20]. One of the key signalling pathways associated with inflammation is the JAK/STAT signalling cascade, activated in response to interferons type I (IFNs  $\alpha$ ,  $\beta$ ,  $\omega$ ) or type II (IFN $\gamma$ ). Upon type I IFN binding to its receptor, Janus kinase 1 (Jak1) and tyrosine kinase 2 (Tyk2) phosphorylate signal transducer and activator of transduction 1 and 2 (Stat1 and Stat2), which dimerize and bind IRF9, resulting in the formation of the Stat1/Stat2/IRF9 complex (referred to as ISGF3) [21]. The type II IFN response is mediated by Stat1 homodimers [22]. Secretion of IFNs is generally activated in response to viral infection but is also induced in response to various stress factors, and cancers often show an intrinsic IFN signature [23,24]. This modulates cancer immunosurveillance and response to therapy. IFN- $\beta$  is widely used as an adjuvant for melanoma therapy and has been shown to prolong overall and relapse-free survival [25]. Moreover, IFN- $\beta$  increases tumour infiltration by immune cell subsets, including CD4+ and CD8+ T-cells [26]. Consistently, IFN- $\beta$  treatment was shown to prolong survival and increase T-cell recruitment into the tumour tissue of B16F10-bearing mice, which could contribute to the therapeutic efficacy of immune checkpoint inhibitors [27]. Peritumourally administered IFN- $\beta$  enhances the antitumor effect of anti-PD-1 antibody against B16F10 melanoma [28].

In this study, we demonstrate that pro-inflammatory signalling mediated by IFN $\beta$  is associated with the amoeboid phenotype of cancer cells and suggest a novel role of IFN $\beta$  in promoting cancer invasion plasticity, aside from its known role as a tumour suppressor.

## 2. Results

### 2.1. Data Analysis Reveals Upregulation of Inflammation-Associated Genes after MAT

To determine amoeboid phenotype associated signalling, we analysed previously published transcriptomic data from human fibrosarcoma HT1080 cells in 3D collagen before and after MAT induced either by the expression of doxycycline-inducible constitutively active RhoA (iRhoA) or by the treatment of the cells with a Src/Abl kinase inhibitor dasatinib (DAS) [16]. To identify functional gene categories upregulated in amoeboid cells, we performed an enrichment analysis for Gene Ontology (GO) Biological Process terms on genes affected by both treatments [29]. We revealed a strong similarity in the spectra of upregulated genes to type I IFN response (Figure 1a). To affirm that type I IFN signalling is elevated in amoeboid cells, we measured the expression of genes encoding Stat transcription factors (TFs) and IRF9, a component of ISGF3, by RT-qPCR in HT1080 cells undergoing MAT induced by

both iRhoA expression and DAS treatment in a 3D environment (Figure 1b). We detected significantly increased levels of STAT1, STAT2 and IRF9 transcripts after both treatments inducing MAT. Next, we determined the activation status of the corresponding Stat TF proteins measured as phosphorylation detected by immunoblotting, which revealed a predominant activation of Stat1/2 compared to Stat3, in agreement with the upregulation of type I IFN response identified in the transcriptomic data (Figure 1c).

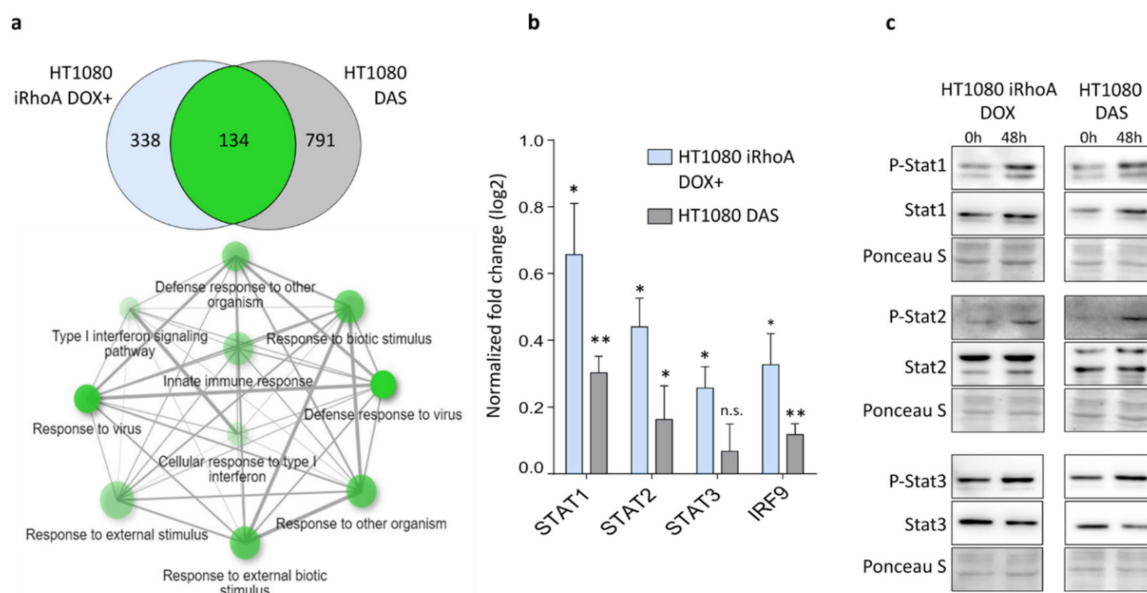


**Figure 1.** Interferon response-like signalling is upregulated in amoeboid cells. (a) Ten most significant GO Biological Process terms enriched in the genes affected concordantly by both iRhoA and dasatinib (DAS) treatment. Only transcripts with adjusted  $p$ -value  $\leq 0.25$  and fold change  $>1.5$  in either direction were considered differentially expressed. Network plot was generated using ShinyGO v0.61 online tool [30]. (b) Gene expression (log<sub>2</sub> fold change) of STAT1, STAT2, STAT3 and IRF9 in cells after mesenchymal–amoeboid transition (MAT) in 3D collagen (48 h) determined by RT-qPCR, normalized to control cells without MAT induction. (c) Immunoblotting detection of Stat transcription factors Stat1, Stat2 and Stat3 in HT1080 cells before and after MAT.  $p$ -values: \*\*  $p < 0.01$ , \*  $p < 0.05$ . Detailed information about Western blot can be found in Figure S1.

## 2.2. Inflammation-Associated Signalling Affects Invasion Plasticity in Melanoma Models

Transcriptomic analysis and the subsequent data validation of genes upregulated after MAT suggested that amoeboid cells display intrinsically upregulated type I IFN signalling. To study the role of IFN signalling in invasion plasticity further, we focused on human melanoma cell lines, since they are known to exhibit high inherent invasion plasticity governed by autocrine and paracrine production of various cytokines [31–33]. Initially, we tested the effect of IFN signalling suppression by Ruxolitinib, a Jak1/2 inhibitor, on a panel of amoeboid and mixed-morphology melanoma cell lines. The inhibition of Jak1/2 significantly promoted the elongated, mesenchymal migratory phenotype of five tested melanoma cell lines in 3D collagen (Figure 2a,b). Next, we tested the effect of IFN signalling activation on three selected cell lines with mixed morphology—namely WM3629, G361 and WM88. We treated the cells with IFNs of both type I (IFN $\omega$  and  $\beta$ ) and type II (IFN $\gamma$ ). Interestingly, IFN $\beta$ —but neither IFN $\omega$  nor IFN $\gamma$ —promoted the round amoeboid phenotype in all three cell lines (Figure 2d,e), and this could be blocked by Ruxolitinib (Figure 2c). To compare the activity of all three IFNs and disclose their differing effect on cell morphology, we assessed the phosphorylation levels of Stat1, 2 and 3 at different time points (Figure 2f; Figures S2a and S3). Only IFN $\beta$  induced a long-term response, observed as the prolonged phosphorylation of Stat1 and Stat2, but interestingly also as the accumulation of Stat1 and Stat2 proteins, which are known to sustain inflammatory signalling [34]. To exclude that the round

phenotype observed in response to IFN $\beta$  is caused by the induction of apoptosis, we measured cell proliferation in the 3D collagen of untreated and treated cells and detected a decrease consistent with the anti-proliferative effects of IFN $\beta$  (Figure S2c), but no significant differences in numbers of dead cells were detected (Figure S2d). Moreover, by live cell imaging of cells in 3D collagen, we documented that IFN $\beta$  treated cells invade almost exclusively as round, amoeboid cells (Video S1).

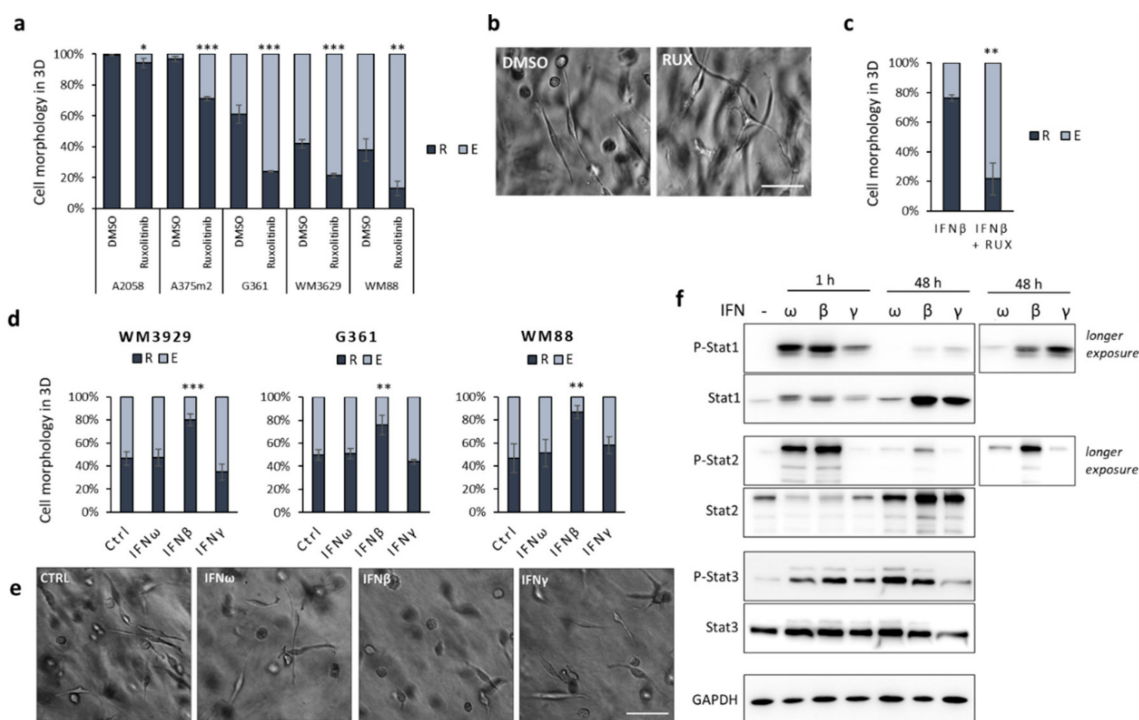


**Figure 2.** Role of IFN signalling in melanoma invasion plasticity. (a) Inhibition of Jak1/2 by Ruxolitinib promotes the elongated, mesenchymal phenotype of melanoma cells cultured in 3D collagen (48 h). (b) Representative image of WM3629 cells after 48 h in 3D collagen treated with DMSO or Ruxolitinib. (c) Quantification of morphology of WM3629 cells treated with IFN $\beta$  alone or IFN $\beta$  plus Ruxolitinib after 48 h in collagen. (d) Quantification of morphology of melanoma cells cultured in 3D collagen for 48 h after treatment with IFNs (overall exposure to IFNs took 96 h). (e) Representative images of WM3629 cells after 48 h in 3D collagen treated with IFNs. (f) Immunoblotting detection of Stat transcription factors Stat1, Stat2 and Stat3 activation after 1 h and 48 h IFN treatment in WM3629 cells. Scale bar 100  $\mu$ m in both (b) and (e). R = round, E = elongated. *p*-values: \*\*\* *p* < 0.001, \*\* *p* < 0.01, \* *p* < 0.05. Detailed information about Western blot can be found at Figure S4.

### 2.3. IFN $\beta$ Treated Cells Upregulate Expression of Pro-Invasive Cytokines and Increase Individual Invasion

To gain insight into the role of IFN signalling in cancer cell invasion plasticity, we prepared protein and RNA lysates from WM3629 cells after IFN treatment in 3D collagen and analysed the expression of Stat TFs and downstream regulated proteins/genes (Figure 3a,b). Both Stat1 and Stat2 showed statistically significant increases in gene expression levels, and at protein level we confirmed the upregulation of both phosphorylated and total proteins after treatment with IFN $\beta$ . We further tested the expression levels of IRF9, the adaptor protein important for binding Stat1/2 heterodimers in the ISGF3 complex, and indeed confirmed its upregulation at both protein and transcript levels in IFN $\beta$  treated cells. Interestingly, the IRF9 levels show similar upregulation time course as Stat1, Stat2, as well as Jak1 (Figure S2b and Figure S3). This points to the role of the long-term type I IFN response in promoting the amoeboid phenotype. IFN $\beta$  also increased the expression of MX1, ISG15, IFITM1 and PDL1, known interferon responsive genes, and of genes encoding secreted cytokines IL6, IL8 and IL24. We also detected the increased expression of IFNB1 gene in response to IFN $\beta$ , suggesting a positive feedback loop, maintaining the sustained IFN signalling. Since we detected the upregulation

of pro-invasive molecules (MX1, IFITM1, IL6, IL8), we sought to investigate the effect of IFN $\beta$  on cell invasion from multicellular spheroids. We cultivated cell spheroids in control media and in the presence of IFN $\beta$ , and then tested their invasion in 3D collagen. Interestingly, IFN $\beta$  pre-treatment did not increase the overall size of the spheroids, but increased the number of individually migrating cells, most of which acquired the amoeboid invasion phenotype (Figure 3c).

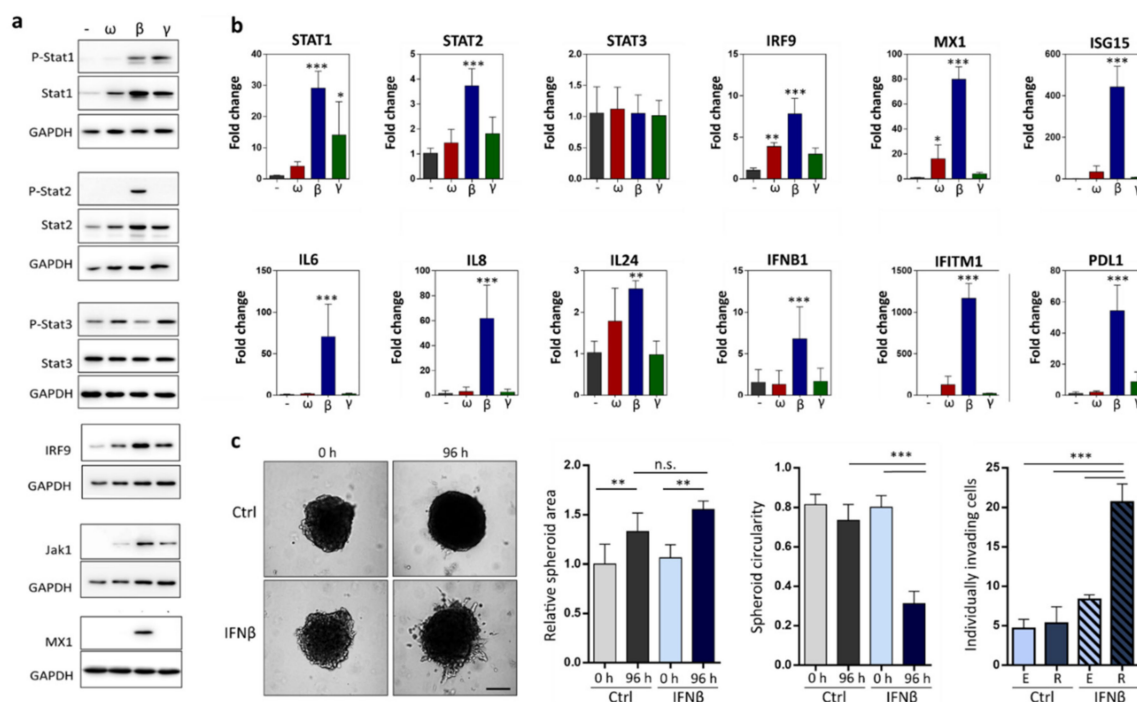


**Figure 3.** Characterization of IFN treated cells. (a) Immunoblotting detection of proteins from WM3629 cells cultured in 3D collagen for 48 h after treatment with IFNs (overall exposure to IFNs was 96 h). (b) Gene expression changes in WM3629 cells cultured in 3D collagen for 48 h (overall exposure to IFNs 96 h). (c) Spheroids of WM3629 cells, quantification of spheroid area, circularity, and the number of individually invading cells after 96 hours in 3D collagen. Scale bar 500  $\mu$ m. R = round, E = elongated. *p*-values: \*\*\* *p* < 0.001, \*\* *p* < 0.01, \* *p* < 0.05. Detailed information about Western blot can be found at Figure S5.

#### 2.4. Suppression of IFN Signalling by SOCS1 Expression or IRF9 Knockdown Promotes the Mesenchymal Phenotype

In cells, the fine tuning of the JAK/STAT signalling is naturally provided by the suppressor of cytokine signalling (SOCS) proteins, which function as negative regulators of the signalling pathway. To determine whether the overexpression of the SOCS proteins can directly affect melanoma invasion and/or suppress the effect of IFN $\beta$ , we prepared stable cell lines bearing EGFP-tagged doxycycline-inducible SOCS1 and SOCS3 (iSOCS1 and iSOCS3) gene expression constructs (Figure S6a). We confirmed the high efficacy of iSOCS1 and iSOCS3 proteins by testing their ability to block interferon-induced phosphorylation of Stat1 and Stat2 proteins (Figures S3 and S6b). The induced expression of both SOCS1 and SOCS3 was able to block the IFN $\beta$  mediated round phenotype (Figure 4b); however, only SOCS1 altered WM3629 morphology directly by promoting the mesenchymal phenotype (Figure 4a,b). To study this further, we analysed cell lysates from WM3629 control cells and cells with induced expression of iSOCS1 and iSOCS3 untreated and treated with IFN $\beta$ . We revealed that, unlike SOCS3, SOCS1 decreases the total level of Stat1, but also IRF9, providing an explanation for its stronger pro-mesenchymal activity (Figure 4c). Accordingly, the induced expression of SOCS1, but not SOCS3, was able to prevent HT1080 cells from undergoing MAT in response to DAS (Figures S3 and S7).

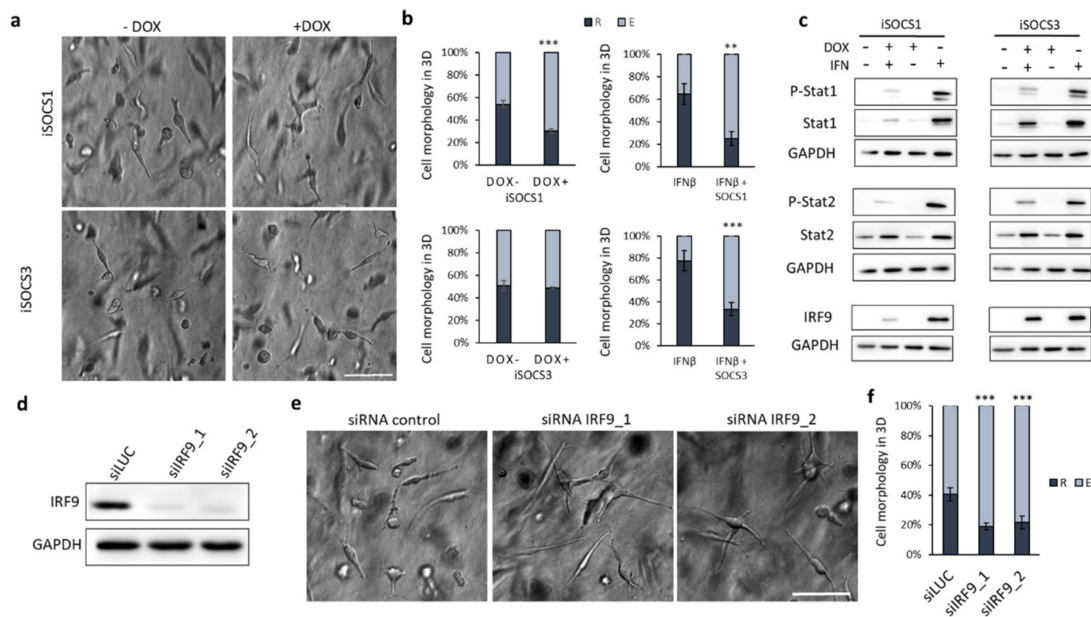


**Figure 4.** Downregulation of IFN signalling by IRF9 knockdown or SOCS1 expression promotes the mesenchymal phenotype. **(a)** Representative image of WM3629 after 48 h in 3D collagen expressing inducible SOCS1 and SOCS3 (iSOCS1 and iSOCS3). **(b)** Quantification of morphology of WM3629 cells with induced expression of iSOCS1 and iSOCS3 alone (left) and pre-treated with IFN $\beta$  (right) cultured in 3D collagen for 48 h (overall exposure to IFN $\beta$  96 h). **(c)** Immunoblotting for proteins in samples of WM3629 cells with iSOCS1 and iSOCS3 expression treated with doxycycline (DOX) and/or IFN $\beta$  (48 h). **(d)** Downregulation of IRF9 after siRNA KD verified by immunoblotting. **(e)** Representative image of WM3629 cells in 3D collagen treated with siRNA. **(f)** Quantification of morphology of WM3629 cells with siRNA KD of IRF9 in 3D collagen. Scale bar 100  $\mu$ m. R = round, E = elongated. *p*-values: \*\*\* *p* < 0.001, \*\* *p* < 0.01. Detailed information about Western blot can be found at Figure S8.

After demonstrating that SOCS1 decreases IRF9 protein levels, we went further and investigated the effect of siRNA knockdown (KD) of IRF9. Using two different siRNAs, we successfully decreased the expression of IRF9 (Figure 4d), which, in turn, shifted the cells to more mesenchymal phenotypes, presumably by disrupting the ISGF3 complex (Figure 4e). IRF9 KD also significantly decreased the pro-amoeboid effect of IFN $\beta$  (Figure S2e). Collectively, our results demonstrate that ISGF3 activity contributes to the maintenance of the amoeboid phenotype and its suppression results in the loss of amoeboid traits and cell elongation.

### 3. Discussion

Here, we have identified a novel mechanism of invasion plasticity regulation governed by IFN signalling mediated by Stat1/Stat2/IRF9 (ISGF3). We show that HT1080 cells induced to undergo MAT upregulate type I IFN signalling (Figure 1). Concordantly, the upregulation of ISGF3 signalling by IFN $\beta$  treatment induces MAT in melanoma cells (Figure 2d,e). Notably, the downregulation of ISGF3 signalling by various approaches suppresses the round amoeboid phenotype and leads to cell elongation (Figures 2a–c and 4). Thus, ISGF3 signalling might act as a rheostat favouring either the amoeboid phenotype or the mesenchymal phenotype depending on the activation level, providing cells with an invasion plasticity regulatory mechanism responsive to extra- and intracellular signalling cues.

IFN $\beta$  has been demonstrated to exert anti-cancer activities mainly through the attenuation of cell proliferation [35] and the facilitation of anti-tumour immune reaction [26] and has, therefore, been utilized in the treatment of melanoma as a form of cytokine therapy [36]. However, it was also identified as a pro-tumorigenic factor in fibromatosis [37]. Moreover, Stat1, the key effector of the IFN $\beta$  signal, was found to play a tumour promoter role in some cases of carcinoma, lymphoma and

leukaemia [38]. Proteomic analysis of human triple negative breast tumours revealed that Stat1-positive tumours were more aggressive with increased invasion and lymph node metastasis [39]. Recently, a study analysing three public datasets to identify an epithelial–mesenchymal–amoeboid transition gene signature as a metastasis risk predictor in breast cancer was published [40]. Interestingly, the MAT-associated gene signature derived from this analysis is enriched with type I interferon-response genes (adj.  $p$ -value  $4.3 \times 10^{-7}$ ) and shows a similar gene enrichment profile as HT1080 cells after MAT (for further information see File S1).

The tumour mass is exposed to various endogenous stress signals, such as hypoxia, nutrient deprivation but also exogenous stress arising in response to chemotherapy and radiation, which all result in upregulated stress signalling, leading to the secretion of various soluble factors, including IFN $\beta$  [41]. Moreover, it was demonstrated that direct contact between cancer cells and cancer-associated fibroblasts (CAFs) can lead to the transfer of double stranded DNA from cancer cells to fibroblasts. This interaction triggers the cGAS-STING mediated production of IFN $\beta$  in CAFs [42]. This can result in prolonged activation of Stat1/Stat2/IRF9 and, as we suggest, promote amoeboid invasion. In line with this hypothesis, it was recently described that, under hypoxia, epithelial cells undergo a switch from collective to amoeboid invasion [43]. Amoeboid migration is the primordial way of cell migration in metazoans, in an adult organism normally used only by cells of the immune system, but inducible in many (if not all) cancer cells by specific conditions in the tumour microenvironment. Such conditions seem to be de-adhesion from ECM in necrotic areas and dense cell masses, hypoxia, and signalling induced by inflammatory and other ligands released by both the tumour stroma cells and cancer cells themselves [3,43].

There is also increasing evidence that the upregulation of interferon signalling intrinsically present in TME or in response to cell stress promotes the resistance of cancer cells to therapy. IFN $\beta$  activated ISGF3 is responsible for constitutive resistance to DNA damage [44]. The upregulation of IRF9 was observed in cells when cultivated in 3D spheroids compared to 2D cultures [45], which was shown to promote resistance to chemotherapeutic drugs [46]. Moreover, IRF9 overexpression leads to resistance to microtubule-targeting drugs [47], and the overexpression of Stat1 is associated with resistance to radiation [48]. IFN $\beta$  also promotes the immune escape of glioma cells [49] by increased expression of PDL-1, which we also detected in our samples (Figure 3b).

The precise molecular mechanism underlying the MAT induced by IFN $\beta$  is still to be discovered; nevertheless, some clues and parallels can be found in published works. The activation of microglia results in a change in their morphology into an amoeboid shape and an enhanced migratory capacity [50]. This could be among other stimuli also achieved by IFN $\beta$  produced by microglia or added exogenously [51]. IFN $\beta$  might promote invasion plasticity by upregulating the expression of pro-invasive cytokines, such as IL6 or invasion-associated molecules, such as IFITM1 [52–54] or MX1 [55]. Accordingly, we show that treatment with IFN $\beta$  promotes the invasion of WM3629 cells from spheroids and increases the number of individually invading cells, most of which utilize the round, amoeboid invasion mode (Figure 3c).

There are several crosstalk mechanisms connecting JAK/STAT signalling to key cytoskeleton dynamics regulators. The ISG15 gene, regulated by Stat1, is one of the crucial effectors of interferon signalling. The ISG15 protein, a small ubiquitin-like covalent modifier, gets attached to numerous target proteins in a process called “isgylation” to affect their activities. ISG15 can disrupt cytoskeletal architecture and promote motility in human breast cancer cells [56,57]. Cytoskeleton remodelling and associated signalling was found to be regulated by the isgylation of IQGAP1 [58,59], non-muscle myosin IIA [60] and filamin B [61]. The activation of Stat1 by focal adhesion kinase FAK is involved in integrin-mediated cell migration and adhesion [62,63]. Cancer cell invasion plasticity is known to be controlled by shifting the balance in the mutually antagonistic regulation of Rac1 and RhoA. Interestingly, the loss of Rac1 in murine keratinocytes decreased actin polymerization and caused the Arp2/3-dependent upregulation of STAT1 and increased interferon sensitivity [64]. Altogether these

results show that interferon signalling and Stat1 expression and activity are integrated in a complex regulatory network, also encompassing the actin cytoskeleton.

Here we show that exposure of human melanoma cells to IFN $\beta$  may lead to acquisition of the amoeboid phenotype and greatly increase the number of individually migrating cells from spheroids in 3D collagen in vitro. We are aware that these conditions cannot reflect the complexity of TME in vivo, nor can the use of cancer cell lines remove the heterogeneity of cell populations within the tumour microenvironment and crosstalk between malignant and healthy cells. However, various studies have shown that in vitro cultured melanoma cells are a relevant models for primary melanomas [65,66]. Therefore, it may be anticipated that the demonstrated effects of IFN $\beta$  on cancer cells kept in 3D culture are paralleled in primary tumours where IFN $\beta$  is known to come from several sources. Notably, human melanoma cells were shown to produce IFN $\beta$  and are capable of suppressing their own proliferation via the secretion of endogenous IFN $\beta$  [36]. It can be speculated that this mechanism could be potentially involved in the switching of human melanoma cells between proliferative and invasive states [67]. Since invasiveness is the most dangerous characteristic of melanoma cells [1], altogether these findings may have important implications for melanoma therapy with IFN $\beta$ .

## 4. Materials and Methods

### 4.1. Data Analysis

Transcriptomic data used for the analysis are available from ArrayExpress database at EMBL-EBI under accession number E-MTAB-6823. Only genes significantly affected in both MAT datasets (with criteria FC  $\geq$  1.5, adjusted *p*-value  $\leq$  0.25) were selected for the subsequent analysis of gene enrichment using the online tool ShinyGO v0.61 [30].

### 4.2. Cell Lines, Constructs, and Transfection

All cell lines used were of human origin and were routinely cultivated in DMEM medium supplemented by 10% FBS and 10  $\mu$ g/ $\mu$ L ciprofloxacin (Sigma, Piscataway, NJ, USA) in a humidified atmosphere with 5% CO $_2$  at 37  $^{\circ}$ C. Transfections were performed using polyethylenimine (Polysciences, Inc., Warrington, PA, USA) or GenMute transfection reagent (SignaGen Laboratories, Frederick, MD, USA) in the case of DNA and siRNA, respectively, according to manufacturer's protocol. Stable cell lines were prepared by lentiviral transduction using the second-generation packaging system (pLVX constructs, Tet-On Advanced Gene expression system, Clontech, Mountain View, CA, USA) and enriched by cell sorting, based on EGFP expression. In the case of IFN-treated cells used for morphology studies, RNA and protein lysates, cells were pre-treated with 10 ng/mL recombinant human IFNs (Peprotech, Cranbury, NJ, USA) for 48 hours and IFNs were also present during subsequent 3D cultures (overall exposure time 96 h). Ruxolitinib (Sigma) was used at a concentration of 10  $\mu$ M, dasatinib (LC Laboratories, Woburn, MA, USA) at 1  $\mu$ M and doxycycline (Sigma, Piscataway, NJ, USA) at 250 ng/mL. The siRNA sequences targeting IRF9 mRNA were: siIRF9\_1: 5'-GCAGAGACUUGGUCAGGUC-3' and siIRF9\_2 5'-CACAGAAUCUUAUCACAGU-3'.

### 4.3. Three-Dimensional Cell Culture and Morphology Analysis

For 3D collagen cultures, cells were mixed with buffer solution and rat tail collagen on ice and plated in wells. After 15 min incubation at 37  $^{\circ}$ C, the gelled samples were overlaid with cultivation medium containing 1% FBS. The resulting composition of the collagen matrix was 1 mg/mL collagen, 1 $\times$ RPMI medium, 15 mM HEPES, 1% foetal bovine serum and 50  $\mu$ g/mL gentamicin. For treated samples, compounds were added to overlaying medium. Cells were cultivated in 3D collagen for 48 hours before further analysis for all applications, except for siRNA treatments that were analysed after 24 h. All images of cells were acquired by Nikon ECLIPSE TE2000-S microscope using Hoffman modulation contrast (10 $\times$ /0.25 objectives). The morphology of cells was analysed using Fiji software. Cells were considered "elongated" (E) when their length/width ratio was greater than 2, otherwise

they were considered “round” (R). A minimum of 100 cells per condition and replicate was analysed and the presented data are summarized from at least 3 independent biological replicates.

#### 4.4. Immunoblotting

Protein lysates were prepared from 2D cell cultures, or 3D collagen cultures, where indicated. In the case of 2D samples, cells were harvested and transferred to 1× lysis buffer (1% SDS, 10% glycerol, 60 mM Tris, pH 6.8). For 3D protein lysates, cells were seeded at a density of 1 million cells per 500 µL of 3D collagen gel and cultivated for 48 hours. Gels from two wells per sample were transferred to tubes containing 2× lysis buffer and homogenized using Tissue Tearor (BioSpec Products, Bartlesville, OK, USA). The lysates were processed as described previously [68]. Briefly, lysates were centrifuged, supernatant transferred to new tubes and protein concentration was determined using the DCTM Protein Assay (Bio-Rad Laboratories, Hercules, California, CA, USA) and adjusted to the same protein concentration with 1× SDS lysis buffer. Before SDS-PAGE, DTT (final concentration 50 mM) and bromophenol blue (final concentration 30 µM) were added, and the samples were incubated at 95 °C for 10 min. Samples were run on 10% SDS-polyacrylamide gels and transferred onto nitrocellulose membrane. To prevent non-specific binding, membranes were incubated in TBST with 5% BSA or skim milk and incubated with primary antibodies at 4 °C overnight. The following primary antibodies were used: P-Stat1 (Thermo Fisher Scientific, Waltham, MA, USA; #MA5-15071), P-Stat2 (CST, Danvers, MA, USA; #88410), P-Stat3 (CST; #9145), Stat1 (Thermo Fisher Scientific; #MA5-15129), Stat2 (CST; #72604), Stat3 (CST; #12640), IRF9 (CST; #76684), Jak1 (CST; #3344), MX1 (CST; #37849) and GAPDH (Thermo Fisher Scientific; #MA5-15738). The Western blot images shown are representative of 3 independent biological replicates.

#### 4.5. Reverse Transcription–Quantitative Polymerase Chain Reaction (RT-qPCR)

For RNA lysates, cells were seeded at a density of 1 million per 500 µL 3D collagen gel and cultivated for 48 hours. In the case of IFN-treated samples, IFNs were added to overlaying medium (1% FBS). For RNA isolation, two collagen gels per sample were added to tubes containing 600 µL RNA extraction solution (60% *v/v* water-saturated phenol, 3.25 M guanidine thiocyanate, 400 mM sodium acetate buffer pH 4.0, 0.4% *w/v* N-lauroylsarcosine and 160 mM 2-mercaptoethanol) and 100 µL of 6.1 M sodium chloride. Samples were then homogenized using Tissue Tearor (BioSpec Products). RNA was isolated using the modified Trizol method, as described previously [68] and used further for reverse transcription. All RT-qPCR experiments were performed according to MIQE guidelines [69]. For primer details, see Table S1. The C<sub>q</sub> values were set by applying a single threshold value for each target using Bio-Rad CFX Manager 3.1 (Bio-Rad Laboratories, Hercules, CA, USA) and exported and further analysed using qBase+ 3.1 software (Biogazelle, Zwijnaarde, Belgium). The list of primers and reference genes is available in Table S1. The obtained data were statistically analysed in GraphPad Prism 6 (GraphPad Software, Inc., San Diego, CA, USA) using paired two-tailed t-test for HT1080 data and one-way ANOVA for WM3629 data.

#### 4.6. Three-Dimensional Invasion Spheroid Assay

To obtain spheroids, cells were grown in a 3D Petri Dish<sup>®</sup> (Microtissues<sup>®</sup>; #12-81 large spheroids, Sigma, Piscataway, NJ, USA) according to manufacturer’s protocol for 2 days in cultivation medium (in case of IFN-treated samples, IFN $\beta$  was added). Next, the spheroids were embedded into the 3D collagen matrix and overlaid with cultivation medium. Images of spheroids were taken immediately after embedding into collagen (before) and after 96 hours (after). The area and circularity of the spheroids before and after invasion was assessed using Fiji software (Rasband, W.S., ImageJ, NIH, Bethesda, MD, USA). The data were statistically analysed in GraphPad Prism 6 using one-way ANOVA. Presented data were summarized from 4 independent biological replicates, and at least 4 spheroids per condition, and replicates were analysed.



#### 4.7. Proliferation Assay in 3D Collagen

Untreated and IFN-treated cells were seeded into collagen matrix (40,000 cells/100 µL collagen matrix; 4 technical replicates per sample) in a 96-well and cultivated for 48 h. Next, the overlaying medium was replaced by phenol-red free medium containing AlamarBlue reagent (Invitrogen, Carlsbad, CA, USA) in a 5:1 ratio and cultivated for 4 hours. The medium containing AlamarBlue was then transferred to new wells and fluorescence (excitation 550 nm; emission 590 nm) was measured using the Infinite M200 Pro plate fluorimeter (TECAN, Mannedorf, Switzerland). Collagen without cells served as a blank for the experiment. The results are summarized from 3 independent biological replicates. The data were statistically analysed in GraphPad Prism 6 using one-way ANOVA.

## 5. Conclusions

Collectively, previous studies and our results suggest that, in response to stress, metastatic cells may activate IFN associated signalling and gain a rounded amoeboid phenotype. We show that although IFN $\beta$  decreases cancer cell proliferation, it promotes invasion plasticity, which can endow cancer cells with an escape mechanism from local stress inducing conditions. In summary, we point out the role of IFN $\beta$  activated Stat1/Stat2/IRF9 signalling in cancer invasion plasticity, aside from its known role as a tumour suppressor.

**Supplementary Materials:** The following are available online at <http://www.mdpi.com/2072-6694/12/9/2450/s1>, Figure S1: Detailed information about Western blot in Figure 1, Figure S2: Additional Characterization of IFN treated cells, Figure S3: Detailed information about Western blot, Figure S4: Detailed information about Western blot in Figure 2, Figure S5: Detailed information about Western blot in Figure 3, Figure S6: Establishment of WM3629 stable cell lines expressing EGFP-tagged doxycycline-inducible SOCS1 and SOCS3, Figure S7: Expression of iSOCS1 can prevent dasatinib-induced MAT in HT1080 cells, Figure S8: Detailed information about Western blot in Figure 4, Table S1: RT-qPCR primers used in the work, Video S1: WM3629 IFN $\beta$ . File S1: Gene Ontology Enrichment Analysis.

**Author Contributions:** Conceptualization, A.G., V.Č., J.B. and D.R.; methodology, A.G., A.-M.Š.; validation, A.G. and A.-M.Š.; investigation, A.G., A.-M.Š., V.Č. and L.M.; writing—original draft preparation, A.G.; writing—review and editing, A.G., V.Č., J.B. and D.R.; visualization, A.G.; supervision, J.B. and D.R.; funding acquisition, A.G., J.B. and D.R. All authors have read and agreed to the published version of the manuscript.

**Funding:** The research was funded by the Charles University Grant Agency, project GA UK No. 1292217. The project was also supported by the project “Center for Tumour Ecology – Research of the Cancer Microenvironment Supporting Cancer Growth and Spread” (CZ.02.1.01/0.0/0.0/16\_019/ 0000785), supported by the Operational Programme Research, Development, and Education. Part of the study was performed using the equipment for metabolomics and cell analyses (Grant no. CZ.1.05/2.1.00/19.0400) supported by the Research and Development for Innovations Operational Program, co-financed by the European regional development fund and the state budget of the Czech Republic.

**Acknowledgments:** The authors thank Marie Charvátová for excellent technical support. We acknowledge the BIOCEV Gene Core facility.

**Conflicts of Interest:** The authors declare no conflict of interest.

## References

1. Gandalovičová, A.; Rosel, D.; Fernandes, M.; Veselý, P.; Heneberg, P.; Čermák, V.; Petruželka, L.; Kumar, S.; Sanz-Moreno, V.; Brábek, J. Migrastatics—Anti-metastatic and Anti-invasion Drugs: Promises and Challenges. *Trends Cancer* **2017**, *3*, 391–406. [[CrossRef](#)]
2. Rosel, D.; Fernandes, M.; Sanz-Moreno, V.; Brábek, J. Migrastatics: Redirecting R&D in Solid Cancer towards Metastasis? *Trends Cancer* **2019**, *5*, 755–756. [[CrossRef](#)]
3. Odenthal, J.; Takes, R.; Friedl, P. Plasticity of tumor cell invasion: Governance by growth factors and cytokines. *Carcinogenesis* **2016**. [[CrossRef](#)]
4. Roizen, M. Hallmarks of Cancer: The Next Generation. *Cell* **2011**, *144*, 646–674. [[CrossRef](#)]
5. Brábek, J.; Mierke, C.T.; Rosel, D.; Veselý, P.; Fabry, B. The role of the tissue microenvironment in the regulation of cancer cell motility and invasion. *Cell Commun. Signal.* **2010**, *8*, 22. [[CrossRef](#)] [[PubMed](#)]

6. Parekh, A.; Weaver, A.M. Regulation of cancer invasiveness by the physical extracellular matrix environment. *Cell Adhes. Migr.* **2009**, *3*, 288–292. [[CrossRef](#)] [[PubMed](#)]
7. Friedl, P.; Alexander, S. Cancer Invasion and the Microenvironment: Plasticity and Reciprocity. *Cell* **2011**, *147*, 992–1009. [[CrossRef](#)] [[PubMed](#)]
8. Pánková, K.; Rosel, D.; Novotný, M.; Brábek, J. The molecular mechanisms of transition between mesenchymal and amoeboid invasiveness in tumor cells. *Cell. Mol. Life Sci.* **2009**, *67*, 63–71. [[CrossRef](#)] [[PubMed](#)]
9. Friedl, P.; Locker, J.; Sahai, E.; Segall, J.E. Classifying collective cancer cell invasion. *Nat. Cell Biol.* **2012**, *14*, 777–783. [[CrossRef](#)] [[PubMed](#)]
10. Tolde, O.; Gandalovičová, A.; Křížová, A.; Veselý, P.; Chmelík, R.; Rosel, D.; Brábek, J. Quantitative phase imaging unravels new insight into dynamics of mesenchymal and amoeboid cancer cell invasion. *Sci. Rep.* **2018**, *8*, 12020. [[CrossRef](#)]
11. Friedl, P.; Wolf, K. Proteolytic interstitial cell migration: A five-step process. *Cancer Metastasis Rev.* **2009**, *28*, 129–135. [[CrossRef](#)] [[PubMed](#)]
12. Wyckoff, J.B.; Pinner, S.E.; Gschmeissner, S.; Condeelis, J.S.; Sahai, E. ROCK- and Myosin-Dependent Matrix Deformation Enables Protease-Independent Tumor-Cell Invasion In Vivo. *Curr. Biol.* **2006**, *16*, 1515–1523. [[CrossRef](#)] [[PubMed](#)]
13. Lämmermann, T.; Sixt, M. Mechanical modes of ‘amoeboid’ cell migration. *Curr. Opin. Cell Biol.* **2009**, *21*, 636–644. [[CrossRef](#)] [[PubMed](#)]
14. Pandya, P.; Orgaz, J.L.; Sanz-Moreno, V. Modes of invasion during tumour dissemination. *Mol. Oncol.* **2016**, *11*, 5–27. [[CrossRef](#)]
15. Gandalovičová, A.; Vomastek, T.; Rosel, D.; Brábek, J. Cell polarity signaling in the plasticity of cancer cell invasiveness. *Oncotarget* **2016**, *7*, 25022–25049. [[CrossRef](#)]
16. Čermák, V.; Gandalovičová, A.; Merta, L.; Harant, K.; Rösel, D.; Brábek, J. High-throughput transcriptomic and proteomic profiling of mesenchymal-amoeboid transition in 3D collagen. *Sci. Data* **2020**, *7*, 1–11. [[CrossRef](#)]
17. Boekhorst, V.T.; Friedl, P. Plasticity of Cancer Cell Invasion—Mechanisms and Implications for Therapy. *Adv. Cancer Res.* **2016**, *132*, 209–264. [[CrossRef](#)]
18. Sanz-Moreno, V.; Gaggioli, C.; Yeo, M.; Albregues, J.; Wallberg, F.; Virós, A.; Hooper, S.; Mitter, R.; Féral, C.C.; Cook, M.; et al. ROCK and JAK1 Signaling Cooperate to Control Actomyosin Contractility in Tumor Cells and Stroma. *Cancer Cell* **2011**, *20*, 229–245. [[CrossRef](#)]
19. Georgouli, M.; Herraiz, C.; Crosas-Molist, E.; Fanshawe, B.; Maiques, O.; Perdrix, A.; Pandya, P.; Rodriguez-Hernandez, I.; Ilieva, K.M.; Cantelli, G.; et al. Regional Activation of Myosin II in Cancer Cells Drives Tumor Progression via a Secretory Cross-Talk with the Immune Microenvironment. *Cell* **2019**, *176*, 757–774. [[CrossRef](#)]
20. Hölzel, M.; Tüting, T. Inflammation-Induced Plasticity in Melanoma Therapy and Metastasis. *Trends Immunol.* **2016**, *37*, 364–374. [[CrossRef](#)]
21. Ivashkiv, L.B.; Donlin, L.T. Regulation of type I interferon responses. *Nat. Rev. Immunol.* **2013**, *14*, 36–49. [[CrossRef](#)] [[PubMed](#)]
22. Platanias, L.C. Mechanisms of type-I- and type-II-interferon-mediated signalling. *Nat. Rev. Immunol.* **2005**, *5*, 375–386. [[CrossRef](#)] [[PubMed](#)]
23. Einav, U.; Tabach, Y.; Getz, G.; Yitzhaky, A.; Ozbek, U.; Amariglio, N.; Izraeli, S.; Rechavi, G.; Domany, E. Gene expression analysis reveals a strong signature of an interferon-induced pathway in childhood lymphoblastic leukemia as well as in breast and ovarian cancer. *Oncogene* **2005**, *24*, 6367–6375. [[CrossRef](#)] [[PubMed](#)]
24. Weichselbaum, R.R.; Ishwaran, H.; Yoon, T.; Nuyten, D.S.A.; Baker, S.W.; Khodarev, N.; Su, A.W.; Shaikh, A.Y.; Roach, P.; Kreike, B.; et al. An interferon-related gene signature for DNA damage resistance is a predictive marker for chemotherapy and radiation for breast cancer. *Proc. Natl. Acad. Sci. USA* **2008**, *105*, 18490–18495. [[CrossRef](#)] [[PubMed](#)]
25. Aoyagi, S.; Hata, H.; Homma, E.; Shimizu, H. Sequential Local Injection of Low-Dose Interferon-Beta for Maintenance Therapy in Stage II and III Melanoma: A Single-Institution Matched Case-Control Study. *Oncology* **2012**, *82*, 139–146. [[CrossRef](#)]
26. Fujimura, T.; Okuyama, R.; Ohtani, T.; Ito, Y.; Haga, T.; Hashimoto, A.; Aiba, S. Perilesional treatment of metastatic melanoma with interferon- $\beta$ . *Clin. Exp. Dermatol.* **2009**, *34*, 793–799. [[CrossRef](#)]

27. Uehara, J.; Ohkuri, T.; Kosaka, A.; Ishibashi, K.; Hirata, Y.; Ohara, K.; Nagato, T.; Oikawa, K.; Aoki, N.; Harabuchi, Y.; et al. Intratumoral injection of IFN- $\beta$  induces chemokine production in melanoma and augments the therapeutic efficacy of anti-PD-L1 mAb. *Biochem. Biophys. Res. Commun.* **2017**, *490*, 521–527. [[CrossRef](#)]
28. Kakizaki, A.; Fujimura, T.; Furudate, S.; Kambayashi, Y.; Yamauchi, T.; Yagita, H.; Aiba, S. Immunomodulatory effect of peritumorally administered interferon-beta on melanoma through tumor-associated macrophages. *OncoImmunology* **2015**, *4*, e1047584. [[CrossRef](#)]
29. Čermák, V. Differential Expression Analyses Figshare Dataset. 2019. Available online: [https://figshare.com/articles/Differential\\_expression\\_analyses/10329281/2](https://figshare.com/articles/Differential_expression_analyses/10329281/2) (accessed on 25 August 2020).
30. Ge, S.; Jung, D.; Yao, R. ShinyGO: A graphical gene-set enrichment tool for animals and plants. *Bioinformatics* **2019**, *36*, 2628–2629. [[CrossRef](#)]
31. Cooper, S.; Sadok, A.; Bousgouni, V.; Bakal, C. Apolar and polar transitions drive the conversion between amoeboid and mesenchymal shapes in melanoma cells. *Mol. Biol. Cell* **2015**, *26*, 4163–4170. [[CrossRef](#)]
32. Arozarena, I.; Wellbrock, C. Phenotype plasticity as enabler of melanoma progression and therapy resistance. *Nat. Rev. Cancer* **2019**, *19*, 377–391. [[CrossRef](#)] [[PubMed](#)]
33. Lazar-Molnar, E.; Hegyesi, H.; Tóth, S.; Falus, A. Autocrine and Paracrine Regulation by Cytokines and Growth Factors in Melanoma. *Cytokine* **2000**, *12*, 547–554. [[CrossRef](#)] [[PubMed](#)]
34. Michalska, A.; Blaszczyk, K.; Wesoly, J.; Bluysen, H.A. A Positive Feedback Amplifier Circuit That Regulates Interferon (IFN)-Stimulated Gene Expression and Controls Type I and Type II IFN Responses. *Front. Immunol.* **2018**, *9*, 1135. [[CrossRef](#)] [[PubMed](#)]
35. Medrano, R.F.; Hunger, A.; Mendonça, S.A.; Barbuto, J.A.M.; Strauss, B.E. Immunomodulatory and antitumor effects of type I interferons and their application in cancer therapy. *Oncotarget* **2017**, *8*, 71249–71284. [[CrossRef](#)]
36. Satomi, H.; Wang, B.; Fujisawa, H.; Otsuka, F. Interferon- $\beta$  from melanoma cells suppresses the proliferations of melanoma cells in an autocrine manner. *Cytokine* **2002**, *18*, 108–115. [[CrossRef](#)]
37. Tjandra, S.S.; Hsu, C.; Goh, I.; Gurung, A.; Poon, R.; Nadesan, P.; Alman, B.A. IFN- Signaling Positively Regulates Tumorigenesis in Aggressive Fibromatosis, Potentially by Modulating Mesenchymal Progenitors. *Cancer Res.* **2007**, *67*, 7124–7131. [[CrossRef](#)]
38. Zhang, Y.; Liu, Z. STAT1 in cancer: Friend or foe? *Discov. Med.* **2017**, *24*, 19–29.
39. Greenwood, C.; Metodiev, G.; Al-Janabi, K.; Lausen, B.; Alldridge, L.; Leng, L.; Bucala, R.; Fernández, N.; Metodiev, M.V. Stat1 and CD74 overexpression is co-dependent and linked to increased invasion and lymph node metastasis in triple-negative breast cancer. *J. Proteom.* **2012**, *75*, 3031–3040. [[CrossRef](#)]
40. Emad, A.; Ray, T.; Jensen, T.W.; Parat, M.; Natrajan, R.; Sinha, S.; Ray, P.S. Superior breast cancer metastasis risk stratification using an epithelial-mesenchymal-amoeboid transition gene signature. *Breast Cancer Res.* **2020**, *22*, 1–13. [[CrossRef](#)]
41. Cheon, H.; Borden, E.C.; Stark, G.R. Interferons and Their Stimulated Genes in the Tumor Microenvironment. *Semin. Oncol.* **2014**, *41*, 156–173. [[CrossRef](#)]
42. Iriarte, A.R.; Arwert, E.; Milford, E.; Chakravarty, P.; Melcher, A.; Harrington, K.; Sahai, E. Interaction between cancer associated fibroblasts and cancer cells influence immune infiltrate and is modulated by therapeutic agents. *Ann. Oncol.* **2018**, *29*, viii657. [[CrossRef](#)]
43. Lehmann, S.; Boekhorst, V.T.; Odenthal, J.; Bianchi, R.; Van Helvert, S.; Ikenberg, K.; Ilina, O.; Stoma, S.; Xandry, J.; Jiang, L.; et al. Hypoxia Induces a HIF-1-Dependent Transition from Collective-to-Amoeboid Dissemination in Epithelial Cancer Cells. *Curr. Biol.* **2017**, *27*, 392–400. [[CrossRef](#)] [[PubMed](#)]
44. Cheon, H.; Holvey-Bates, E.G.; Schoggins, J.W.; Forster, S.C.; Hertzog, P.; Imanaka, N.; Rice, C.M.; Jackson, M.W.; Junk, D.J.; Stark, G.R. IFN $\beta$ -dependent increases in STAT1, STAT2, and IRF9 mediate resistance to viruses and DNA damage. *EMBO J.* **2013**, *32*, 2751–2763. [[CrossRef](#)] [[PubMed](#)]
45. Edsbäcker, E.; Serviss, J.T.; Kolosenko, I.; Palm-Apergi, C.; De Milito, A.; Tamm, K.P. STAT3 is activated in multicellular spheroids of colon carcinoma cells and mediates expression of IRF9 and interferon stimulated genes. *Sci. Rep.* **2019**, *9*, 536. [[CrossRef](#)] [[PubMed](#)]
46. Kolosenko, I.; Fryknäs, M.; Forsberg, S.; Johnsson, P.; Cheon, H.; Holvey-Bates, E.G.; Edsbäcker, E.; Pellegrini, P.; Rassoolzadeh, H.; Brnjic, S.; et al. Cell crowding induces interferon regulatory factor 9, which confers resistance to chemotherapeutic drugs. *Int. J. Cancer* **2014**, *136*, E51–E61. [[CrossRef](#)]
47. E Luker, K.; Pica, C.M.; Schreiber, R.D.; Piwnica-Worms, D. Overexpression of IRF9 confers resistance to antimicrotubule agents in breast cancer cells. *Cancer Res.* **2001**, *61*, 6540–6547.

48. Khodarev, N.N.; Beckett, M.; Labay, E.; Darga, T.; Roizman, B.; Weichselbaum, R.R. STAT1 is overexpressed in tumors selected for radioresistance and confers protection from radiation in transduced sensitive cells. *Proc. Natl. Acad. Sci. USA* **2004**, *101*, 1714–1719. [[CrossRef](#)]
49. Silginer, M.; Nagy, S.; Happold, C.; Schneider, H.; Weller, M.; Roth, P. Autocrine activation of the IFN signaling pathway may promote immune escape in glioblastoma. *Neuro Oncol.* **2017**, *19*, 1338–1349. [[CrossRef](#)]
50. Ransohoff, R.M.; Cardona, A.E. The myeloid cells of the central nervous system parenchyma. *Nature* **2010**, *468*, 253–262. [[CrossRef](#)]
51. Scheu, S.; Ali, S.; Mann-Nüttel, R.; Richter, L.; Arolt, V.; Dannlowski, U.; Kuhlmann, T.; Klotz, L.; Alferink, J. Interferon  $\beta$ -Mediated Protective Functions of Microglia in Central Nervous System Autoimmunity. *Int. J. Mol. Sci.* **2019**, *20*, 190. [[CrossRef](#)]
52. Ogony, J.; Choi, H.J.; Lui, A.; Cristofanilli, M.; Lewis-Wambi, J. Interferon-induced transmembrane protein 1 (IFITM1) overexpression enhances the aggressive phenotype of SUM149 inflammatory breast cancer cells in a signal transducer and activator of transcription 2 (STAT2)-dependent manner. *Breast Cancer Res.* **2016**, *18*, 25. [[CrossRef](#)] [[PubMed](#)]
53. Nan, J.; Wang, Y.; Yang, J.; Stark, G.R. IRF9 and unphosphorylated STAT2 cooperate with NF- $\kappa$ B to drive IL6 expression. *Proc. Natl. Acad. Sci. USA* **2018**, *115*, 3906–3911. [[CrossRef](#)] [[PubMed](#)]
54. Jobe, N.P.; Rosel, D.; Dvořánková, B.; Kodet, O.; Lacina, L.; Mateu, R.; Smetana, K.; Brábek, J.; Smetana, K. Simultaneous blocking of IL-6 and IL-8 is sufficient to fully inhibit CAF-induced human melanoma cell invasiveness. *Histochem. Cell Biol.* **2016**, *146*, 205–217. [[CrossRef](#)]
55. Croner, R.S.; Sturzl, M.; Rau, T.T.; Metodieva, G.; Geppert, C.I.; Naschberger, E.; Lausen, B.; Metodiev, M.V. Quantitative proteome profiling of lymph node-positive vs. -negative colorectal carcinomas pinpoints MX1 as a marker for lymph node metastasis. *Int. J. Cancer* **2014**, *135*, 2878–2886. [[CrossRef](#)]
56. Desai, S.D.; E Reed, R.; Burks, J.; Wood, L.M.; Pullikuth, A.K.; Haas, A.L.; Liu, L.F.; Breslin, J.W.; Meiners, S.; Sankar, S. ISG15 disrupts cytoskeletal architecture and promotes motility in human breast cancer cells. *Exp. Biol. Med.* **2012**, *237*, 38–49. [[CrossRef](#)]
57. Burks, J.; Reed, R.E.; Desai, S.D. ISGylation governs the oncogenic function of Ki-Ras in breast cancer. *Oncogene* **2013**, *33*, 794–803. [[CrossRef](#)]
58. Cruz, A.C.T.; González, C.C.C.; Cruz-Ramos, E.; Jarquín, J.O.R.; Romero-Mandujano, A.K.; Sosa-Garrocho, M. Interplay between interferon-stimulated gene 15/ISGylation and interferon gamma signaling in breast cancer cells. *Cell. Signal.* **2019**, *54*, 91–101. [[CrossRef](#)]
59. Cerikan, B.; Shaheen, R.; Colo, G.P.; Gläßer, C.; Hata, S.; Knobloch, K.-P.; Alkuraya, F.S.; Fässler, R.; Schiebel, E. Cell-Intrinsic Adaptation Arising from Chronic Ablation of a Key Rho GTPase Regulator. *Dev. Cell* **2016**, *39*, 28–43. [[CrossRef](#)]
60. Cruz-Ramos, E.; Macías-Silva, M.; Sandoval-Hernández, A.; Tecalco-Cruz, A.C. Non-muscle myosin IIA is post-translationally modified by interferon-stimulated gene 15 in breast cancer cells. *Int. J. Biochem. Cell Biol.* **2019**, *107*, 14–26. [[CrossRef](#)]
61. Jeon, Y.J.; Choi, J.S.; Lee, J.Y.; Yu, K.R.; Kim, S.M.; Ka, S.H.; Oh, K.H.; Kim, K.I.; Zhang, D.-E.; Bang, O.S.; et al. ISG15 modification of filamin B negatively regulates the type I interferon-induced JNK signalling pathway. *EMBO Rep.* **2009**, *10*, 374–380. [[CrossRef](#)]
62. Xie, B.; Zhao, J.; Kitagawa, M.; Durbin, J.; Madri, J.A.; Guan, J.-L.; Fu, X.-Y. Focal Adhesion Kinase Activates Stat1 in Integrin-mediated Cell Migration and Adhesion. *J. Biol. Chem.* **2001**, *276*, 19512–19523. [[CrossRef](#)] [[PubMed](#)]
63. Zhang, L.; Zou, W. Inhibition of integrin  $\beta$ 1 decreases the malignancy of ovarian cancer cells and potentiates anticancer therapy via the FAK/STAT1 signaling pathway. *Mol. Med. Rep.* **2015**, *12*, 7869–7876. [[CrossRef](#)] [[PubMed](#)]
64. Pedersen, E.; Wang, Z.; Stanley, A.; Peyrollier, K.; Roesner, L.M.; Werfel, T.; Quondamatteo, F.; Brakebusch, C. RAC1 in keratinocytes regulates crosstalk to immune cells by Arp2/3-dependent control of STAT1. *J. Cell Sci.* **2012**, *125*, 5379–5390. [[CrossRef](#)] [[PubMed](#)]
65. Vincent, K.M.; Postovit, L.M. Investigating the utility of human melanoma cell lines as tumour models. *Oncotarget* **2017**, *8*, 10498–10509. [[CrossRef](#)]
66. Lin, W.M.; Baker, A.C.; Beroukhim, R.; Winckler, W.; Feng, W.; Marmion, J.M.; Laine, E.; Greulich, H.; Tseng, H.; Gates, C.; et al. Modeling Genomic Diversity and Tumor Dependency in Malignant Melanoma. *Cancer Res.* **2008**, *68*, 664–673. [[CrossRef](#)] [[PubMed](#)]

67. Hoek, K.S.; Eichhoff, O.M.; Schlegel, N.C.; Döbbling, U.; Kobert, N.; Schaerer, L.; Hemmi, S.; Dummer, R. In vivo Switching of Human Melanoma Cells between Proliferative and Invasive States. *Cancer Res.* **2008**, *68*, 650–656. [[CrossRef](#)]
68. Merta, L.; Gandalovičová, A.; Cermak, V.; Dibus, M.; Gutschner, T.; Diederichs, S.; Rosel, D.; Brábek, J. Increased Level of Long Non-Coding RNA MALAT1 is a Common Feature of Amoeboid Invasion. *Cancers* **2020**, *12*, 1136. [[CrossRef](#)]
69. Bustin, S.A.; Benes, V.; Garson, J.; Hellemans, J.; Huggett, J.F.; Kubista, M.; Mueller, R.; Nolan, T.; Pfaffl, M.W.; Shipley, G.L.; et al. The MIQE Guidelines: Minimum Information for Publication of Quantitative Real-Time PCR Experiments. *Clin. Chem.* **2009**, *55*, 611–622. [[CrossRef](#)]



© 2020 by the authors. Licensee MDPI, Basel, Switzerland. This article is an open access article distributed under the terms and conditions of the Creative Commons Attribution (CC BY) license (<http://creativecommons.org/licenses/by/4.0/>).

Supplementary Materials

# Sustained Inflammatory Signalling through Stat1/Stat2/IRF9 Is Associated with the Amoeboid Phenotype of Melanoma Cells

Aneta Gandalovičová, Anna-Marie Šuchová, Vladimír Čermák, Ladislav Merta, Daniel Rösel and Jan Brábek

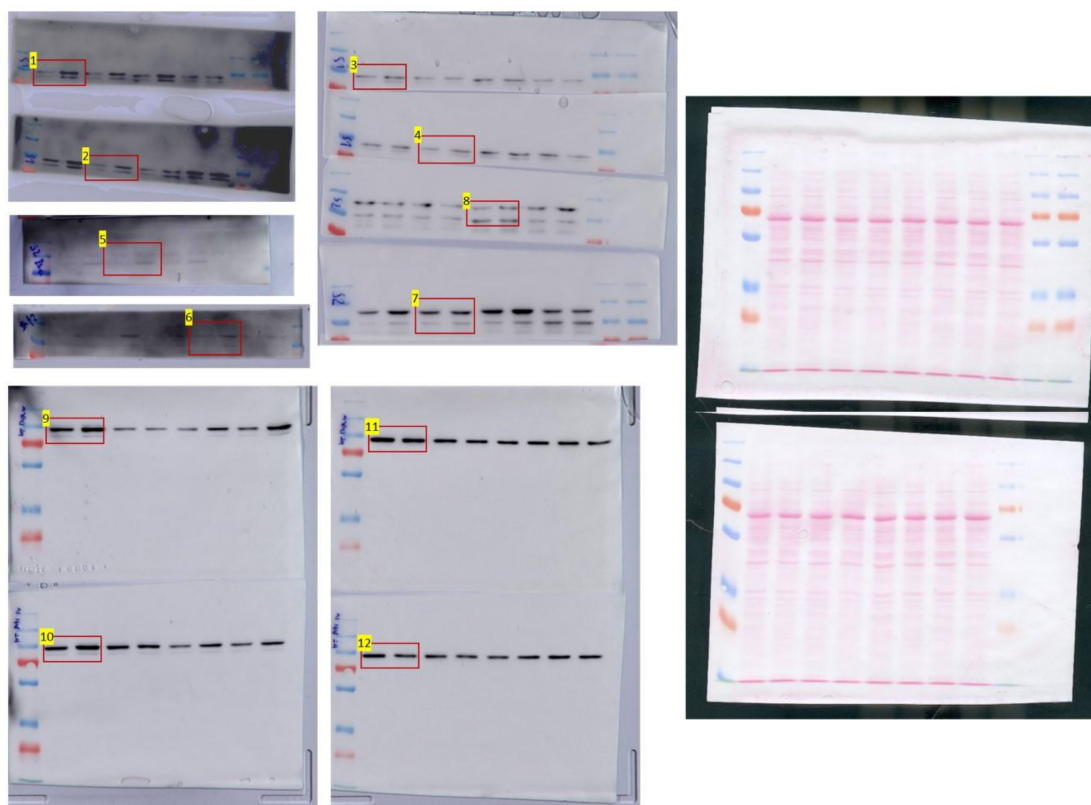
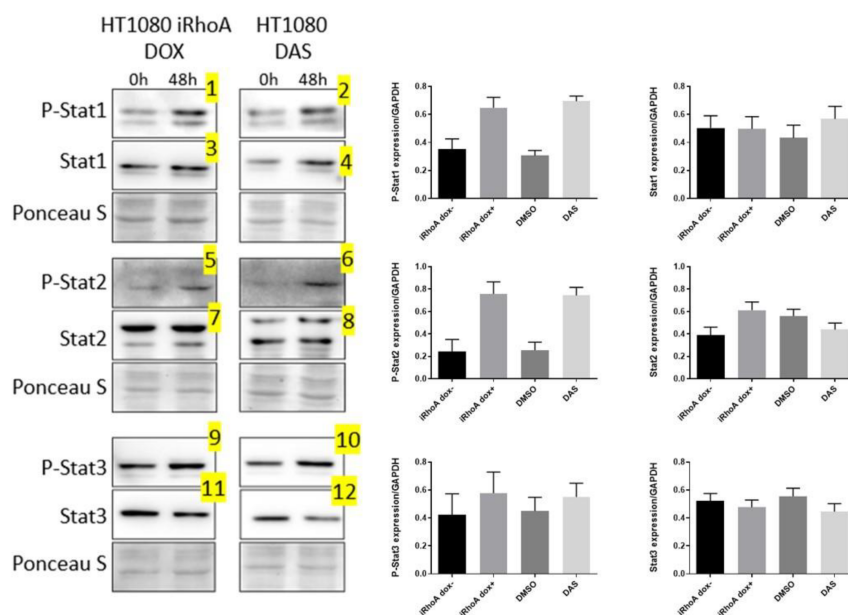
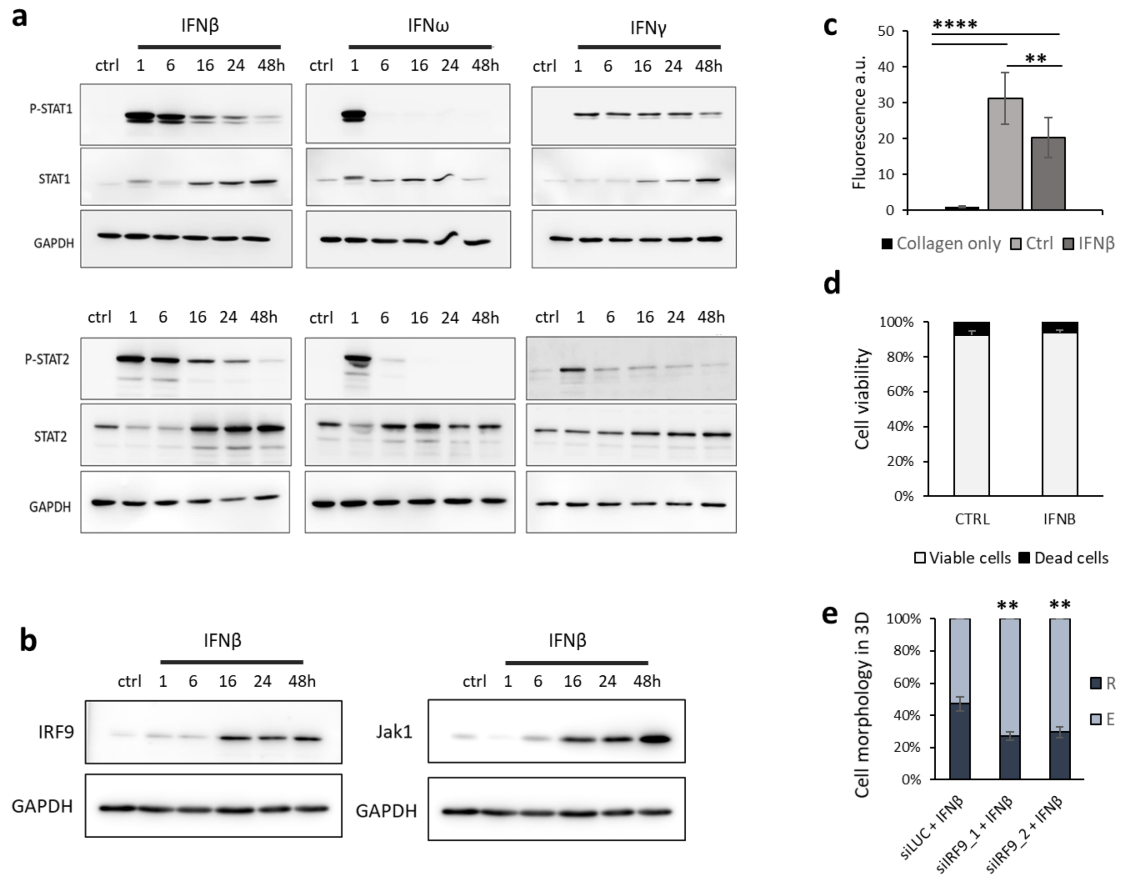
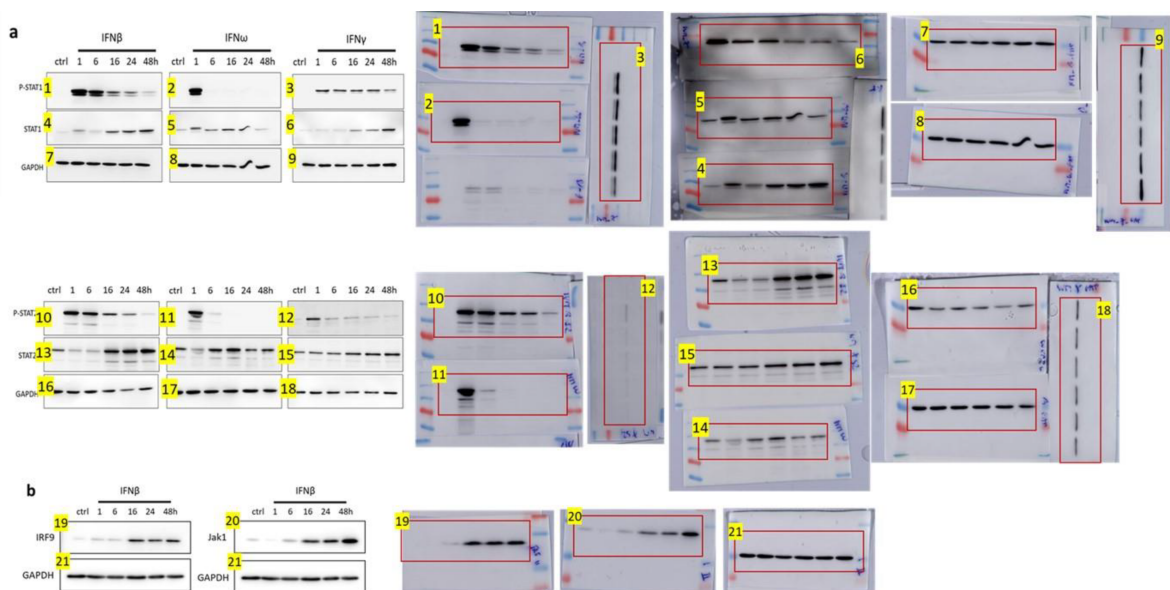


Figure S1. Detailed information about western blot in Figure 1.



**Figure S2.** Additional Characterization of IFN treated cells (a) Immunoblotting for the activation of Stat1 and Stat2 in time course samples of WM3629 cells treated with IFNs. (b) Immunoblotting for IRF9 and Jak1 in time course samples of WM3629 cells treated with IFN $\beta$ . (c) Proliferation of control and IFN $\beta$  treated WM3629 cells in 3D collagen after 48 h measured by modified Alamar Blue assay. (d) Cell viability of control and IFN $\beta$  treated WM3629 cells after 48 h assessed by trypan blue exclusion assay. (e) Quantification of morphology of WM3629 cells with siRNA KD of IRF9 treated with IFN $\beta$  in 3D collagen. *p*-values: \*\*\*\* *p* < 0.0001, \*\* *p* < 0.01.



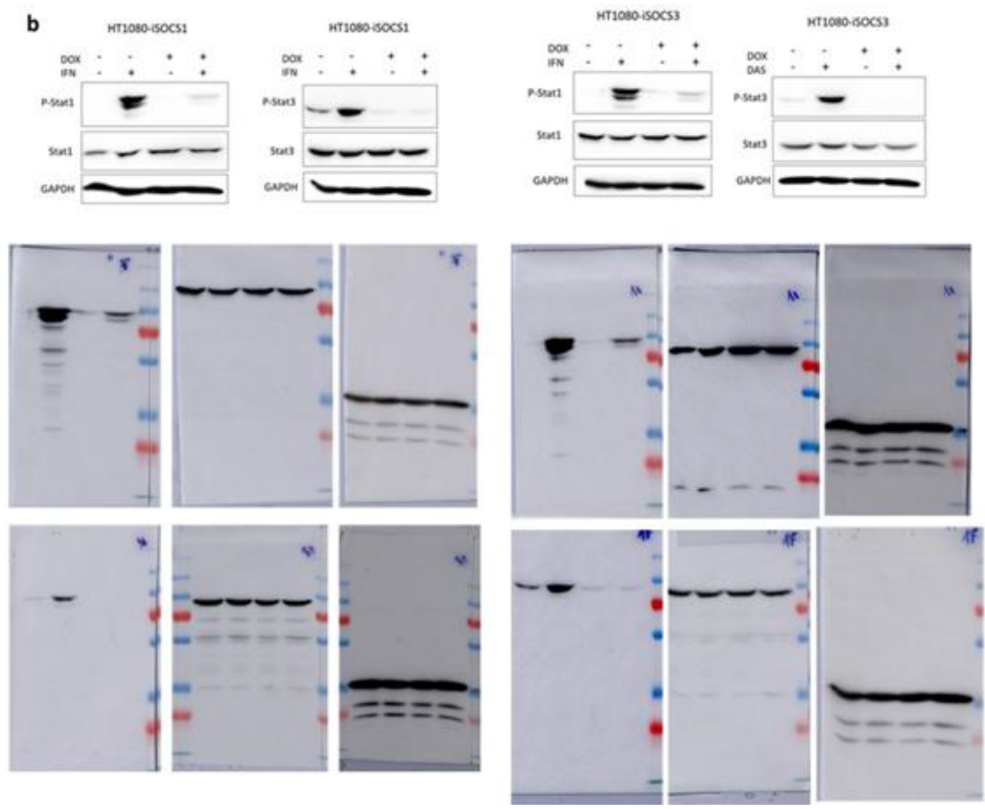
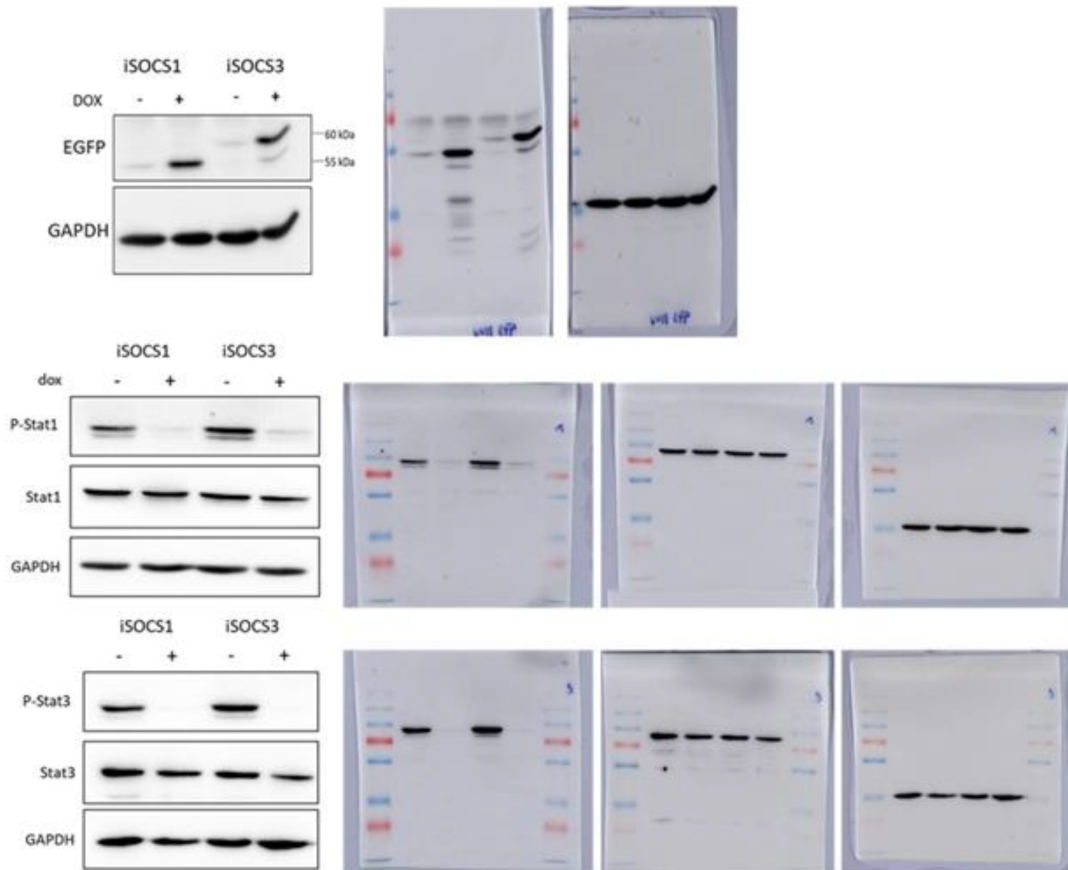
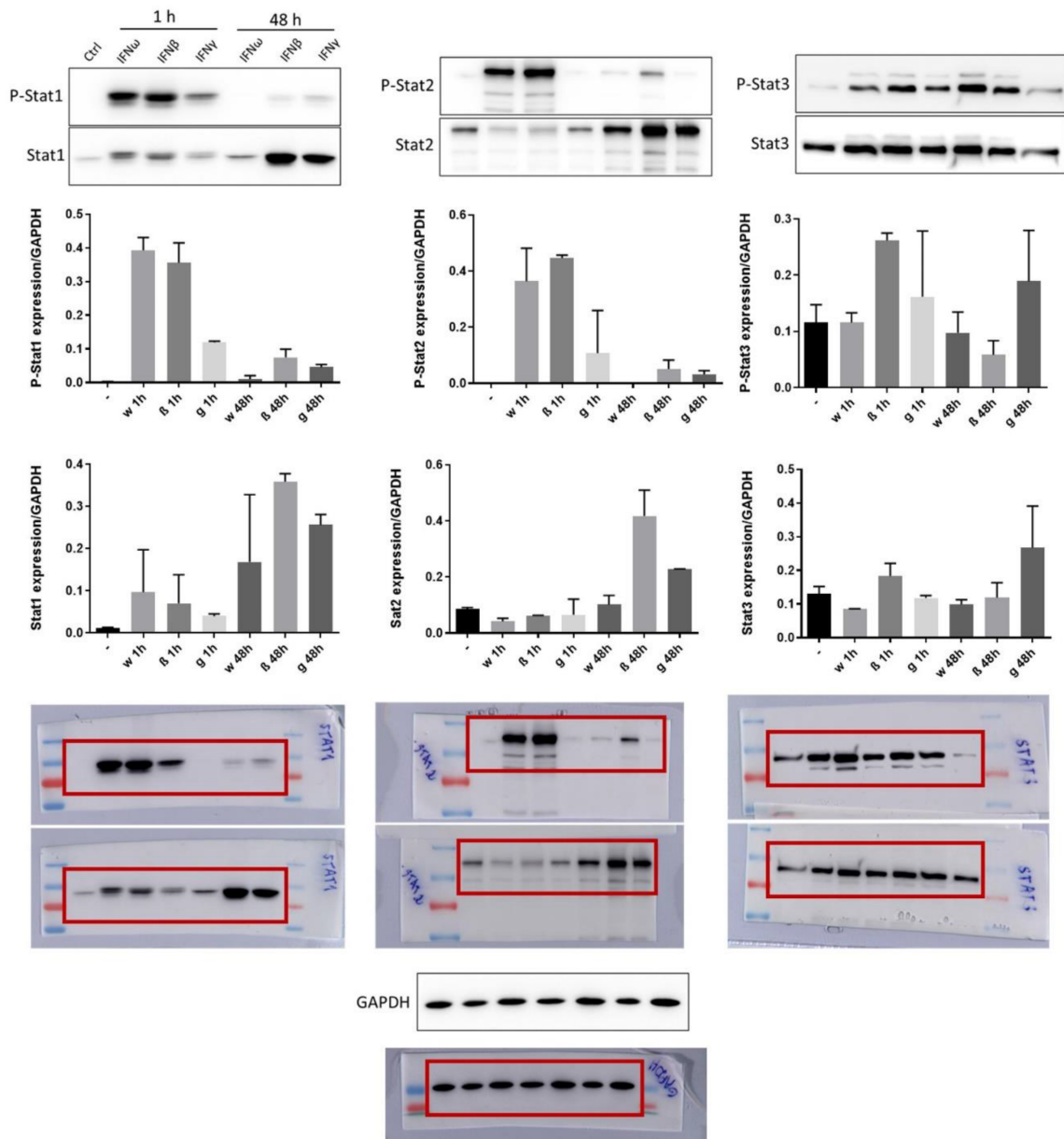


Figure S3. Detailed information about western blot.





**Figure S4.** Detailed information about western blot in Figure 2.

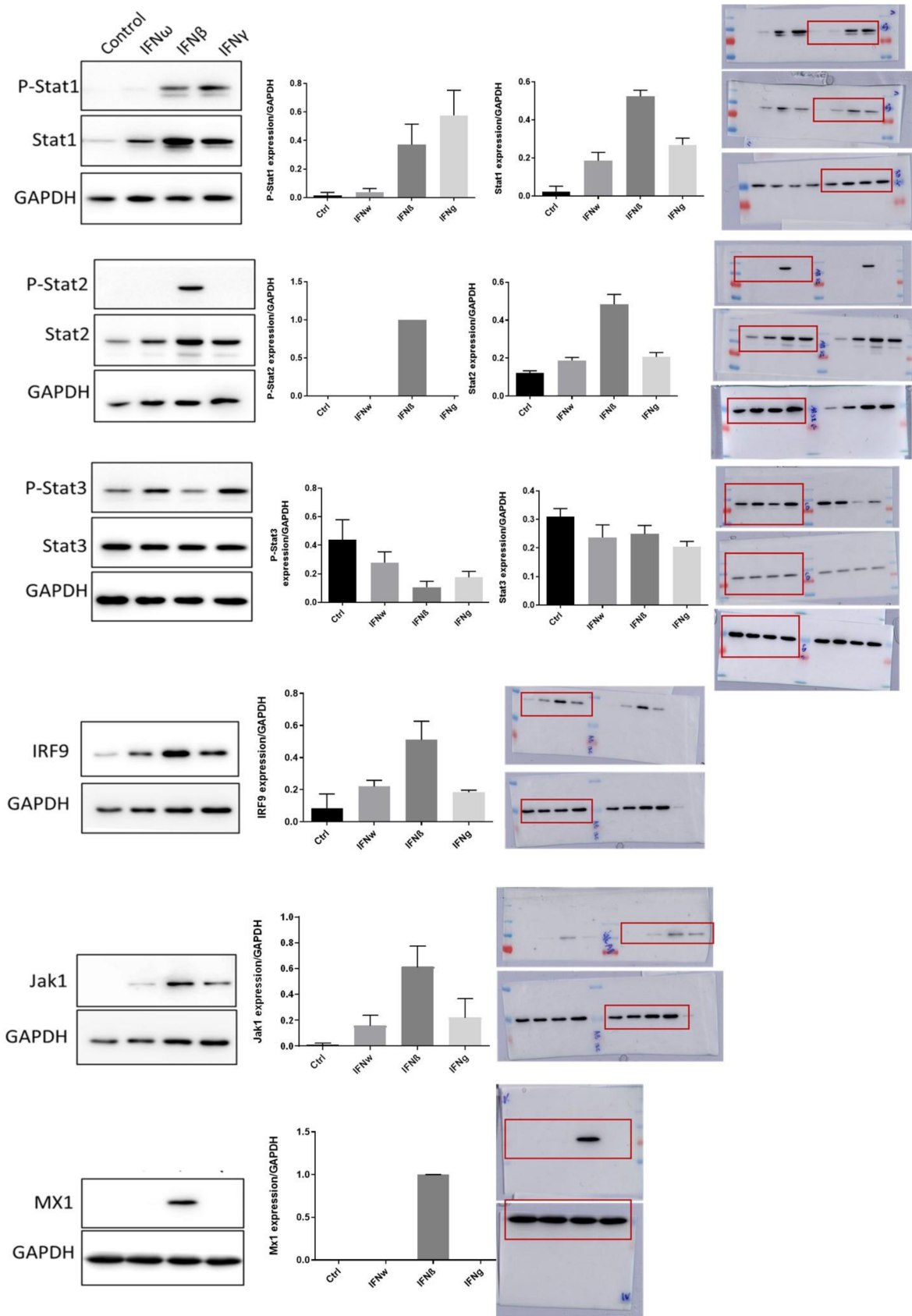
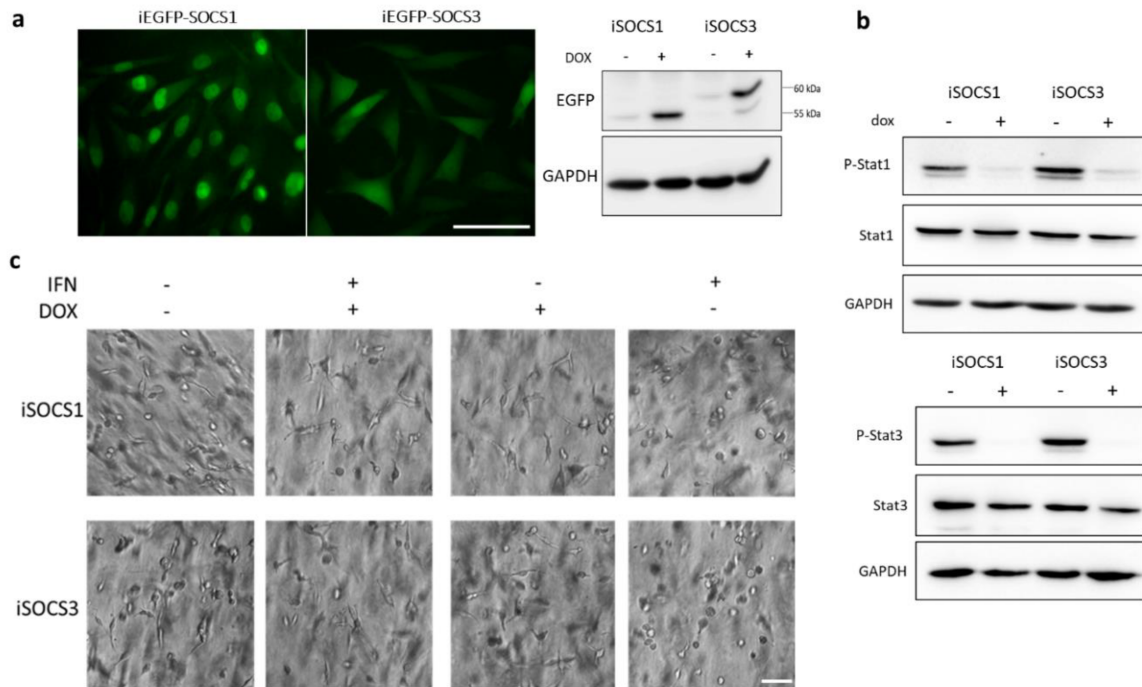
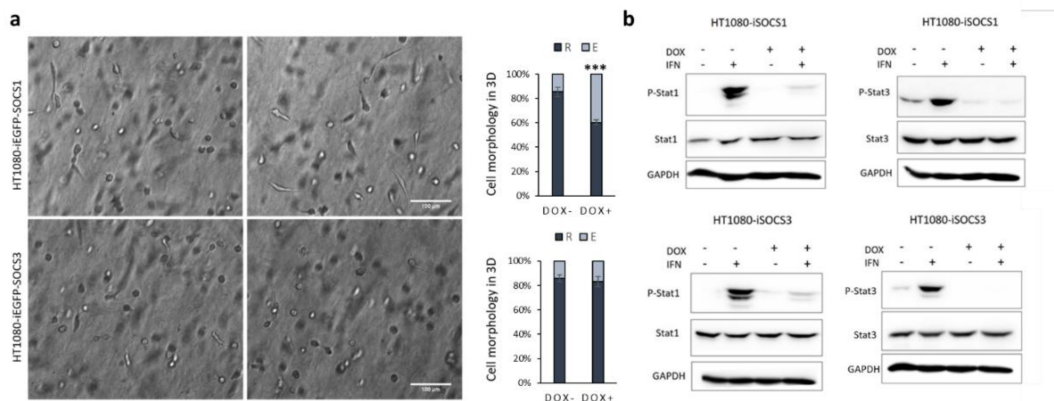


Figure S5. Detailed information about western blot in Figure 3.



**Figure S6.** Establishment of WM3629 stable cell lines expressing EGFP-tagged doxycycline-inducible SOCS1 and SOCS3. (a) Validation of expression of inducible SOCS1 and SOCS3 (iSOCS1, iSOCS3) visualized by fluorescence microscopy of EGFP signal after addition of doxycycline (DOX) (left) and by immunoblotting for EGFP. (b) Immunoblotting for Stat transcription factors Stat1 and Stat3 activation after induced expression of iSOCS1 and iSOCS3 in WM3629 cells. (c) Representative image of WM3629 stable cell lines expressing iSOCS1 and iSOCS3 treated with IFN $\beta$  without or with induced expression of iSOCS1 and iSOCS3 in 3D collagen. Scale bar 100  $\mu$ m.



**Figure S7.** Expression of iSOCS1 can prevent dasatinib induced MAT in HT1080 cells. (a) Representative image of HT1080 stable cell lines expressing EGFP-tagged doxycycline-inducible SOCS1 and SOCS3 (iSOCS1, iSOCS3) treated with dasatinib (DAS) to induce MAT without or with induced expression of iSOCS1 and iSOCS3 in 3D collagen and quantification of cell morphology. (b) Immunoblotting for Stat transcription factors Stat1 and Stat3 activation after IFN treatment and induced expression of iSOCS1 and iSOCS3 in HT1080 cells. Scale bar 100  $\mu$ m. R = round, E = elongated. *p*-values: \*\*\* *p* < 0.001.

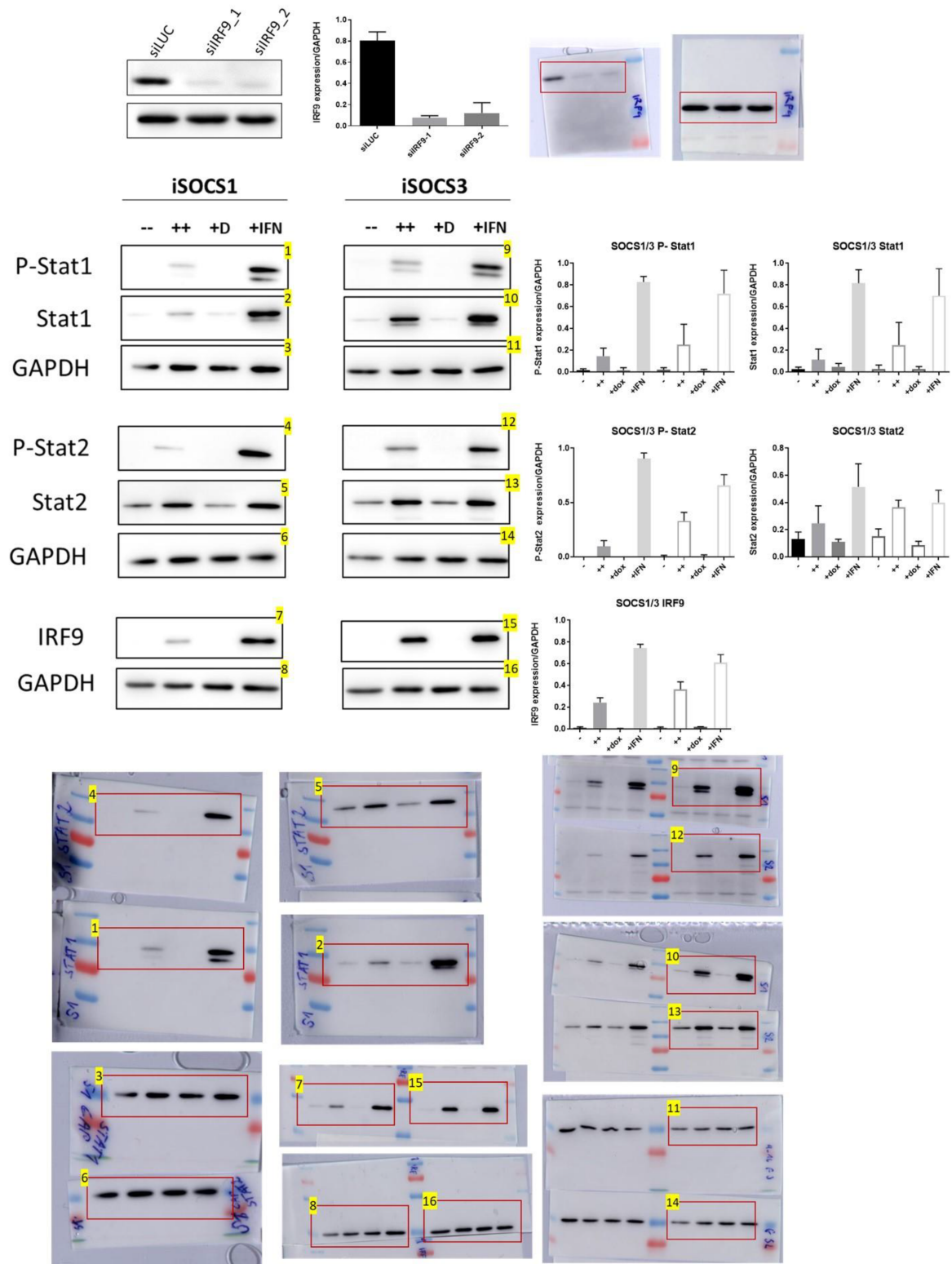


Figure S8. Detailed information about western blot in Figure 4.

**Table S1.** RT-qPCR primers used in the work.

Target Gene	Forward Primer	Reverse Primer
STAT1	CTGAATTCGGCACCTGCAAT	GCTCTTCAGTAACGATGAGAGGA
STAT2	GGGACTTTGGTTACCTGACTCT	CAGTTCCTCTGTACACCTAGT
STAT3	AGTGTGCATTGACAAAGACTCTG	CGTTGTTGGATTCTTCCATGTTG
IRF9	AGCTCTTCAGAACCGCCTAC	CAGTGTACCTGGAACCTTCGGT
MX1	CACAGAACCGCCAAGTCCAA	ACCTGGTCTGGCAGTAGAC
ISG15	GAGAGGCAGCGAACTCATCT	CTTCAGCTCTGACACCGACA
IL6	GTTCTGCAGAAAAAGGCAAAGA	GTCAGCAGGCTGGCATTGT
IL8	CACACTGCGCCAACACAGAAA	CTCAGCCCTCTTCAAAAACTTCTC
IL24	CCTGTGGACTTTAGCCAGACC	GCAGGGTAAAACCCAGGCAA
IFNB1	CTAGCACTGGCTGGAATGAGAC	CCAGGACTGTCTTCAGATGGTTT
IFITM1	TCAACACCCTCTTCTGAACTGG	CTTCCTGTCCCTAGACTTCAGC
PDL1	CTGGCATTGCTGAACGCAT	TTAGTGCAGCCAGGTCTAATTGT
Reference gene (HT1080)		
EIF4H	CCTTCTGGCTACGGGAACCAT	CTTCGACACCTACGACGATCG
GAPDH	GCATGGACTGTGGTCATGAG	CTGCACCACCAACTGCTTAG
Reference gene (WM3629)		
HNRNLP	GCGCTCACTTTTGCCCTGAGAA	CTGGAGGTGACCGAGGAGAA
PPIA	GCCGAGGAAAACCGTGTACTA	CTGCAAAACAGCTCAAAGGAGAC



© 2020 by the authors. Licensee MDPI, Basel, Switzerland. This article is an open access article distributed under the terms and conditions of the Creative Commons Attribution (CC BY) license (<http://creativecommons.org/licenses/by/4.0/>).

## Discussion of results

The study of cancer invasion plasticity is crucial for our understanding of metastatic processes and may help identify novel therapeutic opportunities. Metastasis is the leading cause of death in cancer patients, accounting for an estimated 90% of deaths (Sleeman and Steeg, 2010). It has become clearly evident that while the proliferation of tumour cells underlies tumour growth, the most jeopardising event in cancer progression is the gain of an invasive, metastasizing phenotype. This may arise as a consequence of genetic alterations gained during abnormal proliferation, such as chromosomal instability, or as a result of epigenetic modifications or aberrant signalling. There is also an undeniable role of the signalling cues from the TME that contribute to pro-invasive behaviour. Altogether this gives rise to a fraction of highly motile, invading cells, capable of enduring (and surviving) the metastatic process. Moreover, the selection of invasive cells and their interaction with non-cancer counterparts and the surrounding ECM promotes invasion plasticity, enabling the acquisition of various invasion modes that enhance the cells' capability to adapt to and invade heterogeneous environments (**Fig. 6**). Due to the multiplexity of genetic aberrations, intratumor heterogeneity, and invasion plasticity, even with the advancement of sequencing technologies, the promising identification of key cancer-promoting genes has not achieved expected outcomes. As a result, effective therapies targeting tumour invasion are still unavailable, although there is a strive to identify anti-invasion drugs, coined under the term migrastatics. Nevertheless, this demands rigorous characterization of the multiple invasive phenotypes. Even after decades since metastatic behaviour was first described, reports of newly identified invasion strategies and mechanisms of cancer invasion plasticity arise, fuelling further research in this direction.

The invasive phenotypes and transitions among them fully manifest in 3D conditions (Even-Ram and Yamada, 2005) and inducing MAT or AMT in 2D cultures is associated with only a limited morphological change. Although cells cultured in 2D conditions also show shape heterogeneity, it does not predict their invasion phenotype in 3D, and 2D migration analysis was shown to be uncorrelated with 3D invasion (Baskaran et al., 2020). It is therefore critical to study cancer invasion plasticity in 3D matrices, and their main requirement is the support of cell growth, motility and viability. Commonly used matrices include Matrigel, a mixture of basal lamina proteins, and collagen I, the most abundant ECM protein in humans. In addition, collagen I is secreted by cancer cells and thus is upregulated within the tumour stroma, making it a suitable and relevant model for 3D cancer invasion studies (Xu et al., 2019). Therefore, all results presented in this thesis were performed in 3D collagen I environments, unless specifically stated otherwise.

There is only a limited number of studies offering datasets from invasion studies with regard to cancer invasion phenotypes. Microarray transcriptomic data are available for melanoma cells cultivated on both thin, rigid layers of collagen or thick, deformable collagen either treated or untreated with ROCK kinase inhibitors (Sanz-Moreno et al., 2011). Also, transcriptomic profiling of melanoma cells after MAT was published, although this study was based merely on 2D cell cultures (Taddei et al., 2014). Recently, transcriptomes of squamous carcinoma cells that adopted a round phenotype were published (Caley et al., 2021). Proteomic data focused on cancer invasion modes include data from AMT in melanoma seeded in 3D collagen (Vaškovičová et al., 2015). Nevertheless, comprehensive transcriptomic and proteomic profiling of paired mesenchymal and amoeboid cells from 3D environments was missing.

Therefore, to describe signalling underlying invasion plasticity, we established two independent inducible systems of MAT in 3D collagen gels. The induction of MAT in mesenchymal cell lines enables direct comparison of mesenchymal and amoeboid cells within one cell line, discriminating cell-line specific differences caused by a different genetic background and oncogenic mutation status. On the other hand, induction of MAT by exogenous factors can induce treatment-specific responses, we, therefore, sought to implement two independent approaches to allow for comparison of two independent datasets. The first MAT system is based on the preparation of stable cell lines with doxycycline-inducible expression of constitutively active RhoA (icaRhoA). RhoA activity is tightly coupled to the amoeboid state and expression of its constitutively active version has been previously linked to a round morphology and membrane blebbing (MacKay and Kumar, 2014; Sahai and Marshall, 2003). The second approach takes advantage of dasatinib, a Src/Abl kinase inhibitor. Dasatinib was shown to induce rounding of melanoma cells plated on top of collagen and has also been linked to activation of RhoA signalling (Ahn et al., 2012; Dasgupta et al., 2017). We have thus implemented these systems for 3D collagen cultures and verified the induction of motile, amoeboid invasion phenotype. Both systems enabled us to induce the MAT in a time-controlled manner within 3D collagen matrices in a variety of mesenchymally migrating cancer cell lines of different origin, including fibrosarcoma HT1080, MDA-MB-231 breast carcinoma and BLM melanoma cells (**Fig. 7**), proving to be a universal and robust approach of MAT induction.

The effectiveness of the MAT induction was verified by multiple approaches, including detection of active RhoA by pulldown assays and analysis of cell morphology measured as a decrease of length/width ratio in amoeboid cells. We also confirmed the independence of the induced amoeboid phenotype on ECM proteolysis by tracking cell invasion in 3D collagen and showed that unlike invasion of control mesenchymal cells, invasion of cells after MAT was not halted in the presence of GM6001, a MMP inhibitor. Moreover, due to the morphological resemblance of blebbing amoeboid cells to dying apoptotic cells, we excluded cell death by detecting the levels of

activated caspase-3 by western blot, which disclosed unchanged levels before and after MAT. All results confirmed that we are able to induce an invasive amoeboid phenotype in the originally mesenchymal cells (Čermák et al., 2020). ([Publication #2](#))

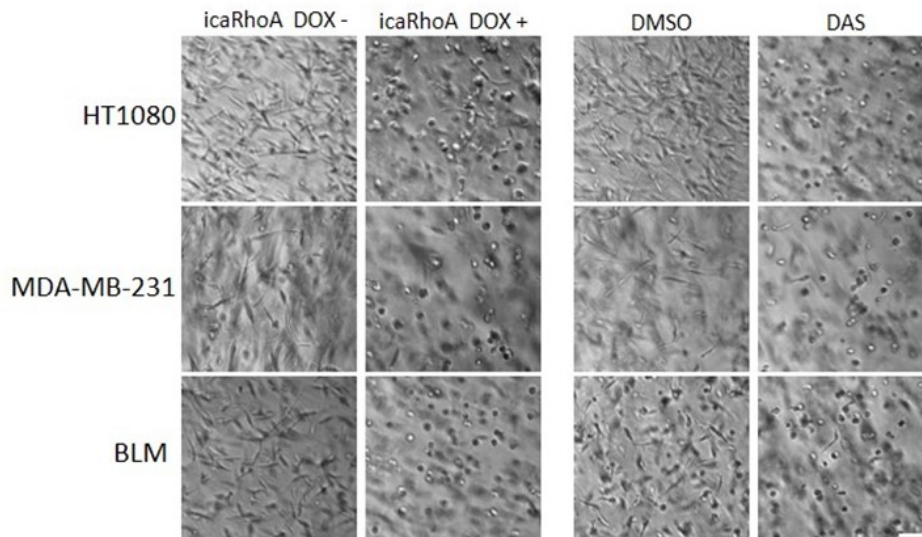


**Figure 7: Established model systems of MAT induction in 3D collagen.** Representative images of cell morphology of three cell lines in 3D collagen without induction of MAT and after induction of MAT induced by icaRhoA expression (left) or treatment of cells with dasatinib (right). Scale bar 100  $\mu$ m.

Imaging cell invasion within 3D environments brings along various challenges not encountered when cells are seeded on 2D substrates. First, imaging cells embedded in 3D gels requires larger working distances, which demands a compromise between numerical aperture and the working distance, obtainable due to the use of specialized objectives. Bright-field imaging is unsatisfactory for detailed resolution due to light diffraction. The limitations of wide-field imaging are avoided when fluorescence microscopy is employed, although this brings into light issues such as phototoxicity. Progressive techniques such as light sheet microscopy limit phototoxicity and bleaching and thus enable long-term live cell imaging, however, sample preparation issues and their general unavailability renders them difficult to employ. A promising tool is represented by digital holographic microscopy, which enables live cell, label-free and high contrast imaging (Kasprowicz et al., 2017).

Therefore, to gain further insight into the mechanisms of the mesenchymal and amoeboid invasion mode, we took use of quantitative phase imaging provided by coherence-controlled holographic microscopy (CCHM), which enables label-free imaging of live cells in optically scattering environments, such as 3D collagen gels. This is possible due to a coherence gate effect that allows to filter out strongly scattered light paths and includes only those, which meet at the detector level



after initial splitting into the subject and reference light paths. The camera of the microscope captures the interference of the subject path, which passes through the sample, with respect to the reference path, and records a hologram image. Due to the nature of this imaging technique, it is quantitative and provides information on the amount of cell dry mass in  $\text{pg}/\mu\text{m}^2$ . Using this unique approach, we recorded the invasion of HT1080-icaRhoA cells before and after MAT. We documented a direct interaction of mesenchymal cells with collagen fibres, including their ability to bundle together several collagen fibres, presumably to strengthen the cell-ECM adhesion. On the other hand, we observed only short-lived interactions with the ECM in the case of amoeboid cells, which agrees with the current concept that amoeboid invasion is independent of stable, integrin based adhesions (Paluch et al., 2016). Instead, amoeboid cells form transient contact with the ECM mediated by the glycocalyx (Schmidt et al., 2020). Interestingly, the NG2 glycoprotein was previously linked to the amoeboid phenotype, and its overexpression increased invasion (Paňková et al., 2012). Whether this was due to NG2-mediated cell-ECM contacts would be an interesting question to address by CCHM. We further documented membrane blebbing, typical of amoeboid cells, also in mesenchymal cells at sites around the nucleus. Since the nucleus is the most rigid cell part, it is often subject to constriction (Krause and Wolf, 2015). We hypothesized that the peri-nuclear blebbing could serve to push away fibres and alleviate the stress formed by the ECM on the nucleus. In agreement, yet unreviewed research shows that localized membrane blebs can promote breakage and internalization of collagen, making space for cell translocation without the need for proteolytical degradation, imposing a novel role for membrane blebbing (Welf et al., 2020).

From image sequences obtained by CCHM, we were able to describe translocation of the cell dry mass within the cell body during invasion. We show that two previously described subtypes of amoeboid invasion, blebby-amoeboid and pseudopodal-amoeboid (Friedl and Wolf, 2010; Petrie and Yamada, 2016), can be distinguished by cell mass translocation, which is unpolarized in blebby-amoeboid cells but shows front-rear polarization in pseudopodal-amoeboid cells. This corresponds with the characterization of blebby amoeboid cell invasion as slower and less polarized compared to pseudopodal amoeboid invasion (Friedl and Wolf, 2010). Moreover, we demonstrate that the distribution of the cell mass is an important determinant of cell directionality, which is a feature shared by both mesenchymal and pseudopodal-amoeboid cells. These findings encourage the design of automatized, machine-learning evaluation methods of cell migration and invasion based on label-free imaging. This has already been proved possible in 2D conditions, where automatized evaluation of digital holographic images was implemented to evaluate cell morphology (Lam et al., 2018) or cell dynamics during EMT (Strbkova et al., 2020). The application of CCHM could enable this in 3D environments. Moreover, the calculation of dynamic

phase differences could further serve to automatically assess the direction of cell invasion (Tolde et al., 2018). ([Publication #1](#))

To disclose the genetic and protein expression changes associated with the transition of mesenchymal cells to amoeboid cells, we performed large scale transcriptomic and proteomic profiling of HT1080 fibrosarcoma cells before and after induction of MAT by both icaRhoA and dasatinib in 3D collagen cultures. After 48h in 3D collagen, control mesenchymal and MAT-induced cells were harvested for RNA or protein lysates, which were further processed for RNA-sequencing or mass spectrometry, respectively (Čermák et al., 2020). ([Publication #2](#))

To eliminate treatment specific changes, only overlapping genes were considered for further enrichment analysis to obtain an amoeboid molecular signature. Gene enrichment analysis disclosed that the most significant upregulated pathways are involved in inflammatory signalling and type I IFN response (Gandalovičová et al., 2020). Concordantly, the overlap of genes upregulated by both icaRhoA and dasatinib, with proteins detected as upregulated by both systems (Čermák, 2019) includes 9 genes/proteins (CEBPB, GDF15, IFIT1, IFITM3, MX1, NNMT, SERPINB2, STAT1, VASN)<sup>2</sup>, out of which 5 represent interferon-associated genes. IFIT1, IFITM3, MX1 and NNMT are IFN-induced genes with a described link to cancer (Aljohani et al., 2020; D'Andrea et al., 2011; Pidugu et al., 2019; Rajapaksa et al., 2020). STAT1 is a direct mediator of IFN signalling and has an ambiguous role for tumour progression, showing both tumour suppressing and promoting roles (Zhang and Liu, 2017). The downregulated genes common to both icaRhoA and dasatinib were enriched with cell-cycle associated genes, pointing to a less proliferative state of amoeboid cells (unpublished results). Whether this is biologically relevant or is an effect of the treatments remains to be addressed.

Thus, to affirm the upregulation of type I IFN signalling in amoeboid cells detected by RNA sequencing, we measured the expression of Stat1/2/3 and IRF9, by RT-qPCR, in HT1080 cells undergoing MAT, and complemented this with Western blot detection of Stats phosphorylation. Results on both gene and protein level pointed to the involvement of Stat1/2 and IRF9, together known as the ISGF3 complex, in the amoeboid phenotype.

To dissect the role of inflammation signalling in cancer invasion plasticity in more detail, we employed a set of melanoma cell lines with mixed invasion phenotypes, which enabled us to test whether manipulation of the type I IFN signalling pathway can induce both MAT when upregulated and AMT when repressed. Indeed, inhibition of Jak/Stat signalling by Ruxolitinib, a

---

<sup>2</sup> CEBPB (*CCAAT/enhancer-binding protein beta*); GDF15 (*growth differentiation factor 15*); IFIT1 (*interferon induced protein with tetratricopeptide repeats 1*); IFITM3 (*interferon induced transmembrane protein 3*); MX1 (*MX dynamin like GTPase 1*); NNMT (*nicotinamide N-methyltransferase*); SERPINB2 (*serpin family B member 2*); STAT1 (*signal transducer and activator of transcription 1*); VASN (*vasorin*)

kinase inhibitor of Jak1/2, led to an increase in elongated, mesenchymal cells, whereas treating melanoma cells with IFN $\beta$  caused cells to switch to the round, amoeboid phenotype. The IFN $\beta$  treatment led to a prolonged expression of ISGF3 components, i.e. IRF9 and unphosphorylated Stat1, Stat2, which is associated with a low level, constitutive expression of interferon induced genes (Cheon et al., 2013; Yamagami et al., 2018). However, we did not observe any pro-amoeboid effect of IFN $\alpha$  nor IFN $\omega$ , which we attribute to their decreased ability to activate the long-term response, since neither IFN $\alpha$  nor IFN $\omega$  increased the levels of ISGF3 components to the same extent as IFN $\beta$ . In addition, when IRF9, the adaptor protein of the ISGF3 complex, was depleted by siRNA, the amoeboid phenotype was downregulated, and an increased number of elongated cells was observed.

In cells, the fine-tuning of the IFN response is regulated by suppressor of cytokine signalling (SOCS) proteins that secure a negative feedback loop for Jak/Stat signalling (Linossi et al., 2018). Thus, we prepared stable cell lines expressing doxycycline-inducible SOCS1 and SOCS3. After confirming their ability to diminish interferon induced phosphorylation of Stat1/3, we tested their effect on preventing MAT. Interestingly, SOCS1, but not SOCS3 expression, had a pro-mesenchymal effect on WM3629 melanoma cells, and could partially prevent dasatinib induced MAT in HT1080 cells. We suggest that this could be explained by the differential effect of SOCS1 and SOCS3 on long-term IFN signalling, with only SOCS1 leading to IRF9 and unphosphorylated Stat1 downregulation. Although we do not know the nature of this downregulation, it supports our theory that sustained ISGF3 signalling is important for amoeboid cells. Apart from its action on the IFN pathway, SOCS1 may repress the amoeboid phenotype by suppressing CEBP $\beta$  expression, which is one of the amoeboid-associated genes identified in our transcriptomic and proteomic analysis (Čermák et al., 2020).

We have also demonstrated that ISGF3 signalling drives cell dissemination from tumour spheres and promotes the amoeboid phenotype by adding IFN $\beta$  to spheroid cultures. Since IFN $\beta$  is present in the tumour stroma, where it is secreted by both tumour cells and CAFs, this finding suggests a mechanism relevant for the *in vivo* situation. In fact, direct contact between cancer cells and CAFs may lead to DNA transfer and enhanced IFN $\beta$  secretion from CAFs (Rullan Iriarte et al., 2018). It has also been described that cancer cells undergoing chemotherapy upregulate secretion of IFN $\beta$ , which reprograms stromal fibroblast into an anti-viral state that supports tumour re-growth after treatment (Maia et al., 2021). Moreover, we have shown that melanoma cells treated with IFN $\beta$  upregulate the expression of cytokines, such as IL6, IL8, IL24 and IFN $\beta$ 1 itself, indicating that IFN $\beta$ 1 issues an autocrine stimulatory program leading to enhanced secretion of pro-invasive molecules. In addition, it upregulates the expression of PD-L1 (*programmed death-ligand 1*), a molecule implicated in the immune escape of cancer cells (Frydenlund and Mahalingam, 2017).

In agreement with our findings, recent data point to a pro-tumorigenic role of IFN signalling in various contexts. Cancers often display an intrinsic inflammatory-like signature (Colotta et al., 2009; Greten and Grivennikov, 2019). In addition, IFN signalling has been linked to increased resistance to anti-cancer drugs (Khodarev et al., 2004; Kolosenko et al., 2015; Luker et al., 2001), and constitutive exposure to IFN $\beta$  confers cells with protection to DNA damage (Cheon et al., 2013).

This is opposed to the previously described role of IFN signalling in suppressing proliferation in cancers cells, and thus its previous implication as a therapeutic strategy against cancer (Kaynor et al., 2002; Musella et al., 2017). Nevertheless, invasive behaviour should be uncoupled from proliferative behaviour, as they may in fact be exclusive to a certain extent (Kohrman and Matus, 2017). For example, in melanoma, a phenotype switch between proliferative and invasive states has been described (Hoek et al., 2008). The diverse effects of IFN signalling on proliferation and invasion may be one of the causes why IFN treatment showed ineffective against cancer in various clinical studies.

Taken together, we have demonstrated that modifying the level of type I interferon signalling modulates the invasive behaviour of cells. Sustained, long-term IFN response, but not the immediate IFN-induced response, seems to underlie the maintenance of the amoeboid phenotype and its upregulation is associated with increased cell dissemination from tumour spheroids. On the other hand, abrogation of ISGF3 signalling by various approaches leads to cell elongation typical of mesenchymal cells (Gandalovičová et al., 2020). ([Publication #3](#))

Inflammation-associated signalling has been previously repeatedly linked to the progression of metastatic disease (Ben-Neriah and Karin, 2011; Opdenakker and Van Damme, 1992; Sistigu et al., 2017). The activation of inflammatory pathways may occur as a result of chromosomal instability, which has been linked to metastatic progression, and often results in presence of cytosolic DNA, activating a self-driven type I IFN response (Tijhuis et al., 2019). Recently, it was shown that inflammatory gene expression profiles were enriched in macrometastases compared to micrometastases, involving an autocrine positive feedback loop of IL1 (Pein et al., 2020). Moreover, there is increasing evidence for the involvement of inflammatory signalling in promoting the amoeboid phenotype. For example, both IL6-Stat3 and IL1-NF $\kappa$ B signalling was shown to promoting the amoeboid phenotype in melanoma cells (Georgouli et al., 2019; Sanz-Moreno et al., 2011). The pro-amoeboid role of IL1 was also identified in our recent transcriptomic analysis of amoeboid A375m2 cells treated with p38 kinase inhibitors, which led to a shift to an elongated, mesenchymal phenotype, corresponding to AMT. In fact, IL1B was among the ten most downregulated genes after the induction of AMT (Čermák et al., 2021). Notably, the amoeboid-associated gene expression signature of breast cancer displays is enriched in inflammation-

associated signalling and displays a striking overlap with genes upregulated after MAT in HT1080 cells – 20 out of the 35 most enriched gene ontology categories are present in both data sets and all 20 represent inflammatory signalling (Čermák et al., 2020; Emad et al., 2020; Gandalovičová et al., 2020).

It is still yet unclear, whether amoeboid cells upregulate inflammatory signalling actively, or as a result of mechanical stress they must endure during their translocation through pores of the ECM. Nevertheless, nuclear deformation is a common accompanying effect during invasion in confinement (Denais et al., 2016), and may be the source of stress signalling due to DNA damage. It may be speculated that the IFN-like signalling identified in amoeboid cancer cells imposes them with adaptability to survive in adhesion-low, cytokine rich environments and renders them more resilient to deformation (**Fig. 8**).

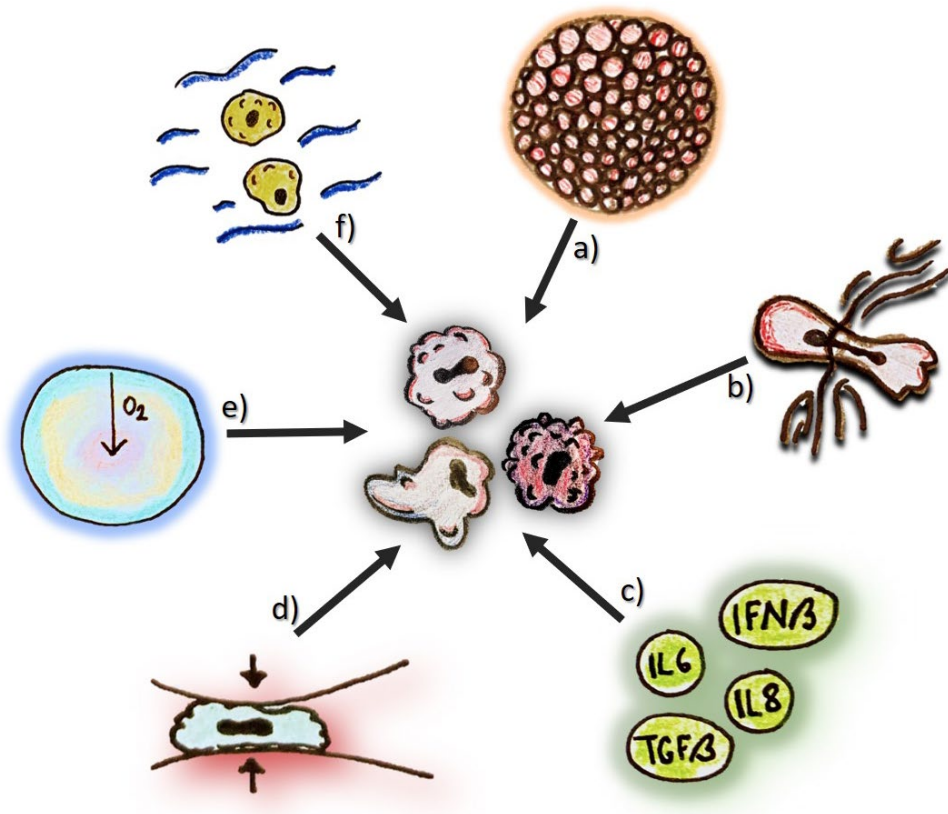


**Figure 8: Stress associated signalling promotes amoeboid invasion.** Amoeboid invasion is induced by various stress-inducing conditions, such as *a*) cell crowding and loss of adhesion, *b*) nuclear stress during invasion, *c*) a cytokine rich environment, *d*) cell confinement, *e*) hypoxia and *f*) shear stress.

It cannot be easily defined as to which invasion mode has the largest metastatic capacity, as this is very dependent on both cell intrinsic, and extrinsic factors. Collective invasion is considered the dominant strategy for dissemination from primary tumours, and mesenchymal invasion, as the net result of EMT was long considered the dominant form of invasive behaviour. In fact, amoeboid invasion was considered an artefact due to collagen matrix preparation (Sabeh et al., 2009). This was later amended by the finding that amoeboid cells metastasize *in vivo*, and the upregulation of Rho/ROCK signalling could actually promote metastatic behaviour of cells (Kosla et al., 2013). Nowadays, the role of amoeboid cells in metastatic disease is becoming more and more profound. This is supported by the observations that highly metastatic melanoma cell lines derived from metastases of parental cell lines often increase amoeboid traits, such as A375m2 and A375P, or WM983B and WM982A cell lines, respectively (Georgouli et al., 2019). Moreover, cells with amoeboid traits are often detected at the leading front of melanoma tumours (Sanz-Moreno et al., 2011) as well as breast cancer tumours (Gao et al., 2017).

*In vitro*, the invasiveness of individual cancer cells can be tested in various matrices, and, importantly, may give varying results based on the chosen ECM. For example, merely increasing the concentration of collagen may favour mesenchymal invasion. In cell cultures, cancer cell lines exhibit phenotypic stability and adopt the amoeboid or mesenchymal phenotype in a large variety of matrices. This may evoke the tempting presumption that tumours exist in either the amoeboid or mesenchymal state, which is very unlikely. Rather, cancers take advantage of different invasion modes during individual steps of the metastatic cascade and commonly adopt hybrid and transitional phenotypes (Friedl and Alexander, 2011; Huang et al., 2014) (**Fig. 6**).

Moreover, the cooperation of mesenchymal and amoeboid cells promotes invasive behaviour. Amoeboid cells can serve as immunomodulatory hubs, producing pro-invasive cytokines to stimulate a pro-invasive environment. In addition, amoeboid cells can modulate the behaviour of surrounding cells by exosome shedding and stimulate their pro-malignant characteristics (Schillaci et al., 2017). A mathematical model suggested that a population with mesenchymal and amoeboid heterogeneity is most effective in invading heterogeneous environments, as the fast, dynamics amoeboid cells take use of paths within the ECM created by mesenchymal cells (Hecht et al., 2015). Concordantly, a different model predicts that heterogeneity in cell size and deformability is desirable and maximizes invasive potential (Asadullah et al., 2021).

During the metastatic cascade, particular invasion modes may be preferentially adopted and bring advantage for each given step. The amoeboid phenotype may be preferentially adopted by cells within the tumour mass due to lack of ECM contact and necessity to survive under stress-inducing conditions including hypoxia, cytokine rich environment and overall cell crowding (**Fig. 8**). At sites of dissociation from the tumour mass, collective or individual invasion may be beneficial

based on the physical properties of the adjacent ECM. Nevertheless, amoeboid cells are often observed at the invasive fronts of melanoma and breast cancer tumours and may arise from direct dissemination or through MAT (Pandya et al., 2017). In dividing mitotic cells, the activation of RhoA/ROCK was shown to promote dissociation of individual cells from epithelial sheets, suggesting a mechanism of cell dissemination from collectively migrating cells (Vasiliev et al., 2004). In the case of transendothelial migration, both amoeboid (RhoA/ROCK, deformability) and mesenchymal phenotypic traits (adhesion and proteolysis) have been described (Onken et al., 2021). Notably, when entering confined spaces, cells autonomously promote amoeboid-associated traits, such as membrane blebbing (Holle et al., 2019). Once within the vessel, circulating tumour cells endure confinement and interstitial flow, both of which has been associated with the amoeboid phenotype (Huang et al., 2015; Liu et al., 2015). Similar to intravasation, the process of extravasation requires both proteolysis and RhoA-mediated signalling (Ladhani et al., 2011). It can be expected that the successful passage of cells through the metastatic cascade will have rendered them more adaptive and resilient, affecting their biophysical properties. Notably, recent findings show that during migration in confinement, cancer cells soften (Rianna et al., 2020). The softness of cells has also been linked to drug resistance in ovarian cells (Kapoor et al., 2018) and tumour progression in glioma cells (Alibert et al., 2020). Intriguingly, cell deformability increases with metastatic progression and cells after lung metastasis display the highest invasion rates and lowest stiffness, which could be correlated with the tendency to adopt the amoeboid phenotype (Liu et al., 2020). Taken together, the metastatic process greatly profits from cancer invasion plasticity, and cells with inherently increased phenotypic plasticity and adaptability may be expected to have most metastatic potential.

## Future challenges and perspectives

It is increasingly more evident that cancer invasion plasticity studies will move from simple 3D models, let alone 2D cell cultures, to complex environments that involve cell co-cultures and multiple ECM components to reconstitute the *in vivo* situation better. This will bring along technical challenges such as imaging cells in optically inhomogeneous environments, complicating live cell imaging. Moreover, whilst co-cultures of multiple cell lines enable to imitate cell interactions within the TME, they complicate read-out on the level of protein and gene expression as it is not possible to separate one cell line from another in bulk analysis. This issue could be resolved by single cell sequencing techniques; however, we still lack the tools required for routine, single cell analysis from 3D cultures. Another limitation that hinders a better understanding of the metastatic processes is the difficulty to maintain long-term 3D cell cultures, limiting studies focusing on e.g., the role of tumour dormancy or senescence in invasion plasticity.

A detailed description of molecular signatures of each cancer invasion mode will help to unravel heterogeneity within individual tumours and predict the level of metastatic propensity. Moreover, it would allow for detection of the implied invasion mode from patient-derived samples, enabling stratification into amoeboid and mesenchymal prognostic subtypes. A recent paper has contributed to this area by disclosing an epithelial-to-mesenchymal-to-amoeboid transition gene signature of breast cancer metastasis and survival, which was shown to improve survival prediction in combination with standard prognosis methods (Emad et al., 2020).

Overall, the characterization of the individual cancer invasion modes will help to unravel heterogeneity within individual tumours and predict the level of metastatic propensity. As such, cancer cell invasion plasticity remains an exciting topic to study and will certainly disclose many targetable mechanisms, raising hope that one day metastasis will be tackled.



## Concluding remarks

This thesis has summarized the results of three publications focusing on mechanisms of cell invasion plasticity within 3D *in vitro* environments.

After initial testing of suitable model systems of MAT in 3D conditions, we established and described two MAT systems that proved effective in various cancer cell lines. The first relies on the generation of stable cell lines expressing doxycycline-inducible constitutively active RhoA, while the other takes advantage of a Src kinase inhibitor dasatinib treatment. Both approaches resulted in the induction of a migratory amoeboid phenotype in the vast majority of cells, exemplified by the gain of round morphology, membrane blebbing and invasion resistant to protease inhibition.

Utilizing the HT1080-iRhoA model system, we employed digital holography microscopy to visualize live, unlabelled mesenchymal or amoeboid invasion in real-time within 3D collagen. The unique method of CCHM provided us with a detailed depiction of cell invasion strategies, including cell interaction with collagen fibres or detailed visualization of membrane blebs, and disclosed changes of mass distribution within the migrating cell.

To identify amoeboid associated gene expression, we performed RNA sequencing and transcriptomic profiling of HT1080 cells after induction of MAT by the two independent systems and focused on the overlapping genes to discriminate treatment-specific effects. This disclosed that amoeboid cells upregulate signalling associated with inflammation, particularly the response to type I IFNs.

The association between inflammatory signalling and amoeboid invasion was further confirmed in a panel of melanoma cell lines of ranging invasion phenotypes. Moreover, by enhancing the Stat1/Stat2 response by treatment of cells with IFN $\beta$ , we could promote the amoeboid phenotype and individual dissemination of single cells from tumour spheres. Oppositely, downregulation of this signalling complex by IRF9 knockdown mediated by siRNA, or induced expression of SOCS1, responsible for negative regulation of Jak/Stat signalling, both promoted mesenchymal features of melanoma cells.

Results presented in this thesis have contributed to the field of cancer invasion plasticity and disclosed signalling mechanisms associated with the amoeboid phenotype, adding another piece to the overwhelmingly complicated biological puzzle of cancer.

## References

- Ahn, J., Sanz-Moreno, V., and Marshall, C.J. (2012). The metastasis gene NEDD9 product acts through integrin 3 and Src to promote mesenchymal motility and inhibit amoeboid motility. *J. Cell Sci.* *125*, 1814–1826.
- Alibert, C., Pereira, D., Lardier, N., Etienne-Manneville, S., Goud, B., Asnacios, A., and Manneville, J.-B. (2020). Intracellular stiffening competes with cortical softening in glioblastoma cells. *BioRxiv* 2020.09.02.279794.
- Aljohani, A.I., Joseph, C., Kurozumi, S., Mohammed, O.J., Miligy, I.M., Green, A.R., and Rakha, E.A. (2020). Myxovirus resistance 1 (MX1) is an independent predictor of poor outcome in invasive breast cancer. *Breast Cancer Res. Treat.* *181*, 541–551.
- Amano, M., Ito, M., Kimura, K., Fukata, Y., Chihara, K., Nakano, T., Matsuura, Y., and Kaibuchi, K. (1996). Phosphorylation and Activation of Myosin by Rho-associated Kinase (Rho-kinase). *J. Biol. Chem.* *271*, 20246–20249.
- Amano, M., Nakayama, M., and Kaibuchi, K. (2010). Rho-kinase/ROCK: A key regulator of the cytoskeleton and cell polarity. *Cytoskeleton (Hoboken)*. *67*, 545–554.
- Arthur, W.T., and Burridge, K. (2001). RhoA inactivation by p190RhoGAP regulates cell spreading and migration by promoting membrane protrusion and polarity. *Mol. Biol. Cell* *12*, 2711–2720.
- Asadullah, Kumar, S., Saxena, N., Sarkar, M., Barai, A., and Sen, S. (2021). Combined heterogeneity in cell size and deformability promotes cancer invasiveness. *J. Cell Sci.* *134*.
- Bartolini, F., Moseley, J.B., Schmoranzler, J., Cassimeris, L., Goode, B.L., and Gundersen, G.G. (2008). The formin mDia2 stabilizes microtubules independently of its actin nucleation activity. *J. Cell Biol.* *181*, 523–536.
- Basbaum, C.B., and Werb, Z. (1996). Focalized proteolysis: spatial and temporal regulation of extracellular matrix degradation at the cell surface. *Curr. Opin. Cell Biol.* *8*, 731–738.
- Baskaran, J.P., Weldy, A., Guarin, J., Munoz, G., Shpilker, P.H., Kotlik, M., Subbiah, N., Wishart, A., Peng, Y., Miller, M.A., et al. (2020). Cell shape, and not 2D migration, predicts extracellular matrix-driven 3D cell invasion in breast cancer. *APL Bioeng.* *4*, 26105.
- Baum, B., Settleman, J., and Quinlan, M.P. (2008). Transitions between epithelial and mesenchymal states in development and disease. *19*, 294–308.
- Belletti, B., Nicoloso, M.S., Schiappacassi, M., Berton, S., Lovat, F., Wolf, K., Canzonieri, V., D’Andrea, S., Zucchetto, A., Friedl, P., et al. (2008). Stathmin activity influences sarcoma cell shape, motility, and metastatic potential. *Mol. Biol. Cell* *19*, 2003–2013.
- Belletti, B., Pellizzari, I., Berton, S., Fabris, L., Wolf, K., Lovat, F., Schiappacassi, M., D’Andrea, S., Nicoloso, M.S., Lovisa, S., et al. (2010). p27kip1 controls cell morphology and motility by regulating microtubule-dependent lipid raft recycling. *Mol. Cell. Biol.* *30*, 2229–2240.
- Ben-Neriah, Y., and Karin, M. (2011). Inflammation meets cancer, with NF- $\kappa$ B as the matchmaker. *Nat. Immunol.* *12*, 715–723.
- Bergert, M., Chandradoss, S.D., Desai, R. a, and Paluch, E. (2012). Cell mechanics control rapid transitions between blebs and lamellipodia during migration. *Proc. Natl. Acad. Sci. U. S. A.* *109*, 14434–14439.
- Bond, M., Chase, a J., Baker, a H., and Newby, a C. (2001). Inhibition of transcription factor NF-kappaB reduces matrix metalloproteinase-1, -3 and -9 production by vascular smooth muscle cells. *Cardiovasc. Res.* *50*, 556–565.
- Bouchet, B.P., and Akhmanova, A. (2017). Microtubules in 3D cell motility. *J. Cell Sci.* *130*, 39–50.
- Bouchet, B.P., Noordstra, I., van Amersfoort, M., Katrukha, E.A., Ammon, Y.C., ter Hoeve, N.D., Hodgson, L., Dogterom, M., Derksen, P.W.B., and Akhmanova, A. (2016). Mesenchymal Cell Invasion Requires Cooperative Regulation of Persistent Microtubule Growth by SLAIN2 and CLASP1. *Dev. Cell* *39*, 708–723.

- Boureux, A., Vignal, E., Faure, S., and Fort, P. (2007). Evolution of the Rho family of ras-like GTPases in eukaryotes. *Mol. Biol. Evol.* *24*, 203–216.
- Byrne, K.M., Monsefi, N., Dawson, J.C., Degasperi, A., Bukowski-Wills, J.-C., Volinsky, N., Dobrzyński, M., Birtwistle, M.R., Tsyganov, M.A., Kiyatkin, A., et al. (2016). Bistability in the Rac1, PAK, and RhoA Signaling Network Drives Actin Cytoskeleton Dynamics and Cell Motility Switches. *Cell Syst.* *2*, 38–48.
- Caley, M.P., Martins, V.L., Moore, K., Lashari, M., Nissinen, L., Kähäri, V.-M., Alexander, S., Jones, E., Harwood, C.A., Jones, J., et al. (2021). Loss of the laminin subunit alpha-3 induces cell invasion and macrophage infiltration in cutaneous squamous cell carcinoma. *Br. J. Dermatol.* *184*, 923–934.
- Cambria, E., Brunner, S., Heusser, S., Fisch, P., Hitzl, W., Ferguson, S.J., and Wuertz-Kozak, K. (2020). Cell-Laden Agarose-Collagen Composite Hydrogels for Mechanotransduction Studies. *Front. Bioeng. Biotechnol.* *8*, 346.
- Cantelli, G., Orgaz, J.L., Rodriguez-Hernandez, I., Karagiannis, P., Maiques, O., Matias-Guiu, X., Nestle, F.O., Marti, R.M., Karagiannis, S.N., and Sanz-Moreno, V. (2015). TGF- $\beta$ -Induced Transcription Sustains Amoeboid Melanoma Migration and Dissemination. *Curr. Biol.* *25*, 2899–2914.
- Carragher, N.O., Walker, S.M., Scott Carragher, L.A., Harris, F., Sawyer, T.K., Brunton, V.G., Ozanne, B.W., and Frame, M.C. (2006). Calpain 2 and Src dependence distinguishes mesenchymal and amoeboid modes of tumour cell invasion: a link to integrin function. *Oncogene* *25*, 5726–5740.
- Čermák, V. (2019). Differential expression analyses.
- Čermák, V., Gandalovičová, A., Merta, L., Fučíková, J., Špišek, R., Rösel, D., and Brábek, J. (2018). RNA-seq of macrophages of amoeboid or mesenchymal migratory phenotype due to specific structure of environment. *Sci. Data* *5*, 180198.
- Čermák, V., Gandalovičová, A., Merta, L., Harant, K., Rösel, D., and Brábek, J. (2020). High-throughput transcriptomic and proteomic profiling of mesenchymal-amoeboid transition in 3D collagen. *Sci. Data* *7*.
- Čermák, V., Škarková, A., Merta, L., Kolomazníková, V., Palušová, V., Uldrijan, S., Rösel, D., and Brábek, J. (2021). RNA-seq Characterization of Melanoma Phenotype Switch in 3D Collagen after p38 MAPK Inhibitor Treatment. *Biomolecules* *11*.
- Chambers, A.F., Groom, A.C., and MacDonald, I.C. (2002). Dissemination and growth of cancer cells in metastatic sites. *Nat. Rev. Cancer* *2*, 563–572.
- Cheon, H., Holvey-Bates, E.G., Schoggins, J.W., Forster, S., Hertzog, P., Imanaka, N., Rice, C.M., Jackson, M.W., Junk, D.J., and Stark, G.R. (2013). IFN $\beta$ -dependent increases in STAT1, STAT2, and IRF9 mediate resistance to viruses and DNA damage. *EMBO J.* *32*, 2751–2763.
- Chrisafis, G., Wang, T., Moissoglu, K., Gasparski, A.N., Ng, Y., Weigert, R., Lockett, S.J., and Mili, S. (2020). Collective cancer cell invasion requires RNA accumulation at the invasive front. *Proc. Natl. Acad. Sci.* *117*, 27423 LP – 27434.
- Colotta, F., Allavena, P., Sica, A., Garlanda, C., and Mantovani, A. (2009). Cancer-related inflammation, the seventh hallmark of cancer: links to genetic instability. *Carcinogenesis* *30*, 1073–1081.
- Cooper, S., Sadok, A., Bousgouni, V., and Bakal, C. (2015). Apolar and polar transitions drive the conversion between amoeboid and mesenchymal shapes in melanoma cells. *Mol. Biol. Cell.*
- Coussens, L.M., and Werb, Z. (2002). Inflammation and cancer. *Nature* *420*, 860–867.
- D’Alterio, C., Scala, S., Sozzi, G., Roz, L., and Bertolini, G. (2020). Paradoxical effects of chemotherapy on tumor relapse and metastasis promotion. *Semin. Cancer Biol.* *60*, 351–361.
- D’Andrea, F.P., Safwat, A., Kassem, M., Gautier, L., Overgaard, J., and Horsman, M.R. (2011). Cancer stem cell overexpression of nicotinamide N-methyltransferase enhances cellular radiation resistance. *Radiother. Oncol.* *99*, 373–378.
- D’Angelo, E., Lindoso, R.S., Sensi, F., Pucciarelli, S., Bussolati, B., Agostini, M., and Collino, F. (2020). Intrinsic and Extrinsic Modulators of the Epithelial to Mesenchymal Transition: Driving the Fate of Tumor Microenvironment. *Front. Oncol.* *10*, 1122.

- Dasgupta, S.K., Le, A., Vijayan, K.V., and Thiagarajan, P. (2017). Dasatinib inhibits actin fiber reorganization and promotes endothelial cell permeability through RhoA-ROCK pathway. *Cancer Med.* 6, 809–818.
- Delgoffe, G.M., and Vignali, D.A.A. (2013). STAT heterodimers in immunity. *JAK-STAT* 2, e23060.
- Denais, C.M., Gilbert, R.M., Isermann, P., McGregor, A.L., te Lindert, M., Weigelin, B., Davidson, P.M., Friedl, P., Wolf, K., and Lammerding, J. (2016). Nuclear envelope rupture and repair during cancer cell migration. *Science* (80-. ). 352, 353–358.
- Diekmann, D., Nobes, C.D., Burbelo, P.D., Abo, A., and Hall, A. (1995). Rac GTPase interacts with GAPs and target proteins through multiple effector sites. *EMBO J.* 14, 5297–5305.
- Dovas, A., and Couchman, J.R. (2005). RhoGDI: multiple functions in the regulation of Rho family GTPase activities. *Biochem. J.* 390, 1–9.
- Dvorak, H.F. (1986). Tumors: wounds that do not heal. Similarities between tumor stroma generation and wound healing. *N. Engl. J. Med.* 315, 1650–1659.
- Eden, S., Rohatgi, R., Podtelejnikov, A. V, Mann, M., and Kirschner, M.W. (2002). Mechanism of regulation of WAVE1-induced actin nucleation by Rac1 and Nck. *Nature* 418, 790–793.
- Eitaki, M., Yamamori, T., Meike, S., Yasui, H., and Inanami, O. (2012). Vincristine enhances amoeboid-like motility via GEF-H1/RhoA/ROCK/Myosin light chain signaling in MKN45 cells. *BMC Cancer* 12, 469.
- Emad, A., Ray, T., Jensen, T.W., Parat, M., Natrajan, R., Sinha, S., and Ray, P.S. (2020). Superior breast cancer metastasis risk stratification using an epithelial-mesenchymal-amoeboid transition gene signature. *Breast Cancer Res.* 22, 74.
- Even-Ram, S., and Yamada, K.M. (2005). Cell migration in 3D matrix. *Curr. Opin. Cell Biol.* 17, 524–532.
- Fares, J., Fares, M.Y., Khachfe, H.H., Salhab, H.A., and Fares, Y. (2020). Molecular principles of metastasis: a hallmark of cancer revisited. *Signal Transduct. Target. Ther.* 5, 28.
- Fernandes, M., Rosel, D., and Brábek, J. (2019). Solid cancer: the new tumour spread endpoint opens novel opportunities. *Br. J. Cancer* 121, 513–514.
- Friedl, P., and Alexander, S. (2011). Cancer invasion and the microenvironment: plasticity and reciprocity. *Cell* 147, 992–1009.
- Friedl, P., and Wolf, K. (2003). Tumour-cell invasion and migration: diversity and escape mechanisms. *Nat. Rev. Cancer* 3, 362–374.
- Friedl, P., and Wolf, K. (2008). Tube Travel: The Role of Proteases in Individual and Collective Cancer Cell Invasion. *Cancer Res.* 68, 7247–7249.
- Friedl, P., and Wolf, K. (2010). Plasticity of cell migration: a multiscale tuning model. *J. Cell Biol.* 188, 11–19.
- Frydenlund, N., and Mahalingam, M. (2017). PD-L1 and immune escape: insights from melanoma and other lineage-unrelated malignancies. *Hum. Pathol.* 66, 13–33.
- Gaggioli, C., Hooper, S., Hidalgo-Carcedo, C., Grosse, R., Marshall, J.F., Harrington, K., and Sahai, E. (2007). Fibroblast-led collective invasion of carcinoma cells with differing roles for RhoGTPases in leading and following cells. *Nat. Cell Biol.* 9, 1392–1400.
- Gandalovičová, A., Vomastek, T., Rosel, D., and Brábek, J. (2016). Cell polarity signaling in the plasticity of cancer cell invasiveness. *Oncotarget; Adv. Online Publ.*
- Gandalovičová, A., Rosel, D., Fernandes, M., Veselý, P., Heneberg, P., Čermák, V., Petruželka, L., Kumar, S., Sanz-Moreno, V., and Brábek, J. (2017). Migrastatics—Anti-metastatic and Anti-invasion Drugs: Promises and Challenges. *Trends in Cancer* 3, 391–406.
- Gandalovičová, A., Šüchová, A.-M., Čermák, V., Merta, L., Rösel, D., and Brábek, J. (2020). Sustained

Inflammatory Signalling through Stat1/Stat2/IRF9 Is Associated with Amoeboid Phenotype of Melanoma Cells. *Cancers (Basel)*. *12*.

Gao, Y., Wang, Z., Hao, Q., Li, W., Xu, Y., Zhang, J., Zhang, W., Wang, S., Liu, S., Li, M., et al. (2017). Loss of ER $\alpha$  induces amoeboid-like migration of breast cancer cells by downregulating vinculin. *Nat. Commun.* *8*, 14483.

Geiger, F., Rüdiger, D., Zahler, S., and Engelke, H. (2019). Fiber stiffness, pore size and adhesion control migratory phenotype of MDA-MB-231 cells in collagen gels. *PLoS One* *14*, e0225215.

Georgouli, M., Herraiz, C., Crosas-Molist, E., Fanshawe, B., Maiques, O., Perdrix, A., Pandya, P., Rodriguez-Hernandez, I., Ilieva, K.M., Cantelli, G., et al. (2019). Regional Activation of Myosin II in Cancer Cells Drives Tumor Progression via a Secretory Cross-Talk with the Immune Microenvironment. *Cell* *176*, 757-774.e23.

Gerashchenko, T.S., Novikov, N.M., Krakhmal, N. V., Zolotaryova, S.Y., Zavyalova, M. V., Cherdyntseva, N. V., Denisov, E. V., and Perelmuter, V.M. (2019). Markers of Cancer Cell Invasion: Are They Good Enough? *J. Clin. Med.* *8*, 1092.

Ghosh, A., and Heston, W.D. (2004). Unique prostate cancer marker, prostate specific membrane antigen or PSMA and its role in prostate cancer metastasis. *Cancer Res.* *64*, 762 LP – 763.

Ghosh, I., Singh, R.K., Mishra, M., Kapoor, S., and Jana, S.S. (2021). Switching between blebbing and lamellipodia depends on the degree of non-muscle myosin II activity. *J. Cell Sci.* *134*.

Gilkes, D.M., Xiang, L., Lee, S.J., Chaturvedi, P., Hubbi, M.E., Wirtz, D., and Semenza, G.L. (2014). Hypoxia-inducible factors mediate coordinated RhoA-ROCK1 expression and signaling in breast cancer cells. *Proc. Natl. Acad. Sci. U. S. A.* *111*, E384–E393.

Van Goethem, E., Poincloux, R., Gauffre, F., Maridonneau-Parini, I., and Le Cabec, V. (2010). Matrix architecture dictates three-dimensional migration modes of human macrophages: differential involvement of proteases and podosome-like structures. *J. Immunol.* *184*, 1049–1061.

Greten, F.R., and Grivennikov, S.I. (2019). Inflammation and Cancer: Triggers, Mechanisms, and Consequences. *Immunity* *51*, 27–41.

Guiet, R., Van Goethem, E., Cougoule, C., Balor, S., Valette, A., Al Saati, T., Lowell, C.A., Le Cabec, V., and Maridonneau-Parini, I. (2011). The Process of Macrophage Migration Promotes Matrix Metalloproteinase-Independent Invasion by Tumor Cells. *J. Immunol.* *187*, 3806–3814.

Guzman, A., Sánchez Alemany, V., Nguyen, Y., Zhang, C.R., and Kaufman, L.J. (2017). A novel 3D in vitro metastasis model elucidates differential invasive strategies during and after breaching basement membrane. *Biomaterials* *115*, 19–29.

Haeger, A., Wolf, K., Zegers, M.M., and Friedl, P. (2015). Collective cell migration: Guidance principles and hierarchies. *Trends Cell Biol.* *25*, 556–566.

Hager, M.H., Morley, S., Bielenberg, D.R., Gao, S., Morello, M., Holcomb, I.N., Liu, W., Mouneimne, G., Demichelis, F., Kim, J., et al. (2012). DIAPH3 governs the cellular transition to the amoeboid tumour phenotype. *EMBO Mol. Med.* *4*, 743–760.

Hecht, I., Bar-El, Y., Balmer, F., Natan, S., Tsarfaty, I., Schweitzer, F., and Ben-Jacob, E. (2015). Tumor Invasion Optimization by Mesenchymal-Amoeboid Heterogeneity. *Sci. Rep.* *5*, 10622.

Hoek, K.S., Eichhoff, O.M., Schlegel, N.C., Dobbeling, U., Kobert, N., Schaerer, L., Hemmi, S., and Dummer, R. (2008). In vivo switching of human melanoma cells between proliferative and invasive states. *Cancer Res.* *68*, 650–656.

Holle, A.W., Govindan Kuty Devi, N., Clar, K., Fan, A., Saif, T., Kemkemer, R., and Spatz, J.P. (2019). Cancer Cells Invade Confined Microchannels via a Self-Directed Mesenchymal-to-Amoeboid Transition. *Nano Lett.* *19*, 2280–2290.

Huang, B., Lu, M., Jolly, M.K., Tsarfaty, I., Onuchic, J., and Ben-Jacob, E. (2014). The three-way switch operation of Rac1/RhoA GTPase-based circuit controlling amoeboid-hybrid-mesenchymal transition. *Sci. Rep.* *4*, 6449.

- Huang, Y.L., Tung, C.-K., Zheng, A., Kim, B.J., and Wu, M. (2015). Interstitial flows promote amoeboid over mesenchymal motility of breast cancer cells revealed by a three dimensional microfluidic model. *Integr. Biol. (Camb)*. 7, 1402–1411.
- Itoh, G., Chida, S., Yanagihara, K., Yashiro, M., Aiba, N., and Tanaka, M. (2017). Cancer-associated fibroblasts induce cancer cell apoptosis that regulates invasion mode of tumours. *Oncogene* 36, 4434–4444.
- Jacquemet, G., Hamidi, H., and Ivaska, J. (2015). Filopodia in cell adhesion, 3D migration and cancer cell invasion. *Curr. Opin. Cell Biol.* 36, 23–31.
- Jiu, Y., Peränen, J., Schaible, N., Cheng, F., Eriksson, J.E., Krishnan, R., and Lappalainen, P. (2017). Vimentin intermediate filaments control actin stress fiber assembly through GEF-H1 and RhoA. *J. Cell Sci.* 130, 892–902.
- Jolly, M.K., Ware, K.E., Gilja, S., Somarelli, J.A., and Levine, H. (2017). EMT and MET: necessary or permissive for metastasis? *Mol. Oncol.* 11, 755–769.
- Jones, B.C., Kelley, L.C., Loskutov, Y. V, Marinak, K.M., Kozyreva, V.K., Smolkin, M.B., and Pugacheva, E.N. (2017). Dual Targeting of Mesenchymal and Amoeboid Motility Hinders Metastatic Behavior. *Mol. Cancer Res.* 15, 670 LP – 682.
- Kapoor, A., Barai, A., Thakur, B., Das, A., Patwardhan, S.R., Monteiro, M., Gaikwad, S., Bukhari, A.B., Mogha, P., Majumder, A., et al. (2018). Soft drug-resistant ovarian cancer cells migrate via two distinct mechanisms utilizing myosin II-based contractility. *Biochim. Biophys. Acta - Mol. Cell Res.* 1865, 392–405.
- Kasprowicz, R., Suman, R., and O’Toole, P. (2017). Characterising live cell behaviour: Traditional label-free and quantitative phase imaging approaches. *Int. J. Biochem. Cell Biol.* 84, 89–95.
- Kaynor, C., Xin, M., Wakefield, J., Barsoum, J., and Qin, X.Q. (2002). Direct evidence that IFN-1 $\beta$  functions as a tumor-suppressor protein. *J. Interf. Cytokine Res.* 22, 1089–1098.
- Khodarev, N.N., Beckett, M., Labay, E., Darga, T., Roizman, B., and Weichselbaum, R.R. (2004). STAT1 is overexpressed in tumors selected for radioresistance and confers protection from radiation in transduced sensitive cells. *Proc. Natl. Acad. Sci. U. S. A.* 101, 1714–1719.
- Kim, D.H., Xing, T., Yang, Z., Dudek, R., Lu, Q., and Chen, Y.-H. (2018). Epithelial Mesenchymal Transition in Embryonic Development, Tissue Repair and Cancer: A Comprehensive Overview. *J. Clin. Med.* 7.
- Kim, Y.H., Choi, Y.W., Lee, J., Soh, E.Y., Kim, J.-H., and Park, T.J. (2017). Senescent tumor cells lead the collective invasion in thyroid cancer. *Nat. Commun.* 8, 15208.
- Kimura, K., Ito, M., Amano, M., Chihara, K., Fukata, Y., Nakafuku, M., Yamamori, B., Feng, J., Nakano, T., Okawa, K., et al. (1996). Regulation of Myosin Phosphatase by Rho and Rho-Associated Kinase (Rho-Kinase). *Science* (80-. ). 273, 245–248.
- Kohrman, A.Q., and Matus, D.Q. (2017). Divide or Conquer: Cell Cycle Regulation of Invasive Behavior. *Trends Cell Biol.* 27, 12–25.
- Kolosenko, I., Fryknäs, M., Forsberg, S., Johnsson, P., Cheon, H., Holvey-Bates, E.G., Edsbäcker, E., Pellegrini, P., Rassoolzadeh, H., Brnjic, S., et al. (2015). Cell crowding induces interferon regulatory factor 9, which confers resistance to chemotherapeutic drugs. *Int. J. Cancer* 136, E51–E61.
- Kosla, J., Paňková, D., Plachý, J., Tolde, O., Bicanová, K., Dvořák, M., Rösel, D., and Brábek, J. (2013). Metastasis of aggressive amoeboid sarcoma cells is dependent on Rho/ROCK/MLC signaling. *Cell Commun. Signal.* 11, 51.
- Krakhmal, N. V, Zavyalova, M. V, Denisov, E. V, Vtorushin, S. V, and Perelmuter, V.M. (2015). Cancer Invasion: Patterns and Mechanisms. *Acta Naturae* 7, 17–28.
- Krause, M., and Wolf, K. (2015). Cancer cell migration in 3d tissue: Negotiating space by proteolysis and nuclear deformability. *Cell Adhes. Migr.* 9, 357–366.
- Krendel, M., Zenke, F.T., and Bokoch, G.M. (2002). Nucleotide exchange factor GEF-H1 mediates cross-

talk between microtubules and the actin cytoskeleton. *Nat. Cell Biol.* 4, 294–301.

Ladhani, O., Sanchez-Martinez, C., Orgaz, J.L., Jimenez, B., and Volpert, O. V (2011). Pigment epithelium-derived factor blocks tumor extravasation by suppressing amoeboid morphology and mesenchymal proteolysis. *Neoplasia* 13, 633–642.

Lam, V.K., Nguyen, T.C., Chung, B.M., Nehmetallah, G., and Raub, C.B. (2018). Quantitative assessment of cancer cell morphology and motility using telecentric digital holographic microscopy and machine learning. *Cytom. Part A* 93, 334–345.

Lambert, A.W., Pattabiraman, D.R., and Weinberg, R.A. (2017). Emerging Biological Principles of Metastasis. *Cell* 168, 670–691.

Lamouille, S., Subramanyam, D., Billelo, R., and Derynck, R. (2013). Regulation of epithelial-mesenchymal and mesenchymal-epithelial transitions by microRNAs. *Curr. Opin. Cell Biol.* 25, 200–207.

Lauffenburger, D., and Horwitz, F. (1996). Cell migration: a physically integrated molecular process. *Cell* 84, 359–369.

Lavenus, S.B., Tudor, S.M., Ullo, M.F., Vosatka, K.W., and Logue, J.S. (2020). A flexible network of vimentin intermediate filaments promotes migration of amoeboid cancer cells through confined environments. *J. Biol. Chem.* 295, 6700–6709.

Lehmann, S., te Boekhorst, V., Odenthal, J., Bianchi, R., van Helvert, S., Ikenberg, K., Ilina, O., Stoma, S., Xandry, J., Jiang, L., et al. (2017). Hypoxia Induces a HIF-1-Dependent Transition from Collective-to-Amoeboid Dissemination in Epithelial Cancer Cells. *Curr. Biol.* 27, 392–400.

Lewis, D.M., Park, K.M., Tang, V., Xu, Y., Pak, K., Eisinger-Mathason, T.S.K., Simon, M.C., and Gerecht, S. (2016). Intratumoral oxygen gradients mediate sarcoma cell invasion. *Proc. Natl. Acad. Sci. U. S. A.* 113, 9292–9297.

Li, L., Dragulev, B., Zigrino, P., Mauch, C., and Fox, J.W. (2009). The invasive potential of human melanoma cell lines correlates with their ability to alter fibroblast gene expression in vitro and the stromal microenvironment in vivo. *1804*, 1796–1804.

Linder, S., Wiesner, C., and Himmel, M. (2011). Degrading devices: invadosomes in proteolytic cell invasion. *Annu. Rev. Cell Dev. Biol.* 27, 185–211.

Linke, F., Zaunig, S., Nietert, M.M., VonBonin, F., Lutz, S., Dullin, C., Janovská, P., Beissbarth, T., Alves, F., Klapper, W., et al. (2017). WNT5A: A motility-promoting factor in Hodgkin lymphoma. *Oncogene* 36, 13–23.

Linossi, E.M., Calleja, D.J., and Nicholson, S.E. (2018). Understanding SOCS protein specificity. *Growth Factors* 36, 104–117.

Liu, Y.J., Le Berre, M., Lautenschlaeger, F., Maiuri, P., Callan-Jones, A., Heuzé, M., Takaki, T., Voituriez, R., and Piel, M. (2015). Confinement and low adhesion induce fast amoeboid migration of slow mesenchymal cells. *Cell* 160, 659–672.

Liu, Z., Lee, S.J., Park, S., Konstantopoulos, K., Glunde, K., Chen, Y., and Barman, I. (2020). Cancer cells display increased migration and deformability in pace with metastatic progression. *FASEB J. Off. Publ. Fed. Am. Soc. Exp. Biol.* 34, 9307–9315.

Lorentzen, A., Bamber, J., Sadok, A., Elson-Schwab, I., and Marshall, C.J. (2011). An ezrin-rich, rigid uropod-like structure directs movement of amoeboid blebbing cells. *J. Cell Sci.* 124, 1256–1267.

Lorusso, G., and Rüegg, C. (2008). The tumor microenvironment and its contribution to tumor evolution toward metastasis. *Histochem. Cell Biol.* 130, 1091–1103.

Luker, K.E., Pica, C.M., Schreiber, R.D., and Piwnica-Worms, D. (2001). Overexpression of IRF9 confers resistance to antimicrotubule agents in breast cancer cells. *Cancer Res.* 61, 6540–6547.

Luzzi, K.J., MacDonald, I.C., Schmidt, E.E., Kerkvliet, N., Morris, V.L., Chambers, A.F., and Groom, A.C. (1998). Multistep Nature of Metastatic Inefficiency: Dormancy of Solitary Cells after Successful Extravasation and Limited Survival of Early Micrometastases. *Am. J. Pathol.* 153, 865–873.

- MacKay, J.L., and Kumar, S. (2014). Simultaneous and independent tuning of RhoA and Rac1 activity with orthogonally inducible promoters. *Integr. Biol.* *6*, 885–894.
- Maia, A., Gu, Z., Koch, A., Berdiel-Acer, M., Will, R., Schlesner, M., and Wiemann, S. (2021). IFN $\beta$ 1 secreted by breast cancer cells undergoing chemotherapy reprograms stromal fibroblasts to support tumour growth after treatment. *Mol. Oncol.* *15*, 1308–1329.
- Mendez, M.G., Restle, D., and Janmey, P.A. (2014). Vimentin enhances cell elastic behavior and protects against compressive stress. *Biophys. J.* *107*, 314–323.
- Messica, Y., Laser-Azogui, A., Volberg, T., Elisha, Y., Lysakovskaia, K., Eils, R., Gladilin, E., Geiger, B., and Beck, R. (2017). The role of Vimentin in Regulating Cell Invasive Migration in Dense Cultures of Breast Carcinoma Cells. *Nano Lett.* *17*, 6941–6948.
- Montano, N., D’Alessandris, Q.G., Izzo, A., Fernandez, E., and Pallini, R. (2016). Biomarkers for glioblastoma multiforme: status quo. *J. Clin. Transl. Res.* *2*, 3–10.
- Musella, M., Manic, G., De Maria, R., Vitale, I., and Sistigu, A. (2017). Type-I-interferons in infection and cancer: Unanticipated dynamics with therapeutic implications. *Oncoimmunology* *6*, e1314424–e1314424.
- Nabeshima, K., Inoue, T., Shima, Y., Kataoka, H., and Koono, M. (1999). Cohort migration of carcinoma cells: differentiated colorectal carcinoma cells move as coherent cell clusters or sheets. *Histol. Histopathol.* *14*, 1183–1197.
- Nabeshima, K., Inoue, T., Shima, Y., Okada, Y., Itoh, Y., Seiki, M., and Koono, M. (2000). Front-Cell-specific Expression of Membrane-Type 1 Matrix Metalloproteinase and Gelatinase A during Cohort Migration of Colon Carcinoma Cells Induced by Hepatocyte Growth Factor/Scatter Factor. *Cancer Res.* *60*, 3364–3369.
- Nguyen, L.K., Kholodenko, B.N., and von Kriegsheim, A. (2018). Rac1 and RhoA: Networks, loops and bistability. *Small GTPases* *9*, 316–321.
- O’Neill, P.R., Castillo-Badillo, J.A., Meshik, X., Kalyanaraman, V., Melgarejo, K., and Gautam, N. (2018). Membrane Flow Drives an Adhesion-Independent Amoeboid Cell Migration Mode. *Dev. Cell* *46*, 9-22.e4.
- Odenthal, J., Takes, R., and Friedl, P. (2016). Plasticity of tumor cell invasion: governance by growth factors and cytokines. *Carcinogenesis*.
- Onken, M.D., Blumer, K.J., and Cooper, J.A. (2021). Uveal melanoma cells use amoeboid and mesenchymal mechanisms of cell motility crossing the endothelium. *Mol. Biol. Cell* *32*, 413–421.
- Opdenakker, G., and Van Damme, J. (1992). Cytokines and proteases in invasive processes: Molecular similarities between inflammation and cancer. *Cytokine* *4*, 251–258.
- Orgaz, J.L., Benguria, A., Sanchez-Martinez, C., Ladhani, O., Volpert, O. V., and Jimenez, B. (2011). Changes in the gene expression profile of A375 human melanoma cells induced by overexpression of multifunctional pigment epithelium-derived factor. *Melanoma Res.* *21*, 285–297.
- Osmani, N., Peglion, F., Chavrier, P., and Etienne-Manneville, S. (2010). Cdc42 localization and cell polarity depend on membrane traffic. *J. Cell Biol.* *191*, 1261–1269.
- Pagès, D.-L., Dornier, E., De Seze, J., Wang, L., Luan, R., Cartry, J., Canet-Jourdan, C., Raingeaud, J., Voituriez, R., Coppey, M., et al. (2020). Cell clusters adopt a collective amoeboid mode of migration in confined non-adhesive environments. *BioRxiv* 2020.05.28.106203.
- Paluch, E.K., Aspalter, I.M., and Sixt, M. (2016). Focal Adhesion-Independent Cell Migration. *Annu. Rev. Cell Dev. Biol.* *32*, 469–490.
- Pan, Y.R., Chen, C.C., Chan, Y.T., Wang, H.J., Chien, F.T., Chen, Y.L., Liu, J.L., and Yang, M.H. (2018). STAT3-coordinated migration facilitates the dissemination of diffuse large B-cell lymphomas. *Nat. Commun.* *9*.
- Pandya, P., Orgaz, J.L., and Sanz-Moreno, V. (2017). Modes of invasion during tumour dissemination. *Mol. Oncol.* *11*, 5–27.



- Panková, K., Rösel, D., Novotný, M., and Brábek, J. (2010). The molecular mechanisms of transition between mesenchymal and amoeboid invasiveness in tumor cells. *Cell. Mol. Life Sci.* *67*, 63–71.
- Paňková, D., Jobe, N., Kratochvílová, M., Buccione, R., Brábek, J., and Rösel, D. (2012). NG2-mediated Rho activation promotes amoeboid invasiveness of cancer cells. *Eur. J. Cell Biol.* *91*, 969–977.
- Patteson, A.E., Pogoda, K., Byfield, F.J., Mandal, K., Ostrowska-Podhorodecka, Z., Charrier, E.E., Galie, P.A., Deptuła, P., Bucki, R., McCulloch, C.A., et al. (2019). Loss of Vimentin Enhances Cell Motility through Small Confining Spaces. *Small* *1903180*, 1–10.
- Pein, M., Insua-Rodríguez, J., Hongu, T., Riedel, A., Meier, J., Wiedmann, L., Decker, K., Essers, M.A.G., Sinn, H.-P., Spaich, S., et al. (2020). Metastasis-initiating cells induce and exploit a fibroblast niche to fuel malignant colonization of the lungs. *Nat. Commun.* *11*, 1494.
- Pertz, O., Hodgson, L., Klemke, R.L., and Hahn, K.M. (2006). Spatiotemporal dynamics of RhoA activity in migrating cells. *Nature* *440*, 1069–1072.
- Petrie, R.J., and Yamada, K.M. (2016). Multiple mechanisms of 3D migration: the origins of plasticity. *Curr. Opin. Cell Biol.* *42*, 7–12.
- Petrie, R.J., Gavara, N., Chadwick, R.S., and Yamada, K.M. (2012). Nonpolarized signaling reveals two distinct modes of 3D cell migration. *J. Cell Biol.* *197*, 439–455.
- Pidugu, V.K., Pidugu, H.B., Wu, M.-M., Liu, C.-J., and Lee, T.-C. (2019). Emerging Functions of Human IFIT Proteins in Cancer . *Front. Mol. Biosci.* *6*, 148.
- Pietrovito, L., Leo, A., Gori, V., Lulli, M., Parri, M., Becherucci, V., Piccini, L., Bambi, F., Taddei, M.L., and Chiarugi, P. (2018). Bone marrow-derived mesenchymal stem cells promote invasiveness and transendothelial migration of osteosarcoma cells via a mesenchymal to amoeboid transition. *Mol. Oncol.* *12*, 659–676.
- Rajapaksa, U.S., Jin, C., and Dong, T. (2020). Malignancy and IFITM3: Friend or Foe? . *Front. Oncol.* *10*, 2539.
- Rawlings, J.S., Rosler, K.M., and Harrison, D. a. (2004). The JAK/STAT signaling pathway. *J. Cell Sci.* *117*, 1281–1283.
- Rianna, C., Radmacher, M., and Kumar, S. (2020). Direct evidence that tumor cells soften when navigating confined spaces. *Mol. Biol. Cell* *31*, 1726–1734.
- Ridley, A.J. (2006). Rho GTPases and actin dynamics in membrane protrusions and vesicle trafficking. *Trends Cell Biol.* *16*, 522–529.
- Ridley, A.J., and Hall, A. (1992). The small GTP-binding protein rho regulates the assembly of focal adhesions and actin stress fibers in response to growth factors. *Cell* *70*, 389–399.
- Ridley, A.J., Schwartz, M. a, Burridge, K., Firtel, R. a, Ginsberg, M.H., Borisy, G., Parsons, J.T., and Horwitz, A.R. (2003). Cell migration: integrating signals from front to back. *Science (80- )*. *302*, 1704–1709.
- Rodriguez-Hernandez, I., Maiques, O., Kohlhammer, L., Cantelli, G., Perdrix-Rosell, A., Monger, J., Fanshawe, B., Bridgeman, V.L., Karagiannis, S.N., Penin, R.M., et al. (2020). WNT11-FZD7-DAAM1 signalling supports tumour initiating abilities and melanoma amoeboid invasion. *Nat. Commun.* *11*.
- Rohatgi, R., Ma, L., Miki, H., Lopez, M., Kirchhausen, T., Takenawa, T., and Kirschner, M.W. (1999). The interaction between N-WASP and the Arp2/3 complex links Cdc42-dependent signals to actin assembly. *Cell* *97*, 221–231.
- Rosel, D., Fernandes, M., Sanz-Moreno, V., and Brábek, J. (2019). Migrastatics: Redirecting R&D in Solid Cancer Towards Metastasis? *Trends in Cancer* *5*, 755–756.
- Rösel, D., Brábek, J., Tolde, O., Mierke, C.T., Zitterbart, D.P., Raupach, C., Bicanová, K., Kollmannsberger, P., Panková, D., Vesely, P., et al. (2008). Up-regulation of Rho/ROCK signaling in sarcoma cells drives invasion and increased generation of protrusive forces. *Mol. Cancer Res.* *6*, 1410–1420.

- Rullan Iriarte, A.J., Arwert, E., Milford, E., Chakravarty, P., Melcher, A., Harrington, K., and Sahai, E. (2018). Interaction between cancer associated fibroblasts and cancer cells influence immune infiltrate and is modulated by therapeutic agents. *Ann. Oncol.* *29*, viii657.
- Ruprecht, V., Wieser, S., Callan-Jones, A., Smutny, M., Morita, H., Sako, K., Barone, V., Ritsch-Marte, M., Sixt, M., Voituriez, R., et al. (2015). Cortical contractility triggers a stochastic switch to fast amoeboid cell motility. *Cell* *160*, 673–685.
- Sabeh, F., Shimizu-Hirota, R., and Weiss, S.J. (2009). Protease-dependent versus-independent cancer cell invasion programs: Three-dimensional amoeboid movement revisited. *J. Cell Biol.* *185*, 11–19.
- Sadok, A., McCarthy, A., Caldwell, J., Collins, I., Garrett, M.D., Yeo, M., Hooper, S., Sahai, E., Kuemper, S., Mardakheh, F.K., et al. (2015). Rho kinase inhibitors block melanoma cell migration and inhibit metastasis. *Cancer Res.* *75*, 2272–2284.
- Sahai, E., and Marshall, C.J. (2003). Differing modes of tumour cell invasion have distinct requirements for Rho/ROCK signalling and extracellular proteolysis. *Nat. Cell Biol.* *5*, 711–719.
- Sahai, E., Garcia-Medina, R., Pouyssegur, J., and Vial, E. (2007). Smurf1 regulates tumor cell plasticity and motility through degradation of RhoA leading to localized inhibition of contractility. *J. Cell Biol.* *176*, 35–42.
- Salbreux, G., Charras, G., and Paluch, E. (2012). Actin cortex mechanics and cellular morphogenesis. *Trends Cell Biol.* *22*, 536–545.
- Sanz-Moreno, V., Gadea, G., Ahn, J., Paterson, H., Marra, P., Pinner, S., Sahai, E., and Marshall, C.J. (2008). Rac activation and inactivation control plasticity of tumor cell movement. *Cell* *135*, 510–523.
- Sanz-Moreno, V., Gaggioli, C., Yeo, M., Albrengues, J., Wallberg, F., Viros, A., Hooper, S., Mitter, R., Féral, C.C., Cook, M., et al. (2011). ROCK and JAK1 signaling cooperate to control actomyosin contractility in tumor cells and stroma. *Cancer Cell* *20*, 229–245.
- Saxena, K., Jolly, M.K., and Balamurugan, K. (2020). Hypoxia, partial EMT and collective migration: Emerging culprits in metastasis. *Transl. Oncol.* *13*, 100845.
- Schillaci, O., Fontana, S., Monteleone, F., Taverna, S., Di Bella, M.A., Di Vizio, D., and Alessandro, R. (2017). Exosomes from metastatic cancer cells transfer amoeboid phenotype to non-metastatic cells and increase endothelial permeability: their emerging role in tumor heterogeneity. *Sci. Rep.* *7*, 4711.
- Schmidt, A., and Hall, A. (2002). Guanine nucleotide exchange factors for Rho GTPases: turning on the switch. *Genes Dev.* *16*, 1587–1609.
- Schmidt, S., and Friedl, P. (2010). Interstitial cell migration: integrin-dependent and alternative adhesion mechanisms. *Cell Tissue Res.* *339*, 83–92.
- Schmidt, S., Weigelin, B., Riet, J. te, Boekhorst, V. te, Lindert, M. te, Wijers-Rouw, M., Lelli, B., Rognoni, L., Krause-Vortmeyer, M., Messent, A., et al. (2020). Glycocalyx-mediated Cell Adhesion and Migration. *BioRxiv* 2020.06.12.149096.
- Schwartz, M.A. (2010). Integrins and extracellular matrix in mechanotransduction. *Cold Spring Harb. Perspect. Biol.* *2*, a005066–a005066.
- Seetharaman, S., and Etienne-Manneville, S. (2019). Microtubules at focal adhesions – a double-edged sword. *J. Cell Sci.* *132*.
- Sero, J.E., Sailem, H.Z., Ardy, R.C., Almuttaqi, H., Zhang, T., and Bakal, C. (2015). Cell shape and the microenvironment regulate nuclear translocation of NF- $\kappa$ B in breast epithelial and tumor cells. *Mol. Syst. Biol.* *11*, 790.
- Sheetz, M.P., Felsenfeld, D., Galbraith, C.G., and Choquet, D. (1999). Cell migration as a five-step cycle. *Biochem. Soc. Symp.* *65*, 233–243.
- Sistigu, A., Di Modugno, F., Manic, G., and Nisticò, P. (2017). Deciphering the loop of epithelial-mesenchymal transition, inflammatory cytokines and cancer immunoediting. *Cytokine Growth Factor Rev.* *36*, 67–77.

- Sleeman, J., and Steeg, P.S. (2010). Cancer metastasis as a therapeutic target. *Eur. J. Cancer* *46*, 1177–1180.
- Solinas, G., Marchesi, F., Garlanda, C., Mantovani, A., and Allavena, P. (2010). Inflammation-mediated promotion of invasion and metastasis. *Cancer Metastasis Rev.* *29*, 243–248.
- Strbkova, L., Carson, B.B., Vincent, T., Vesely, P., and Chmelik, R. (2020). Automated interpretation of time-lapse quantitative phase image by machine learning to study cellular dynamics during epithelial–mesenchymal transition. *J. Biomed. Opt.* *25*, 1–16.
- Strouhalova, K., Přečková, M., Gandalovičová, A., Brábek, J., Gregor, M., and Rosel, D. (2020). Vimentin Intermediate Filaments as Potential Target for Cancer Treatment. *Cancers (Basel)*. *12*.
- Taddei, M.L., Giannoni, E., Morandi, A., Ippolito, L., Ramazzotti, M., Callari, M., Gandellini, P., and Chiarugi, P. (2014). Mesenchymal to amoeboid transition is associated with stem-like features of melanoma cells. *Cell Commun. Signal.* *12*, 24.
- Tijhuis, A.E., Johnson, S.C., and McClelland, S.E. (2019). The emerging links between chromosomal instability (CIN), metastasis, inflammation and tumour immunity. *Mol. Cytogenet.* *12*, 17.
- Tolde, O., Gandalovičová, A., Křížová, A., Veselý, P., Chmelík, R., Rosel, D., and Brábek, J. (2018). Quantitative phase imaging unravels new insight into dynamics of mesenchymal and amoeboid cancer cell invasion. *Sci. Rep.* *8*, 12020.
- Tong, L., and Tergaonkar, V. (2014). Rho protein GTPases and their interactions with NFκB: crossroads of inflammation and matrix biology. *Biosci. Rep.* *34*, e00115.
- Ulrich, T.A., Jain, A., Tanner, K., MacKay, J.L., and Kumar, S. (2010). Probing cellular mechanobiology in three-dimensional culture with collagen-agarose matrices. *Biomaterials* *31*, 1875–1884.
- Vasiliev, J.M., Omelchenko, T., Gelfand, I.M., Feder, H.H., and Bonder, E.M. (2004). Rho overexpression leads to mitosis-associated detachment of cells from epithelial sheets: A link to the mechanism of cancer dissemination. *Proc. Natl. Acad. Sci. U. S. A.* *101*, 12526 LP – 12530.
- Vaškovičová, K., Szabadosová, E., Čermák, V., Gandalovičová, A., Kasalová, L., Rösel, D., and Brábek, J. (2015). PKCα promotes the mesenchymal to amoeboid transition and increases cancer cell invasiveness. *BMC Cancer* *15*.
- Vedula, S.R.K., Hirata, H., Nai, M.H., Brugués, A., Toyama, Y., Trepát, X., Lim, C.T., and Ladoux, B. (2014). Epithelial bridges maintain tissue integrity during collective cell migration. *Nat. Mater.* *13*, 87–96.
- Wang, X., Enomoto, A., Asai, N., Kato, T., and Takahashi, M. (2016). Collective invasion of cancer: Perspectives from pathology and development. *Pathol. Int.* *66*, 183–192.
- Watanabe, N., Kato, T., Fujita, A., Ishizaki, T., and Narumiya, S. (1999). Cooperation between mDial and ROCK in Rho-induced actin reorganization. *Nat. Cell Biol.* *1*, 136–143.
- Welf, E.S., Driscoll, M.K., Sapoznik, E., Murali, V.S., Weems, A., Roh-Johnson, M., Dean, K.M., Fiolka, R., and Danuser, G. (2020). Worrying drives cell migration in mechanically unrestrained environments. *BioRxiv* 2020.11.09.372912.
- Williams, E.D., Gao, D., Redfern, A., and Thompson, E.W. (2019). Controversies around epithelial–mesenchymal plasticity in cancer metastasis. *Nat. Rev. Cancer* *19*, 716–732.
- Wolf, K., Mazo, I., Leung, H., Engelke, K., von Andrian, U.H., Deryugina, E.I., Strongin, A.Y., Bröcker, E.-B., and Friedl, P. (2003). Compensation mechanism in tumor cell migration: mesenchymal-amoeboid transition after blocking of pericellular proteolysis. *J. Cell Biol.* *160*, 267–277.
- Wolf, K., te Lindert, M., Krause, M., Alexander, S., te Riet, J., Willis, A.L., Hoffman, R.M., Figdor, C.G., Weiss, S.J., and Friedl, P. (2013). Physical limits of cell migration: Control by ECM space and nuclear deformation and tuning by proteolysis and traction force. *J. Cell Biol.* *201*, 1069–1084.
- Xu, S., Xu, H., Wang, W., Li, S., Li, H., Li, T., Zhang, W., Yu, X., and Liu, L. (2019). The role of collagen in cancer: from bench to bedside. *J. Transl. Med.* *17*, 309.
- Yamagami, M., Otsuka, M., Kishikawa, T., Sekiba, K., Seimiya, T., Tanaka, E., Suzuki, T., Ishibashi, R.,

Ohno, M., and Koike, K. (2018). ISGF3 with reduced phosphorylation is associated with constitutive expression of interferon-induced genes in aging cells. *Npj Aging Mech. Dis.* *4*, 1–10.

Yang, J., and Stark, G.R. (2008). Roles of unphosphorylated STATs in signaling. *Cell Res.* *18*, 443–451.

Zhang, Y., and Liu, Z. (2017). STAT1 in cancer: friend or foe? *Discov. Med.* *24*, 19–29.